Mechanisms linking *CARS2* to Coronary Artery Disease

ANH-THU DANG

Thesis submitted to the University of Ottawa
in partial Fulfillment of the requirements for the
degree of PhD in Biochemistry

Department of Biochemistry, Microbiology and Immunology
Faculty of Medicine
University of Ottawa

Abstract

Coronary artery disease (CAD) is the leading cause of death worldwide. Genome-wide association studies (GWAS) have identified more than 200 loci associated with CAD. Here, we investigated the functional effects of a locus tagged by rs61969072 (T/G), with the common allele (T) associated with protection from CAD.

Expression quantitative trait loci (eQTL) analysis demonstrated a strong association between rs61969072 and *CARS2* gene expression, which increased with the T allele, in various human tissues. *CARS2* encodes the mitochondrial cysteinyl-tRNA synthetase, an enzyme that attaches cysteine to its cognate tRNA. We hypothesized that *CARS2* is a candidate causal gene and that CARS2 confers a protective effect against CAD.

We characterized *CARS2* expression in macrophages and demonstrated decreased expression in pro-inflammatory M1 macrophages. Gene expression profiling following *CARS2* siRNA knockdown revealed increased levels of several pro-inflammatory cytokines. Functional enrichment analysis identified the anti-inflammatory IL-10 signaling pathway, and western blotting showed that CARS2 attenuated IL-10 pathway activation through STAT3 phosphorylation. We also demonstrated that macrophage *CARS2* knockdown in a macrophage/smooth muscle cell (SMC) co-culture model elicited gene expression changes indicative of a less contractile, pro-inflammatory, SMC phenotype.

We then performed an in-depth analysis of differentially expressed genes following *CARS2* knockdown. Several inflammatory pathways and functions were affected, particularly Protein Kinase R (PKR), implicated in Interferon Induction and Antiviral Response. Downstream of PKR is the NF-κB signaling pathway; *CARS2* knockdown led to increased NF-κB protein expression but not activation, as measured by a luciferase reporter assay.

Finally, we investigated potential mitochondrial mechanisms that could lead to inflammation. Reduced CARS2 levels were found to decrease mitochondrial membrane potential. However, there was a decrease in reactive oxygen species (ROS) levels and no changes in mitochondrial DNA release, metabolism, or mitochondrial bioenergetics. While ROS are often considered harmful due to their role in oxidative damage and inflammation, studies have shown that under certain contexts, ROS can have protective effects. Further studies are required to understand the mechanisms underlying the anti-inflammatory effects of CARS2.

Overall, my findings highlight a novel anti-inflammatory role of CARS2 in human macrophages, consistent with the CAD protective effect of a common GWAS-identified variant.

Acknowledgements

First and foremost, I would like to thank my supervisor Dr. Ruth McPherson for providing me with the opportunity to join the lab as a volunteer and encouraging me to pursue my graduate studies. Over the years, she has provided support and guidance in my research and has allowed the flexibility to have a well-rounded graduate student experience.

I would like to express my gratitude to Dr. Katey Rayner, Dr. Mary-Ellen Harper, and Dr. Alexander Stewart, all members of my thesis advisory committee. Their expertise, insight, and guidance have been invaluable in building my confidence in my research over the years.

To all the present and past members of the lab, thank you for making the lab such a fun and exciting place to work in. Especially to Sebastien Soubeyrand and Paulina Lau for their feedback, advice, and guidance on my project. I want to give special thanks to Adam Turner, who helped me at the start of this project and was a great mentor for a new graduate student. I would also like to thank Anada Silva, whose reference helped me get into this lab.

I cannot forget all the amazing friends I made at the Heart Institute over the years, who were always there to offer understanding, good talks, and laughter.

Thank you to my partner, for being my best cheerleader who keeps me grounded and always believes in me.

Lastly, thank you to mẹ, ba, and Siêu. Their love, support, and never-ending patience gave me strength through my studies.

Table of Contents

Abstract ii
Acknowledgements iv
Table of Contents v
List of Abbreviations viii
List of Figures x
List of Tables xii
Chapter 1: Introduction 1
1.1 Pathogenesis of Coronary Artery Disease 1
1.1.1 The role of inflammation in atherosclerosis 4
1.1.2 Mitochondrial dysfunction in the pathogenesis of atherosclerosis 8
1.2 Genetics of Coronary Artery Disease 8
1.3 Genome Wide Association Studies 10
1.4 Translating genetic risk loci to disease pathology 12
1.5 Aminoacyl tRNA Synthetases 14
1.6 Cysteinyl t-RNA synthetase (CARS2) 18
1.7 Study Rational 19
1.8 Hypothesis 20
1.9 Objectives 20
Chapter 2: Materials and Methods 21
2.1 eQTL Analysis 21
2.2 Cell Culture 21
2.2.1 Co-culture with human coronary artery smooth muscle cells (HCASMC) 22
2.3 siRNA Transfection 23
2.4 Lentiviral overexpression 23
2.5 Luminex Multiplex Assay 24
2.6 Reverse transcription and quantitative real-time PCR 24
2.7 Microarray 26
2.8 Inflammatory Cytokines and Receptors Array by RT2 Profiler PCR array 26
2.9 Western blotting 26
2.9.1 Subcellular Fractionation 28
2.10 Ingenuity Pathway Analysis 28

2.11 RelA Luciferase Cells 29
2.12 Metabolic Cell Phenotype Analysis (Seahorse) 30
2.13 Mitochondrial Membrane Potential (TMRE) 31
2.14 Measurement of Reactive Oxygen Species (ROS) 32
2.15 Mitochondrial DNA (mtDNA) Quantification 33
2.16 Statistical Analysis 34
Chapter 3: A novel anti-inflammatory role links the CARS2 locus to protection from coronary artery disease. 35
3.1 Introduction 35
3.2 Results 36
3.2.1 rs61969072 is strongly associated with *CARS2* expression. 36
3.2.2 CARS2 expression is decreased in pro-inflammatory M1 macrophages. 40
3.2.3 Reduced levels of CARS2 lead to increased pro-inflammatory cytokine expression. 44
3.2.4 CARS2 silencing reduced STAT3 activation in the IL-10 signaling pathway. 50
3.2.5 *CARS2* knockdown in macrophages altered the expression of SMC markers in co-culture. 53
3.2 Discussion 55
Chapter 4: CARS2 knockdown alters NF-κB activity and expression in macrophages. 59
4.1 Introduction 59
4.2 Results 59
4.2.1 IPA Analysis revealed inflammatory pathways relevant to genes differentially regulated in reduced *CARS2* macrophages. 59
4.2.2 Reduced CARS2 levels increased NFKB protein expression. 70
4.2.3 NF-κB translocation is not affected by lower CARS2 expression. 73
4.2.4 NF-κB activation is decreased following reduced CARS2 levels. 76
4.3 Discussion 78
Chapter 5: Effects of CARS2 on mitochondrial bioenergetics and function 82
5.1 Introduction 82
5.2 Results 82
5.2.1 Mitochondrial mass is unchanged by reduced CARS2 levels. 83
5.2.2 Decreasing CARS2 expression did not affect the oxygen consumption rate. 85
5.2.3 Mitochondrial membrane potential decreased following lower CARS2 levels. 87

5.2.4 Cytosolic mitochondrial DNA release was not affected by reduced CARS2 expression. 89
5.2.5 Reduced CARS2 expression decreased reactive oxygen species levels. 91
5.2.6 Mitochondrial biogenesis, measured by MTCO1 protein expression, is decreased with lower CARS2 levels. 93
5.3 Discussion 96
General Discussion and Future Directions 100
References 106
Curriculum Vitae 118
Copyright Statement 121

List of Abbreviations

3-MST	3-mercaptopyruvate sulfurtransferase
ARS	aminoacyl tRNA synthetases
ALFA	Allele Frequency Aggregator
ASAP	Advanced Study of Aortic Pathology
BiKE	Biobank of Karolinska Endarterectomies
CAD	coronary artery disease
CARS2	cysteinyl-tRNA synthetase 2, mitochondrial
CBS	cystathionine β-synthase
CCCP	carbonyl cyanide m-chlorophenyl hydrazone
CMT	Charcot-Marie-Tooth disease
COXPD	combined oxidative phosphorylation deficiency
CPERS	principal cysteine persulfide
CSE	cystathionine gamma-lyase
CysSSH	cysteine hydopersulfide
DCFDA	dichlorodihydrofluorescein diacetate
DIT	diffuse intimal thickening
ECAR	extracellular acidification rate
ETC	electron transport chain
FCCP	carbonyl cyanide p-trifluoromethoxyphenylhydrazone
FDR	false discovery rate
GSEA	gene set enrichment analysis
GSSSG	glutathione trisulphide
GTEx	Genotype-Tissue Expression
GWAS	genome-wide association study
HCASMC	human coronary artery smooth muscle cells
HMDMs	human monocyte-derived macrophages
IFN-γ	interferon gamma
IKK	IkB kinase
IκB	inhibitor of κB
IL-10	interleukin-10
IL-10R	interleukin-10 receptor
IL-1β	interleukin 1 beta
IPA	Ingenuity Pathway Analysis
IRF	interferon-regulatory factor
JAK1	Janus Kinase 1
KO	knockout
LD	linkage disequilibrium
LDL	low-density lipoprotein
LPS	lipopolysaccharide
MAF	minor allele frequency
MARS2	methionyl-tRNA synthetase 2, mitochondrial
M-CSF	monocyte colony stimulating factor
MERRF	myoclonus epilepsy with ragged red fibers

MSC	multi-tRNA synthetase
mtDNA	mitochondrial DNA
PMA	phorbol-12-myristate-13-acetate
NAFLD	non-alcoholic fatty liver disease
nDNA	nuclear DNA
NF-κB	nuclear factor kappa B
NLRP3	NOD-like receptor family pyrin domain-containing 3
NT2	negative control number 2
OCR	oxygen consumption rate
oxLDL	oxidized LDL
OXPHOS	oxidative phosphorylation
PKR	Protein Kinase R
ROS	reactive oxygen species
SMC	smooth muscle cells
SNP	single nucleotide polymorphisms
STAT3	signal transducer and activator of transcription 3
TMRE	tetramethylrhodamine ethyl ester
TNF-α	tumor necrosis factor
TOMM20	translocase of outer mitochondrial membrane 20
Tyk2	tyrosine kinase 2
WARS	tryptophanyl-tRNA synthetase
YARS	tyrosyl-tRNA synthetase
YARS2	tyrosyl-tRNA synthetase 2, mitochondrial

List of Figures

Figure 1.1 Stages of atherosclerosis plaque progression. 3
Figure 1.2 NF-κB signaling pathway. 6
Figure 1.3 IL-10 signaling pathway. 7
Figure 1.4 Two-step aminoacylation by aminoacyl-tRNA synthetases (ARS). 17
Figure 3.1 The proxy SNPs, rs7991766 and rs7999702, were associated with CARS2 expression. 38
Figure 3.2 Tissue-specific associations between rs61969072 and proximal genes from the ASAP study. 39
Figure 3.3 Tissue-specific pattern of CARS2 mRNA expression. 41
Figure 3.4 Decreased CARS2 expression in pro-inflammatory M1 macrophages. 42
Figure 3.5 Rapid decrease in CARS2 expression following polarisation to M1 macrophages. 43
Figure 3.6 Decreased CARS2 expression increases pro-inflammatory cytokine expression in macrophages 46
Figure 3.7 Expression of inflammatory cytokines in macrophages following aminoacyl tRNA synthetase knockdown. 47
Figure 3.8 CARS2 silencing in M0 macrophages reduced STAT3 phosphorylation in response to IL-10. 52
Figure 3.9 CARS2 knockdown in macrophages altered the expression of major smooth muscle cell markers in co-culture experiments. 54
Figure 4.1 Canonical pathways from the Ingenuity Pathway Analysis (IPA). 63
Figure 4.2 Diseases and Biological functions enriched by IPA. 65
Figure 4.3 Toxicology pathway list from IPA. 66
Figure 4.4 Network analysis using IPA. 67
Figure 4.5 Validation of QPCR array data. 69
Figure 4.7 CARS2 affects protein expression in the PKR pathway. 72
Figure 4.8 NF-κB translocation was examined by protein fractionation. 74
Figure 4.9 Reduced CARS2 levels may reduce NF-κB inhibitor alpha (IKB-α) expression. 75
Figure 4.10 CARS2 decreased NF-κB activation after LPS treatment. 77
Figure 5.1 TOMM20, a marker of mitochondrial mass, remained unchanged under conditions of reduced CARS2 levels. 84
Figure 5.2 Seahorse Cell Energy Phenotype analysis of metabolic potential in THP-1 macrophages. 86

Figure 5.3 CARS2 silencing affects mitochondrial membrane potential in THP-1 cells. 88
Figure 5.4 Assessment of cytosolic mitochondrial DNA (mtDNA) release. 90
Figure 5.5 Decreased reactive oxygen species (ROS) in macrophages with reduced CARS2 levels. 92
Figure 5.6 CARS2 affects MTCO1 protein expression in THP-1 macrophages. 95

List of Tables

Table 3.1 GTEx eQTL data. 37

Table 3.2 Gene Set Enrichment Analysis identifies IL-10 signaling as a positively related category. 48

Table 3.3 Summary of qPCR array results from the CARS2 siRNA-mediated knockdown in M0 macrophages. 49

Table 3.4 IL-10-downregulated/upregulated extracellular and plasma membrane genes. 51

Table 4.1 Top 30 Upstream Regulators from Ingenuity Pathway Analysis (IPA). 64

Table 4.2 Network analysis. 68

Chapter 1: Introduction

1.1 Pathogenesis of Coronary Artery Disease

Despite advances in research and prevention, coronary artery disease (CAD) remains the leading cause of death worldwide[1]. Atherosclerosis is the underlying cause of CAD and is a progressive disease characterised by a chronic inflammatory response to the accumulation of cholesterol in the subendothelial space of large and medium-sized arteries. Atherosclerosis plaque progression can be described in three stages: fatty-streak, fibrous plaque, advanced lesion and thrombosis[2,3] (**Figure 1.1**).

The earliest change that occurs in the arterial wall is diffuse intimal thickening (DIT) which is considered to be related to atherogenesis[4,5]. Intimal thickening, regarded as nonatherosclerotic, is the normal accumulation of smooth muscle cells (SMC), spreading circumferentially and longitudinally in arterial segments with no branches[6,7]. DIT occurs in the intima, which is defined as the innermost layer of the artery, including the endothelial surface of the lumen[6].

In the first stage, early lesions/fatty streaks are formed by the accumulation of extracellular low-density lipoprotein (LDL) in the outer layer of pre-existing DIT[8,9]. LDL is the main carrier of plasma cholesterol and is the predominant atherogenic lipoprotein[10]. LDL can be oxidized by major cell types found in lesions such as SMCs, monocytes, and endothelial cells, resulting in pro-inflammatory and immunogenic oxidized LDL (oxLDL)[11,12]. Modified oxLDLs activate endothelial cells, triggering the expression of adhesion molecules, such as vascular cell adhesion molecule 1 (VCAM-1)[13] and intercellular adhesion molecule-1 (ICAM-1)[14], and the release of chemokines and cytokines, such as monocyte chemotactic protein-1 (MCP-1) and monocyte colony stimulating factor (M-CSF)[15]. Circulating monocytes are recruited to the vessel wall by binding to adhesion molecules, and chemokines promote their migration to the arterial wall[16].

Monocytes differentiate into macrophages to express scavenger receptors, such as scavenger receptor A (SR-A) and cluster of differentiation 36 (CD36)[17], and turn into foam cells by engulfing lipoprotein particles[18].

In the next stage, the fibrous cap forms over the intimal layer, transitioning from a fatty streak to a more complex lesion[19]. This is characterised by the migration of SMCs from the medial layer into the intima and increased synthesis of extracellular matrix components such as collagen, elastin, and proteoglycans which contribute to the thickening of the intimal layer[20]. SMCs also contribute to foam cell populations, making up at least 50% of SMC-derived foam cells in the plaque[21]. Crosstalk between monocytes, macrophages, foam cells, and T cells results in a chronic inflammatory state. For example, T-cells release pro-inflammatory cytokines such as IFN-γ, which can inhibit SMCs from producing collagen, affecting their ability to repair and maintain the fibrous cap[22]. Inside the fibrous cap, foam cells start to die and are not efficiently cleared by efferocytosis, releasing lipids that build up to form a lipid or necrotic core[23]. This results in the formation of fibrous plaques.

In the last stage, the lesion has advanced, and the fibrous cap grows and continues to protrude into the vessel. Advancing plaques contain large amounts of extracellular lipids, cholesterol crystals and necrotic debris[7]. As the plaque becomes unstable, the fibrous cap thins and weakens, leading to an increased susceptibility of the plaque to rupture. Ultimately, thrombosis occurs when the plaque's fibrous cap fractures, enabling blood coagulation components to come into contact with the exposed cholesterol and connective tissue, thereby impeding blood flow.

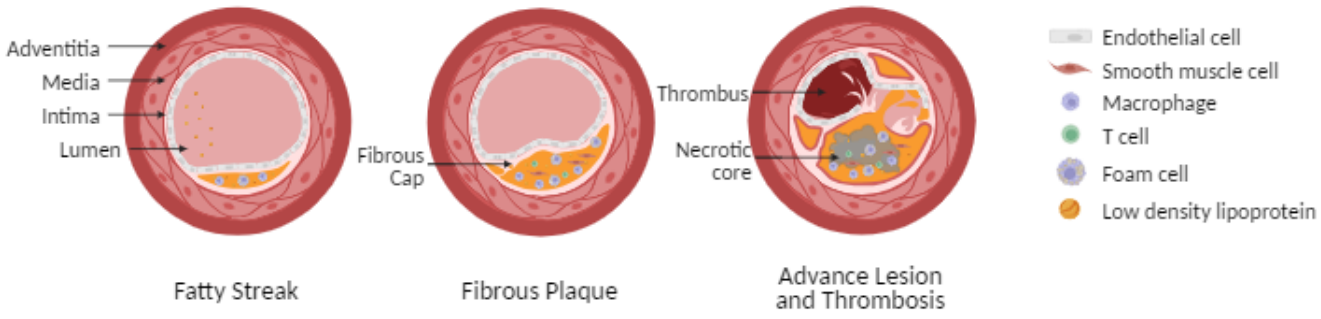

Figure 1.1 Stages of atherosclerosis plaque progression. Early fatty streak lesions are characterised by the accumulation of LDL in the intima where they become modified. Modified oxidized LDL (oxLDL) activates endothelial cells to recruit monocytes that differentiate into macrophages. Macrophages then take up oxLDL to form foam cells. A fibrous cap forms over the intimal layer and SMCs migrate into the intimal layer, resulting in a fibrous plaque. Advanced lesions are characterised by the accumulation of apoptotic cells and defective efferocytosis, resulting in a lipid-filled necrotic core. The plaque becomes more unstable as the thinning fibrous cap decreases lesion stability. Plaques are susceptible to rupture, and thrombus formation ultimately occurs. Created with BioRender.com.

1.1.1 The role of inflammation in atherosclerosis

Atherosclerosis is a chronic inflammatory disease[24]. Inflammation plays a central role in the initiation and progression of atherosclerotic plaques as discussed above. Almost all major cell types involved in this process can produce and are affected by cytokines and chemokines[25]. Proatherogenic cytokines, such as TNF-α, IL-1 family (IL-1, IL-8), Class I cytokines (IL-2, IL-6, IL-12), IFN-γ, M-CSF, and transforming growth factors (TGF-β1, TGF-β2, and TGF-β3), are found in atherosclerosis-prone vessels[25]. THP-1 cells, a cell line derived from the blood of a patient with acute monocytic leukemia[26], are widely used to investigate the function and regulation of monocytes and macrophages in the cardiovascular system. This monocytic cell line can also be stimulated with phorbol-12-myristate-13-acetate (PMA) to differentiate into a macrophage phenotype. Similar to primary macrophages, THP-1 cells can synthesise and secrete cytokines in a relevant cell model to provide insight into inflammation related to atherogenesis[27]. The NF-κB signaling pathway is one of the main pathways activated in response to pro-inflammatory cytokines (TNF-α, IL-1), bacterial lipopolysaccharide (LPS), Toll-like receptors (TLR), and pattern recognition of pathogen-associated molecular patterns (PAMPs)[25,28]. The NF-κB dimer, composed of p65 and p50, is kept inactive by the inhibitor of κB (IκB), forming the IkB kinase (IKK) complex. Extracellular stimuli classically activate the IKK complex, leading to the phosphorylation of IκB and resulting in its ubiquitination and degradation. The NF-κB dimer then translocates to the nucleus to activate specific target genes (**Figure 1.2**). Transcription factor NF-κB mediates the inflammatory response by regulating genes encoding pro-inflammatory cytokines, cell adhesion molecules, growth factors, and other enzymes such as cyclooxygenase-2 (COX2) and inducible nitric oxide synthase (iNOS)[28]. NF-κB contributes to every stage of atherosclerotic plaque development in both proatherogenic and antiatherogenic

ways[29]. Activated NF-κB has been shown in human atherosclerotic lesions[30], SMCs, macrophages and endothelial cells[29].

One anti-inflammatory pathway is the interleukin-10 (IL-10) signaling pathway. IL-10, a pleiotropic cytokine, is produced by Th2-type T cells, B cells, monocytes and macrophages[31]. IL-10 has anti-inflammatory properties in macrophages and T cells and plays an active role in limiting the inflammatory response in the vessel wall[25,32]. IL-10 can also block NF-κB activity by blocking IKBa degradation and NF-κB DNA-binding activity[33]. The JAK1/STAT3 cascade is activated when IL-10 binds to its cognate receptor, IL-10R, a tetramer composed of two distinct chains[34]. IL-10R activates the receptor-associated Janus tyrosine kinases JAK1 and Tyk2. This activation results in the phosphorylation of STAT3 which homodimerizes and translocates to the nucleus to activate the target genes (**Figure 1.3**). A mouse study showed that IL-10 plays critical roles in both atherosclerotic lesion formation and stability. In vivo transfer of murine IL-10 plasmid DNA led to a 60% reduction in lesion size[35].

There are emerging data on the benefits of immunomodulatory agents in experimental models and human studies[36]. The Canakinumab Anti-inflammatory Thrombosis Outcomes Study (CANTOS) demonstrated that targeting inflammation through interleukin 1 beta (IL-1β) in patients with coronary artery disease significantly lowered the incidence of recurrent cardiovascular events compared with placebo[37]. Although the effect size was modest, studies have proven that modulating an inflammatory pathway can reduce cardiovascular events[36,38]. Colchicine, an inhibitor of microtubule polymerization, impairs the assembly of the NLRP3 inflammasome and has been shown to reduce future cardiovascular events by 25% in patients with stable CAD[39].

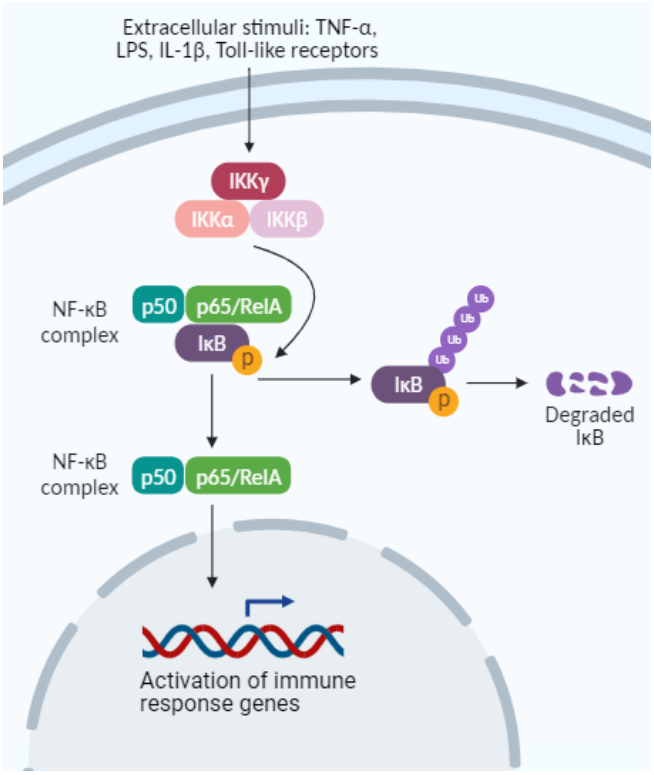

Figure 1.2 NF-κB signaling pathway. The classical NF-κB activation pathway is activated by a variety of external stimuli such as cytokines, LPS, TLRs, and PAMPs. This phosphorylates inhibitory IκB proteins via the IKK complex, leading to ubiquitination and degradation. The NF-κB complex, composed of p50 and p65/RelA dimers, translocates to the nucleus and activates transcription of specific NF-κB target genes. Created with BioRender.com.

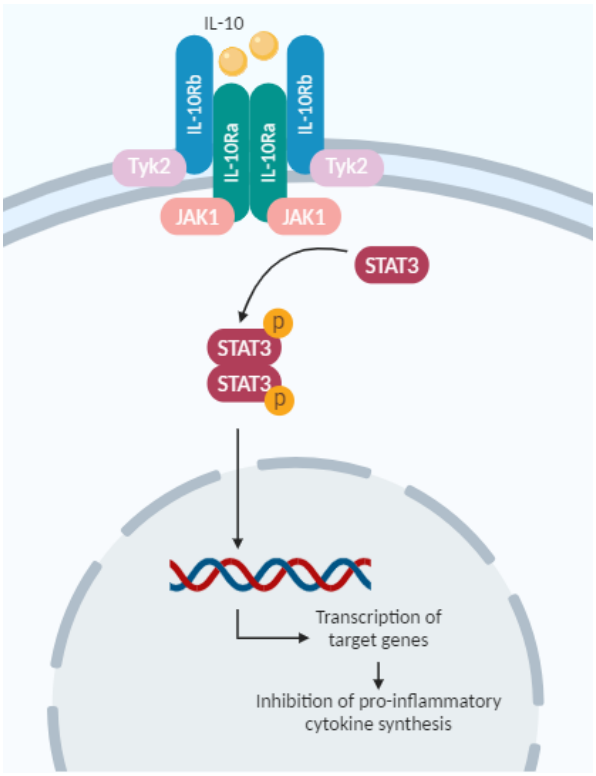

Figure 1.3 IL-10 signaling pathway. IL-10 binds to its receptor (IL-10R), a tetramer composed of two distinct chains (IL-10Ra and IL-10Rb). This activates JAK1 and Tyk2 to phosphorylate STAT3, which homodimerizes and translocates to the nucleus to activate specific target genes. Created with BioRender.com.

1.1.2 Mitochondrial dysfunction in the pathogenesis of atherosclerosis

Mitochondria are the main source of cellular energy and are responsible for meeting the high-energy demands of the heart by providing ATP through oxidative phosphorylation[40]. Mitochondrial dysfunction has emerged as one of the main pathogenic mechanisms underlying cardiovascular disease[41]. Particularly in atherosclerosis, mitochondrial dysfunction has been associated with the initiation and progression of the lesion by increasing the production of reactive oxygen species (ROS), mitochondrial oxidative stress damage, mitochondrial dynamic dysfunction, and energy supply[42]. Mitochondrial dysfunction can affect major cell types in the arterial wall, such as macrophages, SMCs, and endothelial cells due to their metabolic functions[43]. Under pathological conditions, mitochondria can alter inflammation through the production of ROS and release mitochondrial components such as mitochondrial DNA (mtDNA) into the cytoplasm to act as danger signals to innate immune receptors[42,44]. Increased ROS levels affect oxidative stress and chronic inflammation and can result in apoptosis, favoring plaque rupture[43]. Elevated ROS production can damage cellular structures, DNA, proteins, and other molecules[45], and oxidize LDL in the arterial wall[46]. ROS contributes to mtDNA damage, which can result in the weakened expression of respiratory complexes and mitochondrial respiration in smooth muscle cells, monocytes, and macrophages[47]. Damaged mtDNA can also be recognized as an endogenous damage-associated molecular pattern (DAMP) that activates the inflammatory response[43].

1.2 Genetics of Coronary Artery Disease

CAD is a complex disease influenced by a combination of genetic and traditional risk factors. Traditional risk factors include type 2 diabetes mellitus, elevated non-HDL cholesterol, arterial hypertension, smoking, unhealthy diet, and a lack of physical activity. However, these factors do

not fully account CAD risk. Familial studies have estimated CAD heritability to be 40–60%[48]. In a study of over 20,000 Swedish twins, the heritability was 0.57 and 0.38 for men and women, respectively[49]. In the Framingham Offspring Study, individuals with at least one parent with premature cardiovascular disease (defined as onset age <55 years in fathers and <65 years in mothers) had an increased age-specific incidence of CAD by >2-fold[50]. The INTERHEART study further confirmed that a family history of CAD was an independent risk factor after adjusting for age, sex, smoking status, and geographical region[51]. Overall, these findings indicate that genetics plays a major role in coronary artery disease risk.

In family-based studies, linkage analysis has been used to identify monogenic causes of CAD. Linkage analysis is a method based on Mendelian laws of inheritance and is used to identify genetic loci associated with a disease phenotype by examining the family history[52]. Mendelian disorders that predispose individuals to early CAD typically affect plasma lipid levels[53]. Familial hypercholesterolemia (FH), a Mendelian disorder with high levels of LDL-cholesterol culminating in very early atherosclerosis, was first related to a 5 kb deletion of the *LDLR* gene, encoding the LDL receptor[54]. More than 1000 single-nucleotide mutations or extended deletions in the *LDLR* gene have been identified. Impairment of the synthesis or function of the LDL receptor leads to increased levels of circulating LDL cholesterol and premature CAD. Further family-based studies in patients with FH have identified causal mutations in *APOB* (apolipoprotein B), *PCSK9* (proprotein convertase subtilisin/kexin type 9), recessive mutations in *LDLRAP1* (low-density lipoprotein receptor adapter protein 1) and *ABCG5, ABCG8* (ATP-binding cassette subfamily G members 5 or 8)[55–58]. Even so, the use of family studies to identify monogenic causes of CAD can be challenging. For example, a rare mutation leading to a 21 base pair deletion in *MEF2A* was previously proposed to be associated with CAD[59]. However, this

mutation was also observed in unaffected individuals and was not associated with CAD in families. Due to the rarity of some of these genotypes, it is difficult to confirm these findings in the general population.

Although family-based studies can be useful for gene discovery, CAD is a complex disease with a complicated genetic architecture. The majority of individuals with early CAD do not exhibit an autosomal dominant inheritance; thus, CAD is one of many common polygenic disorders.

1.3 Genome Wide Association Studies

Genome-wide association studies (GWAS) scan the human genome for genetic variants that are statistically associated with a specific trait or disease. Single nucleotide polymorphisms (SNPs) are common genetic variants, numbering about 600 million, and are spread across the genome. GWAS typically follows a case and control model, where DNA and phenotypic information are collected from two large groups: patients with the disease (cases) and matched healthy patients (controls). Their DNA is genotyped using high-throughput microarrays that typically contain one million or more SNPs. These are 'tag' SNPs, present throughout the human genome, are highly correlated with neighbouring SNPs through linkage disequilibrium (LD), the non-random coinheritance of proximal genetic variants[60]. However, the causal variant may not be included in the 'tag' SNPs set, requiring fine mapping to identify the causal variant(s).

Collaborative projects like the HapMap Project, which annotated millions of common variant SNPs to their chromosomal location as the 'tag' SNPs and the 1000 Genomes project, which genotyped over 40 million variants including common, low-frequency and rare variants, provided a comprehensive catalogue genetic variation of the haplotyped landscapes of these SNPs[61–63]. A haplotype is a set of variants in a segment of a chromosome that are inherited together. GWAS have imputed variants from the HapMap Project and the 1000 Genomes

Project, which makes use of linkage disequilibrium, to significantly expand the number of interrogated variants.

GWAS tests millions of associations between individual genetic variants and disease outcomes, which requires multiple testing procedures to control for false positives. Typically, statistical tests are considered significant when the null hypothesis is rejected, and the p-value is customarily below 0.05. However, in GWAS where there are a million SNPs genotyped, using a traditional p-value cut-off of 0.05 will inevitably result in false positives. Therefore, genome-wide significance, to account for multiple testing and false-positive discoveries, is set at a p-value threshold of 5×10^{-8} [64]. The Bonferroni correction can also be applied to adjust the p-value for the number of statistical tests performed[65]. However, this correction may generate too many false negatives and may overlook several loci with important biological implications[66]. An alternative to the Bonferroni correction is to use the false discovery rate (FDR) for GWAS thresholding to provide more candidate genes. FDR controls the expected proportion of false positives among the rejected null hypotheses and is therefore less conservative[66].

The first GWAS for CAD was published in 2007. Three independent groups reported common variants at the 9p21 locus associated with a 20-30% increased risk per copy of the risk allele[67–69]. Since this discovery, large GWAS consortiums have been formed and merged to analyze hundreds of thousands of individuals, including the Myocardial Infarction Genomics Consortium[70], CARDIoGRAM consortium[71], Coronary Artery Disease (C4D) Genetics Consortium[72], and CARDIoGRAMplusC4D[73], among others.

To date, GWAS have identified more than 300 loci associated with CAD at a genome-wide level of significance, explaining less than 25% of disease heritability[74]. The majority of these loci are represented by common variants with a minor allele frequency, MAF >2%, with low to modest

effects (odds ratio 1.05-1.20)[75]. There are over 300 additional loci that are suggestive of CAD risk, with FDR values below 5% ($q<0.05$), which together explain approximately 20-30% of the estimated heritability of CAD[76,77]. These data provide an extended list of candidate causal genes that can serve as a resource for functional studies.

1.4 Translating genetic risk loci to disease pathology

GWASs have been successful in identifying numerous genomic loci significantly associated with CAD. These studies have provided new insights into disease biology, while including the genes that play roles in known pathophysiological pathways in atherosclerosis, such as lipid metabolism, inflammation, and vascular remodeling. However, there are many novel CAD-associated loci with unknown functions that are not fully understood. The challenge is to establish a functional relationship between these loci and disease to provide biological insights. In addition, it is difficult to identify the causal variant, corresponding target genes, and relevant cell types.

The first step to prioritize variants in GWAS-associated regions is to conduct fine-mapping. This approach seeks to determine the genetic variants(s) responsible for a complex trait or disease[78]. However, approximately 90% of the causal variants identified by GWAS are in non-coding regions, including intronic or promoter regions, microRNAs, long non-coding RNAs, and antisense and enhancer regions[79,80]. The other challenge is that neighboring genetic variants are correlated with one another through LD making it hard to pinpoint the causal variants. For example, the 9p21.3 risk locus encompasses many SNPs in tight LD, and the causal variants remain to be confirmed[81,82]. Resources such as Open Target Genetics[83] and HaploReg[84] can help with variant prioritisation by visualising epigenetic features, chromatin states, and association data from large populations of various demographics.

Following the identification of the causal variant, the next step is to prioritize the corresponding causal genes. The most straightforward genes would be the ones affected by coding variants, which could directly disrupt the protein structure. Genes located closest to the variants are typically used as the first criteria for causal gene prediction. However, this closest gene approach is arbitrary to a large extent, relying on a linear representation of the genome. In addition, GWAS loci often contain multiple genes. Still, the majority of variants are in non-coding regions, which suggests regulatory changes that contribute to disease risk. Expression quantitative trait loci (eQTL) mapping is a tool used to understand the function of non-coding variants by assessing the association between variants and variations in gene expression. One comprehensive eQTL resource is the Genotype-Tissue Expression (GTEx) project, which profiled 54 non-diseased tissue sites from nearly 1000 individuals[85–87]. Another resource is the Stockholm-Tartu Atherosclerosis Reverse Network Engineering Task Study (STARNET), which characterizes tissue gene expression in patients with CAD matched to patients without CAD[88]. Once the candidate gene(s) are identified, their functions may not be well established. Extensive functional studies are required to determine the mechanism by which a candidate gene leads to CAD risk.

The pathophysiology of complex diseases often involves multiple cell types. For example, multiple cell types are linked in CAD pathogenesis, including macrophages, endothelial cells, and smooth muscle cells. It is important to study the variants and causal genes of relevant cell types. Again, tools such as GTEx can be used to map eQTL data across different human tissues. Overall, functional studies to elucidate the underlying mechanisms are difficult. For example, the 9p21 locus, although strongly associated with CAD, is located in a region that does not contain any protein-coding genes. The 9p21 locus contains 59 linked SNPs located upstream (100,000

base pairs) of the cycle suppressor genes *CDKN2A* (codes for p16 and p14) and *CDKN2B* (codes for p15) and overlaps with the 3' region of *ANRIL* (antisense non-coding RNA at the ink4 locus non-coding gene)[82]. Follow-up studies have suggested that the effectors of this locus include CDKN2A/CDKN2B[89,90], ANRIL[91,92], and interferon-gamma signaling[93,94]. However, the exact mechanism remains debatable even after nearly 15 years of research[82].

1.5 Aminoacyl tRNA Synthetases

Aminoacyl tRNA synthetases (ARSs) are essential enzymes that are present in eukaryotes, archaea, and bacteria[95]. They are universally required for protein synthesis in all organisms and show a high degree of evolutionary conservation[96]. ARSs catalyse the esterification of a tRNA to its cognate amino acid by matching the anticodon triplet of the tRNA[97]. Aminoacylation is a two-step reaction. In the activation step, ARS uses an ATP molecule to activate an amino acid, forming an aminoacyl-adenylate complex and releasing inorganic pyrophosphate as a by-product[97]. In the transfer step, the activated aminoacyl is transferred from the adenylate to the 3'-end of its cognate tRNA, forming aminoacyl-tRNA[97] (**Figure 1.4**).

ARS typically consists of a catalytic domain and an anticodon-binding domain, with some having an editing domain to prevent the insertion of incorrect amino acids during protein synthesis[98]. They are grouped into two classes based on the conserved architecture of their catalytic domains[99,100]. Class I synthetases are structurally similar and contain a Rossman fold with a five-stranded parallel β-sheet connected by α-helices and two highly conserved motifs ('HIGH' and 'KMSKS')[101]. Class II synthetases are less conserved and have a structurally distinct catalytic core composed of a seven-stranded antiparallel β-sheet with flanking α-helices[102].

The human nuclear genome encodes 37 ARS: 18 charge tRNA in the cytoplasm, 17 charge tRNA in the mitochondria[103], and two function in both compartments (glycyl-tRNA synthetase and lysyl-tRNA synthetase)[104]. Mitochondria-specific ARSs are encoded in the nucleus and imported into the mitochondria via their mitochondrial targeting sequence (MTS) which is cleaved upon entry. Mitochondria-specific ARSs are responsible for the synthesis of 13 proteins essential for oxidative phosphorylation[105].

During evolution, ARS acquired additional domains and insertions to expand their functions beyond their tRNA charging activity. In eukaryotes, there is a multi-tRNA synthetase complex (MSC), made up of nine tRNA synthetases (glutamyl-, prolyl-, isoleucyl-, leucyl-, methionyl-, glutaminyl-, lysyl-, arginyl-, and aspartyl-tRNA synthetases) and three scaffold proteins named ARS-interacting multifunctional proteins: AIMP1/p43, AIMP2/p38, and AIMP3/p18[106,107]. Studies have suggested various roles of MSC, such as enhancing translation efficiency by channelling aminoacyl tRNAs for protein biosynthesis[108], acting as a molecular reservoir to regulate the non-translational activities of ARSs[109], and contributing to subcellular localisation of ARS, as MSC have been found in the nucleus[110], among other potential roles. Another example of eukaryotic cytoplasmic ARS with a non-canonical role is the tyrosyl-tRNA synthetase (YARS1). When split by proteolysis, each fragment can act as a cytokine[111,112]. The N-terminus of YARS1 is released by endothelial cells and has angiogenic and leukocyte chemoattractant properties, similar to interleukin-8 (IL-8)[112,113]. The C-terminal fragment is an EMAP-II-like protein with cytokine properties[113]. An alternative function for mitochondrial ARS was identified in tryptophanyl-tRNA synthetases (WARS2). *WARS2* has been identified as a new gene for angiogenesis, both within and outside the heart[114]. Both cytoplasmic and mitochondrial ARSs can have non-canonical roles, unrelated to protein translation.

ARS have been implicated in the pathogenesis of human diseases. To date, 56 human diseases caused by variants in the ARS genes have been identified[115]. The first ARS mutation associated with human disease was glycyl-tRNA synthetase (*GARS1*) in Charcot-Marie-Tooth (CMT) disease[116]. CMT is a neuromuscular disorder characterised by the degeneration of motor and sensory peripheral nerves, leading to the loss of muscle tissue and touch sensation[116]. To date, variants of seven cytoplasmic ARS genes have been established to cause CMT (*YARS1, MARS1, KARS1, WARS1, AARS1, GARS1, and HARS1*)[115]. The most common disease associated with mitochondrial ARSs is Combined oxidative phosphorylation deficiency (COXPD), a group of multisystem disorders caused by defects in the mitochondrial oxidative phosphorylation system[115]. Eight mitochondrial ARS have been found to cause various forms of COXPD: *MARS2*, *CARS2*, *EARS2*, *VARS2*, *TARS2*, *AARS2*, *FARS2*, *and NARS2*[115]. Mutations in various mitochondrial ARS genes (*AARS2*, *PARS2*, *VARS2*, *YARS2*, *KARS2*, *IARS2*, *and DARS2*) are also associated with mitochondrial cardiomyopathy[117], which is myocardial damage caused by mitochondrial dysfunction.

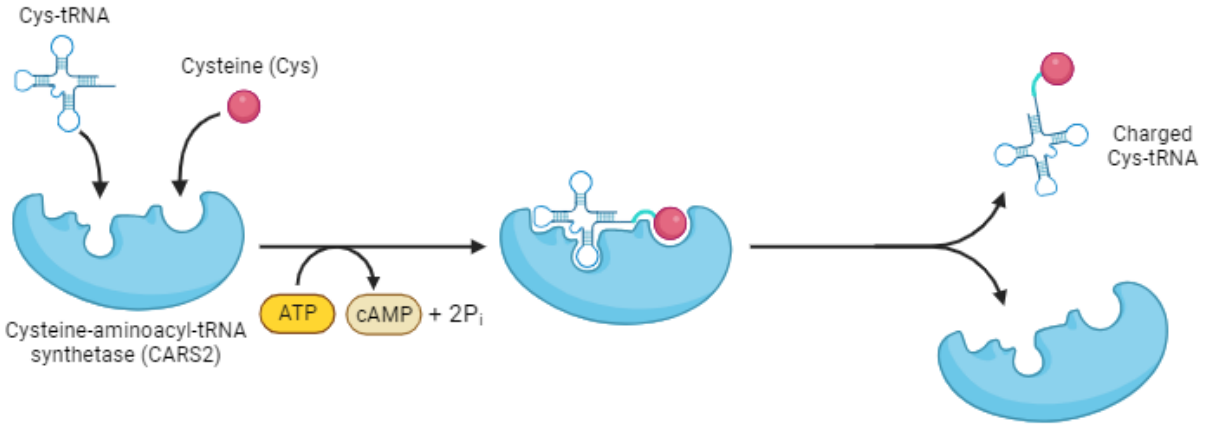

Figure 1.4 Two-step aminoacylation by aminoacyl-tRNA synthetases (ARS). ARS uses an ATP molecule to activate its cognate amino acid to form an aminoacyl-adenylate complex and inorganic pyrophosphate is released as a byproduct. In the transfer step, activated aminoacyl is transferred from the adenylate to the 3'-end of its cognate tRNA to form aminoacyl-tRNA. Created with BioRender.com.

1.6 Cysteinyl t-RNA synthetase (CARS2)

Mitochondrial cysteinyl-tRNA synthetase (CARS2) was first identified with eight other ARS by using known ARSs sequences as queries and searching for mitochondrial targeting sequences[103]. CARS2 is a nuclear-encoded protein involved in mitochondrial translation and belongs to the class I synthetases.

Six cases of CARS2 variants have been described in the literature, which presented developmental delay or neuroregression, cognitive decline, and drug-resistant epilepsy[118–123]. The first disease-gene association of CARS2 was linked to severe progressive myoclonic epilepsy, most resembling myoclonus epilepsy with ragged red fibers (MERRF) syndrome[118]. MERRF syndrome is caused by genetic mutations in the mitochondrial DNA, with a mutation in the tRNA-lysine gene being the most common[124,125]. The homozygous splice-site mutation c.655G>A led to the deletion of 28 amino acids in the conserved surface loop of the cysteinyl-tRNA synthetase protein. It was predicted that this deletion would result in impaired aminoacylation by destabilising the acceptor end hairpin. Coughlin et al. reported a patient with epileptic encephalopathy and combined mitochondrial respiratory chain enzyme deficiency. The patient had two mutations in the highly conserved residues of the functional ligase domain, affecting aminoacylation and leading to decreased mt-tRNA-Cys[119]. Samanta et al. linked the Alpers-Huttenlocher syndrome phenotype, a progressive hepatocerebral mitochondrial DNA depletion syndrome, with CARS2 mutations[120]. Whole exome sequencing revealed compound heterozygous mutations of CARS2 in exons 1 and 5, located in the mitochondrial translocation sequence and cysteinyl-tRNA ligase domain. Hu et al. identified a homozygous mutation on the CARS2 gene causing mitochondrial encephalopathy (progressive myoclonus)[121].

In addition to its role as a cysteinyl tRNA synthetase, CARS2 has also been linked to other functions. In NLT cells, a mouse gonadotropin-releasing hormone (GnRH) cell line, reduced

CARS2 levels reduce neuronal migration, whereas overexpression of CARS2 increases migration[126]. CARS2 also plays a significant role as the principal cysteine persulfide synthase (CPERS) and catalyzes co-translational cysteine polysulfidation, which regulates mitochondrial biogenesis and bioenergetics[127]. In a triple knockout mouse model of cystathionine beta synthase (CBS), mercaptopyruvate sulfurtransferase (3-MST), and cystathionine gamma-lyase (CSE), there were no significance differences between mutant and wild-type mice in terms of reactive persulfide production[128], further implicating CARS2 as the most important CPERS. Additionally, CARS2 plays a role in inflammation-related bone loss through sulfide synthesis. 8-nitroguanosine 3′,5′-cyclic monophosphate (8-nitro-cGMP), a second messenger of NO and ROS, undergoes sulfhydration by hydrogen sulfide, cysteine hydopersulfide (CysSSH), CysSSH-derived persulfides, and polysulfides. Due to CARS2 role as a CPERS, its endogenous production of persulfides is required for the degradation of 8-nitro-cGMP. In mouse osteoblasts with reduced levels of Cars2, there is no degradation of 8-nitro-cGMP leading to inflammation-related bone loss[129]. Moreover, the expression of CARS2 is elevated in human basal-like breast cancer and colorectal cancer tissues, suggesting its involvement as a risk factor for these diseases[130,131].

1.7 Study Rational

For more than a decade, GWAS have identified hundreds of CAD-associated SNPs. However, conducting functional studies to identify the causal loci and elucidate the biological mechanisms involved remains challenging. Only a small number of these associations have been investigated thoroughly. This has resulted in extensive research in functional genomics to identify the causal variants, genes, and mechanisms. The results achieved so far have provided valuable insights

into CAD pathology, and future research will identify new pathways relevant to atherosclerosis to yield therapeutic targets for prevention and treatment.

1.8 Hypothesis

1. The rs61969072 SNP, proximal to *CARS2,* has been reported to be an FDR significant variant[76]. We first hypothesised that *CARS2* was the causal gene.
2. Having demonstrated that altered *CARS2* expression affects inflammation in macrophages, we then hypothesized that CARS2 has a direct or indirect anti-inflammatory function that is protective against atherosclerosis.
3. Finally, we hypothesized that macrophage mitochondrial dysfunction secondary to reduced CARS2 levels elicits a pro-inflammatory response.

1.9 Objectives

This dissertation had two main objectives. First, following the identification of the causal SNP (rs61969072) and gene, we characterize the expression of *CARS2* in macrophages (Chapter 3). The rs61969072 SNP, proximal to *CARS2,* has been reported to be an FDR significant variant[76]. The second aim was to investigate the potential mechanisms through which CARS2 affects inflammation. This is discussed in Chapters 4 and 5. Chapter 4 focuses on the differentially expressed genes in macrophages to determine the signaling pathways affected by CARS2. This allowed us to target candidate signaling pathways that may lead to an increased risk of CAD. Chapter 5 focuses on potential mitochondrial bioenergetics and functions that may in turn affect inflammation due to CARS2's role as a mitochondrial protein.

Chapter 2: Materials and Methods

2.1 eQTL Analysis

Associations between rs61969072 and CARS2 gene expression were determined by querying the public eQTL database from GTEx project (release V7)[85,86]. Expression profiles of rs619169072 in relevant tissues (artery aorta, subcutaneous adipose tissue, artery tibial, and artery coronary) were collected from GTEx. Two other eQTL datasets were also used: the Biobank of Karolinska Endarterectomies (BiKE) study[132] and the Advanced Study of Aortic Pathology (ASAP) study[133]. The BiKE study collected atherosclerotic plaque tissue and blood from patients undergoing carotid endarterectomy and analysed gene expression to identify the pathways linked to plaque instability. As the SNP s61969072 was not present in their array, two SNPs proximal to rs61969072, rs7991766 (LD r^2=0.72), and rs7999702 (LD r^2=0.99) were selected as proxies. The ASAP study collected biopsy specimens (aorta, liver, mammary artery, and carotid atherosclerotic plaque) from patients undergoing aortic valve surgery, and measured gene expression using expression arrays. The SNP rs61969072 was probed in the dataset.

2.2 Cell Culture

THP-1 cells (ATCC, TIB-202), a human monocytic leukaemia cell line, were cultured in RPMI 1640 medium without glucose (Gibco, 11879020), supplemented with 10% FBS, 2 mM L-glutamine, 100 U/mL penicillin, 100 μg/mL streptomycin, 10 mM HEPES, 5.5 mM glucose, 1.0 mM sodium pyruvate and 0.05 mM 2-mercaptoethanol. Monocytes were differentiated into macrophage-like cells (M0) by treatment with 100 nM phorbol-12-myristate 13-acetate (PMA) (Sigma Aldrich, USA, P1585) for 72 h. Macrophages were polarised to pro-inflammatory M1 macrophages by incubation with 20 ng/mL IFN-γ (PeproTech, 300-02) and 100 ng/mL LPS (Sigma, L2630) or with 20 ng/mL IL-4 (PeproTech, 200-04) and 20 ng/mL IL-13 (PeproTech,

200-13) for the anti-inflammatory M2 phenotype. To activate the IL-10 signaling pathway, THP-1 macrophages were treated with 30 ng/mL IL-10 (R&D Systems, Minneapolis, MN, USA, 217-IL) for 15 min before protein harvesting.

Healthy donors on no medication between the ages of 18 and 50 years were recruited for the collection of 35 mL venous blood samples in EDTA tubes. Fresh buffy coats were prepared to isolate and differentiate human monocyte-derived macrophages (HMDMs). Whole blood was diluted with PBS at a 1:2 ratio, gently overlaid on top of a Ficoll-Paque PLUS (GE Healthcare, 17-1440-02), and centrifuged at 900xg for 25 min at room temperature. The buffy coat layer between the plasma and red blood cells was collected and washed with cold PBS 2-4 times to remove platelets. The cells were plated in RPMI 1640 medium without glucose (Gibco, 11879020), supplemented with 10% human serum (Sigma, H4522), 2 mM L-glutamine, 100 U/mL penicillin, and 100 µg/mL streptomycin, and incubated at 37°C for 1.5-2 hours. The cells were then gently washed with warm PBS to remove the lymphocytes and neutrophils. The cells were treated with 25 ng/mL M-CSF (PeproTech, 300-25) for 72 h and refreshed with supplemented medium for the experiments.

Primary human coronary artery smooth muscle cells (HCASMC) (ATCC, PCS-100-021) were grown in Vascular Cell Basal Medium (ATCC PCS100030) supplemented with a Vascular Smooth Muscle Cell Growth Kit (ATCC PCS100042) containing recombinant human (rh) FGFb, rh-insulin, ascorbic acid, L-glutamine, rh-EGF, and 10% FBS.

2.2.1 Co-culture with human coronary artery smooth muscle cells (HCASMC)

THP-1 monocytes ($1.0x10^6$ cells/mL) were plated on cell culture inserts (Falcon, 3.0 um pore size, high pore density, PET track-etched membrane, 12 well format) with 100 nM PMA for 72 h. The cells were transfected with siRNA and incubated in RPMI medium for 48 h. Macrophage-

containing inserts were placed in 12 well plates containing SMCs at the bottom of SMC medium for 48 h. Untreated control THP-1 macrophages and SMCs were maintained in the same medium for the same period of time. The total volume of each well was 2 mL, with 0.5 mL in the insert and 1.5 mL in each well. The cells were harvested separately at the end of the co-culture.

2.3 siRNA Transfection

Cells were seeded onto 12 well plates, at $1.5x10^6$ cells/mL for THP-1 M0 cells and treated with 100 nM PMA for 72 h. CARS2 knockdown using small interfering RNAs (siRNAs) was performed using Lipofectamine RNAiMAX (Life Technologies), with a final siRNA concentration of 16.6 nM. Diluted siRNA and diluted Lipofectamine RNAiMAX was added in a 1:1.25 ratio. The treatment was continued for 72-96 h in a fresh medium. Polarisation of M1 and M2 macrophages with cytokine treatment was performed 48 hours after transfection. The following siRNAs (*Silencer* Select) were purchased from Thermo Fisher Scientific: CARS2 (S140809), MARS2 (S41051), YARS2 (S27340), and the control (Negative Control Number 2 (NT2); 4390846).

2.4 Lentiviral overexpression

The pLVX-CARS2-HA tag plasmid was constructed by subcloning the CARS2-HA tag into the pLVX plasmid using EcoRI restriction sites. Lentivirus particles were generated by co-transfection of the plasmids pLVX-CARS2-HA or pLVX (7.5 μg) with psPAX2 (5 μg) and pMD2.G (2.5 μg) (Addgene) in HEK293FT cells (Thermo Fisher Scientific) using the Lipofectamine 3000 transfection reagent. Lentiviral particles were collected and concentrated in the supernatant 48 h after transfection and stored at -80°C until use. The viral titre was determined in 293FT cells by transducing the cells with various concentrations of lentivirus supplemented with 4 μg/mL polybrene. The next day, 2 μg/mL puromycin was added to the

fresh media to select puromycin-resistant infected cells. THP-1 monocytes were transduced via spinoculation by spinning down the cells (2×10^5 cells/mL in 80 µL of medium) with viral particles. 48 hours post-transduction, the cells were spun down and resuspended in medium supplemented with 2 µg/mL puromycin to select stable cell lines. The cells were grown consistently with 2 µg/mL puromycin for all the passages. Transduced THP-1 monocytes were seeded in 12 well plates and treated with 100 nM PMA for 72 h for differentiation into macrophages.

2.5 Luminex Multiplex Assay

THP-1 monocytes, at $1.5x10^6$ cells/mL, were differentiated into macrophages and transfected with siRNA. After 48 h of transfection, the culture medium was replaced. The supernatant was collected 96 h post-transfection and stored at -80°C until analysis. The seven analytes were quantified using a Human Magnetic Luminex Assay (7-Plex) LXSAHM-07 (R&D Systems). The analytes were tumour necrosis factor-α (TNF-α), interleukins IL-1β/IL-10/IL-13, macrophage colony-stimulating factor (M-CSF), and chemokine CCL3. A customised multiplex kit was used, according to the manufacturer's instructions. A Luminex 200 RUO System was used to obtain results.

2.6 Reverse transcription and quantitative real-time PCR

Total RNA was isolated from all samples using the High Pure RNA Isolation Kit (Roche) and Direct-zol RNA Kits (Zymo Research) following the manufacturer's instructions. cDNA was generated using the Transcriptor First Strand cDNA Synthesis Kit (Roche), with 500 ng – 1 µg of RNA as the template. Quantitative PCR was performed using SYBR Green I Master Mix (Roche) and run on a LightCycler 480 Instrument II (Roche). The PCR protocol was 95°C for 5 min, followed by 45 touchdown cycles at 95°C for 10 s, 65°C to 55°C for 20 s (0.5°C step size

down every cycle), and 72°C for 30 s. Signal Recognition Particle 14 (*SRP14*) was used as the reference gene in all qPCR experiments.

	Primer Sequence	
Gene Name	Forward (5'-3')	Reverse (3'-5')
CARS2	CACTGCTCGCACTGATGAA	ACAAGTATGGCAAATTGGTCG
MARS2	GCCCTGGTCAACTACCTCAC	TGCCGAAGGAGAAAGTAGCG
YARS2	TGCACTGGAGGTCATGTCTG	GCCAACCCTTCAGAGGTCTT
CARS1	GAGGTGTTGCTGGAAGAAGC	CTGCAGAGATGCTCAGGTCA
SRP14	ACTTCCGGCTCTCACTGCTA	TCAAAGCCCTCCACAGTACC
*TNF*α	ACTTTGGAGTGATCGGCCC	TCTGGTAGGAGACGGCGAT
*IL1*β	CTGTCCTGCGTGTTGAAAGA	CCCTAGGGATTGAGTCCACA
IL6	ATCTGGATTCAATGAGGAGACTTG	GGAACTGGATCAGGACTTTTGTACT
CSF1	GAGACCTCGTGCCAAATTACA	GGCCTTGTCATGCTCTTCAT
IL10	TACGGCGCTGTCATCGATTT	TAGAGTCGCCACCCTGATGT
CCL22	CCTGGGCTGAGACATACAGG	GACGTAATCACGGCAGCAGA
IL8	CAAGAGCCAGGAAGAAACCACC	TGCACCCAGTTTTCCTTGGGG
CXCL1	ATTCACCCCAAGAACATCCA	CTTCCTCCTCCCTTCTGGTC
CCL2	ATGAAAGTCTCTGCCGCCCT	AGGTGGTCCATGGAATCCTGA
FN1	CCTGAAGCCTGGTGTGGTAT	CATCTCCCTCCTCACTCAGC
MMP1	AGGGGAGATCATCGGGACAA	GGCTGGACAGGATTTTGGGA
ACTA2	GGAATCCTGTGAAGCAGCTC	CTTTTCCATGTCGTCCCAGT
TAGLN	AACAGCCTGTACCCTGATGG	GCCCATCATTCTTGGTCACT
COL1A2	CCTCTGGAGAGGCTGGTACT	TTGTGTCCGGGTTGACCATC
COL13A1	TCCTGGTCTGCAAGGAATGC	CACCTCTCTCACCAGGGCTA

	Primer Sequence	
Gene Name	Forward (5'-3')	Reverse (3'-5')
OLR1	AAGGACCAGCCTGATGAGAA	CTTCCGAGCAAGGGTTTCTA
SDHB	AGAGCGTGAGAAACTGGACG	ATGGTGTGGCAGCGGTATAG
UQCRC2	TTGCTGCGTCTTACATCCAG	AGCTACTTCCCAACGACGAA
ATP5F1A	CTGGCATTAAGGCTGTGGAT	ACTGGGCAACAGTGGATCTC
COX5A	TCAGTTCGCTGCTATTCCCA	ATTTAACCGTCTGCATGCCC
NDUFB8	CCTAGGACCCCAGAAGAACG	TCACCCCAGTTCAACCTCAG
SRP14	ACTTCCGGCTCTCACTGCTA	TCAAAGCCCTCCACAGTACC

2.7 Microarray

After RNA isolation from *CARS2* knockdown THP-1 macrophages, RNA quality was assessed by 260/280 and 260/230 absorption ratios using a Nanodrop spectrophotometer (Thermo Fisher). The RNA samples were processed using Affymetrix Human Gene 2.0 ST expression arrays at the Center for Applied Genomics, The Hospital for Sick Children (Toronto). Data were analysed using Transcriptome Analysis Console (TAC) software (Affymetrix). Genes that were up- or down-regulated more than 1.5-fold at a significance level of $p < 0.05$ were considered differentially expressed. Further analysis was done with Ingenuity Pathway Analysis (IPA) (Qiagen) to analyze Canonical Pathways, Upstream Analysis and Toxicity Lists. The results were deposited in the Gene Expression Omnibus database (GSE168863).

2.8 Inflammatory Cytokines and Receptors Array by RT2 Profiler PCR array

One microgram of isolated RNA was used to synthesise complementary DNA (cDNA) using the Transcriptor First Strand cDNA Synthesis Kit (Roche). Following RNA isolation and reverse transcription, cDNA was loaded onto an Inflammatory Cytokine and Receptor RT2 Profiler Array (PAHS-011ZA) (Qiagen) according to the manufacturer's instructions. Gene expression was normalised to the average of four housekeeping genes, *ACTB*, *B2M*, *GAPDH*, and *HPRT1*. *RPLP0* was not included because of its inconsistent melting curves. Fold changes were calculated using the $2^{-\Delta\Delta Ct}$ method.

2.9 Western blotting

Protein samples were harvested using RIPA buffer containing a cOmplete Protease Inhibitor Cocktail (Roche) and PhosStop Phosphatase Inhibitor cocktail (Roche). Protein concentrations were determined using a Pierce Bicinchoninic Acid (BCA) protein assay kit (Thermo Fisher Scientific). 10 -15 ug of protein were loaded onto an 8% SDS-PAGE gel and run under reducing

conditions. The samples were then transferred onto a nitrocellulose membrane (Bio-Rad) for 1 h at a constant voltage of 90 V. The blot was blocked for 1 h at room temperature using Odyssey blocking buffer (Licor) or 5% Bovine Serum Albumin (BSA) in Tris-Buffered Saline (TBS). The membranes were incubated with the following primary antibodies overnight at 4°C: CARS2 (Novus, NBP2-32597), STAT3 (Cell Signaling Technologies, 79D7), and pSTAT3 (Tyr705) (Cell Signaling M9C6). As a loading control, all membranes were probed with Beta Tubulin (GeneTex, GTX11307, 1:2000 dilution).

Protein expression in the PKR signaling pathway was assessed as follows: mTOR (Cell Signaling Technology, 2983P), p-mTOR (Ser2448) (Cell Signaling Technology, 5536P), STAT1 (Cell Signaling Technology, 9172S), pSTAT1 (Tyr701) (Santa Cruz Biotechnology, sc-8394), NF-κB p65 (Cell Signaling Technology, 8242S), pNF-κB p65 (Ser 536) (Cell Signaling Technology, 3036S), AMPK (Cell Signaling Technology, 2793S), pAMPK (Thr172) (Cell Signaling Technology, 2535S), ERK1/2 (Cell Signaling Technology, 9107S), and pERK1/2 (Thr202/Tyr204) (Cell Signaling Technology, 4370S). Beta Tubulin (GeneTex, GTX11307) was used as a housekeeping protein.

To assess the structural components of oxidative phosphorylation (OXPHOS), MTCO1 (Thermo Fisher, 1D6E1A8) and a mixture of monoclonal antibodies, Total OXPHOS Human WB Antibody cocktail were used: NDUFB8 of complex I, SDHB subunit of complex II, and UQCRC2 subunit of complex III (Abcam, ab110411), diluted 1:1000. TOMM20 (Abcam, ab56783) was used to assess the mitochondrial mass and as a mitochondrial housekeeping protein.

IRDye secondary antibodies (LI-COR) were used (1:1000 dilution) and the membranes were visualised using the LI-COR Odyssey imaging system.

2.9.1 Subcellular Fractionation

Subcellular fractionation was performed according to a modified protocol[134]. All steps were performed on ice or at 4°C. The cells were washed once with cold PBS, gently scraped in 500 µL PBS, and centrifuged at 300x g for 4 min. Cells were resuspended in 3x volume (based on cell pellet size) of hypotonic buffer (20 mM Tris-HCl (pH 7.4), 10 mM KCl, 2 mM MgCl2, 1 mM EGTA, 0.5 mM DTT, cOmplete Protease Inhibitor Cocktail (Roche), and PhosStop Phosphatase Inhibitor cocktail (Roche)). After 5 min of cell swelling, cells were lysed by adding NP-40 at a final concentration of 0.1% for 3 min and mixed thoroughly. The lysed cells were centrifuged at 1000x g for 10 min. The supernatant was collected, centrifuged at 15,000 g for 3 min, and stored as the cytoplasmic fraction. The cell pellet, containing the nuclei, was resuspended in 3x volume of isotonic buffer (20 mM Tris-HCl (pH 7.4), 150 mM KCl, 2 mM MgCl2, 1 mM EGTA, 0.5 mM DTT, cOmplete Protease Inhibitor Cocktail (Roche), and PhosStop Phosphatase Inhibitor cocktail (Roche)) and a final concentration of 0.1% NP-40. The suspension was constantly rotated for 10 min and then centrifuged at 1000xg for 5 min. The cell pellet was washed twice with PBS and centrifuged at 500 g for 5 min. The remaining cell pellet was incubated with 50 µL ice-cold RIPA buffer for 30 min on ice and centrifuged at 14,000 × g for 15 min. Protein concentrations were determined using a Pierce Bicinchoninic Acid (BCA) protein assay kit (Thermo Fisher Scientific).

2.10 Ingenuity Pathway Analysis

The differential gene expression dataset from the RT2 Profiler PCR array was imported into the Ingenuity Pathway Analysis Tool (version 84978992; Ingenuity Systems, QIAGEN)[135]. Core Analysis were conducted to include canonical pathways, upstream regulators, diseases and functions, regulatory effects, and molecular networks. The analysis cut-off was set for genes with

a fold change>1.5 or <-1.5 and p-value <0.05. The right-tailed Fisher's Exact Test was used to calculate the p-value, which is presented as the negative logarithm of the p-value. For the canonical pathway, disease and function, and tox list analysis, the -log(p-value) > 1.3 was taken as the threshold and a z-score of >2 and <-2 was defined as the threshold of significant activation and inhibition, respectively. The ratio was calculated based on the extent of the overlap of the dataset molecules with the pathway. For upstream regulators, the p-value for overlap was calculated to identify regulators that could explain observed changes in gene expression. The p-value of the overlap measures whether there is a statistically significant overlap between the dataset genes and genes regulated by a regulator. It is calculated using Fisher's Exact test and has a threshold of -log(p-value) > 1.3. For network analysis, the score was the negative exponent of right-tailed Fisher's exact test results. The greater the number of network-eligible molecules, the higher the score (lower the p-value).

2.11 RelA Luciferase Cells

THP-1 NF-κBLuc-2 (TIB-202-NFkB-LUC2, ATCC) human monocytes were cultured according to the manufacturer's protocol. The firefly luciferase gene, luc2, was placed under the control of the NF-κB promoter. NF-κB activation was measured using a luciferase luminescence assay. Monocytes were seeded in 24 well plates at $1.5x10^6$ cells/mL and differentiated into macrophages with 100 nM PMA for 72 h. Cells were transfected with *CARS2* or control siRNA for 96 h. Prior to the assay, the macrophages were treated with 100 ng/mL LPS, 20 ng/mL TNF-α, or 30 ng/mL IL-10 for 6 h. A $1/10^{th}$ volume of alamarBlue reagent (DAL1025; Thermo Fisher Scientific) was added directly to the culture medium. After one hour of incubation, alamarBlue was added to untreated wells as a background. The fluorescence was read at an excitation wavelength of 555 nm and an emission wavelength of 596 nm using a Cytation 5 Cell Imaging

Multimode Reader (BioTek). A Dual-Luciferase Reporter Assay System (E1910, Promega) was used according to the manufacturer's protocol. Cells were lysed with 1X Passive Lysis buffer for 15 min at room temperature and centrifuged at 13000 rpm for 2 min. Ten microlitres was loaded into a white 96-well plate for the assay. A Luciferase Assay Reagent (LARII) was prepared to generate a luminescent signal and was loaded into the injectors. Luminescence analysis was performed by measuring the firefly signals using a GLOMAX Microplate Luminometer (Promega).

2.12 Metabolic Cell Phenotype Analysis (Seahorse)

THP-1 monocytes ($3.5x10^4$ cells/well) were plated on an Agilent Seahorse XFp Cell Culture Miniplate (Agilent) and differentiated into macrophages for three days before transfection with CARS2 siRNA for 72 h. HEK293T cells (2×10^4 cells/mL) were plated in a 12-well plate and transfected on the following day. Prior to the assay, transfected HEK293T cells were lifted and plated onto a miniplate ($3.5x10^4$ cells/well). Cell culture media were added to empty wells on the perimeter to help with the evaporation of the media.

The day before the test, a Seahorse XFp Sensor Cartridge (Agilent) was hydrated by adding 200 µL of Seahorse XF Calibrant (Agilent) to a utility plate. The Sensor Cartridge was submerged in the calibrant for 24 h at 37°C in a humidified non-CO2 incubator. The assay medium was prepared by supplementing Agilent Seahorse XF Base Medium (Agilent) with 4.5 g/L glucose, 2 mM l-glutamine and 1 mM sodium pyruvate. The pH was adjusted to 7.44 with 5M NaOH and the medium was filter-sterilised using a 0.2 µm sterile membrane filter and stored at 4°C.

On the day of the assay, the cells were washed with the prepared assay medium by removing 60 µL of medium from the wells, leaving 20 µL, and adding 180 µL of the medium. The washing

step was repeated twice. The medium was replaced with a final volume of 160 µL and the cells were incubated for 1 h in a humidified, non-CO2 incubator.

10x stock solutions of carbonyl cyanide p-trifluoromethoxyphenylhydrazone (FCCP) (5 µM) and Oligomycin A (10 µM) from the Agilent Seahorse XF Cell Energy Phenotype Test Kit (Agilent Technologies) was prepared in the media. The diluted compounds were added to Port A using a repeater (20 µL/port). The two stressors were injected simultaneously: FCCP depolarised the mitochondrial membrane, driving oxygen consumption rates (OCR) higher by attempting to restore the membrane potential, and Oligomycin A inhibited ATP production in the mitochondria, increasing the rate of glycolysis (ECAR) to meet energy demands. Hoechst 33342 dye (Thermo Fisher) was added to the medium (2 µL/mL) before addition to Port C (25 µL/port). The cartridge and utility plate were transferred to an XFe96/XF96 instrument (Agilent) for calibration. Once the calibration was complete, the cell culture plate was loaded into the instrument to begin the assay. When the assay was completed, the number of cells per well was counted using a Cytation 5 Cell Imaging Multimode Reader (BioTek). The Agilent Seahorse XF Cell Energy Phenotype Test Report Generator was downloaded from Agilent to calculate the baseline phenotype, stress phenotype, and metabolic potential of each group. Data were analyzed through Wave 2.6.1 Software (Agilent Technologies)

2.13 Mitochondrial Membrane Potential (TMRE)

Mitochondrial membrane potential was assessed using tetramethylrhodamine ethyl ester (TMRE), a membrane-potential-dependent fluorescent dye. THP-1 macrophages ($1.0x10^6$ cells/mL) were plated in 24 well plate and transfected with siRNAs for 96 h. Two wells were left empty for blank readings and two wells were plated with THP-1 macrophages and left untreated as the baseline. Negative control cells were treated with carbonyl cyanide m-chlorophenyl

hydrazone (CCCP) (Tocris Bioscience, 0452) at a final concentration of 50 μM for 15 min at 37°C. CCCP is a mitochondrial uncoupling agent that disrupts inner membrane potential. Cells were stained with 200 nM TMRE (Biotium, 70005) and 100 nM MitoTracker Green (Thermo Fisher, M7514) for 30 min at 37°C in the dark. MitoTracker Green localizes to the mitochondria independently of membrane potential and reflects the number of mitochondria in a cell, which was used to normalize the fluorescence values. The cells were washed thrice with warm PBS, and 500 μL of PBS was added to the plate. The total fluorescence of TMRE (Ex/Em = 550 nm/580 nm) and MitoTracker Green (Ex/Em:490 nm/ 516 nm) was measured using a microplate reader (BioTek).

Blank well values were subtracted from all wells to account for the non-specific binding of the dye to the polystyrene plate. The percentage of fluorescence signal was calculated relative to the baseline of untreated cells and normalised to MitoTracker Green.

2.14 Measurement of Reactive Oxygen Species (ROS)

To measure reactive oxygen species levels in live cell samples, the cell-permeant dye 2′,7′-dichlorodihydrofluorescein diacetate (DCFDA, also known as H2DCFDA, DCFH-DA, and DCFH) was used. DCFDA is a fluorogenic dye that measures cellular hydroxyl, peroxyl, and ROS activity. In the presence of ROS, DCFDA is oxidised to the highly fluorescent 2',7'-dichlorofluorescein (DCF).

THP-1 macrophages ($5x10^5$ cells/well) were plated in a 24-well plate and transfected with *CARS2* siRNA for 96 h. Two wells were left empty for blank readings and two wells were plated with THP-1 macrophages and left untreated as the baseline. Following transfection, the cells were stained with 25 μM DCFDA (Thermo Fisher, D399) for 30 min in the dark at 37°C, and then with 1 μM Hoechst for 5 min. The plate was washed three times with PBS before the

addition of PBS (0.5 mL). The total fluorescence of DCF (ex/em,495 nm/529 nm) and Hoechst (ex/em:350 nm/ 461 nm) was measured using a microplate reader (BioTek).

2.15 Mitochondrial DNA (mtDNA) Quantification

Genomic DNA, including mtDNA, was isolated using a modified protocol[136]. The protocol used three detergent-containing buffers and differential centrifugation to harvest DNA from the cytosolic, mitochondrial, and nuclear fractions and whole cells. Following cell fractionation, instead of further extracting/cleaning the DNA fractions, the DNA was diluted in nuclease-free water at a 1:25 ratio.

The relative abundance of mtDNA and nuclear DNA (nDNA) in the total genomic DNA was quantified using qPCR. qPCR was performed using SYBR Green I Master Mix (Roche) and a LightCycler 480 Instrument II (Roche). 2.5 µL of diluted DNA from the whole and cytosolic fractions was loaded into the wells with 7.5 µL of Master Mix (1X SYBR Green (Roche Diagnostics), 5 µM forward and reverse primer). Human mitochondrial genes (*MT-CO1*, *MT-CO3*, and *DLoop*) and the nuclear-encoded gene (*SLCO2B1*) were amplified. mtDNA abundance relative to nDNA was expressed using the ΔΔCt method following a modified protocol[136].

The concentrations of the protein fractions harvested, along with the genomic DNA, were quantified. Fraction purity was assessed by western blotting of the protein fractions. Antibodies against Beta Tubulin (cytosolic extract), CARS2 (mitochondrial extract), and PARP (nuclear extract) were used to assess purity.

	Primer Sequence	
Gene Name	Forward (5'-3')	Reverse (3'-5')
MT-CO1	TTTTCACCGTAGGTGGCCTG	CCGGATAGGCCGAGAAAGTG
MT-CO3	TCACCCCGCTAAATCCCCTA	TGACGTGAAGTCCGTGGAAG
ND1	CACCTCTAGCCTAGCCGTTT	TTCAGGGGAGAGTGCGTCAT
ND5	CCTGACAAGCGCCTATAGCA	GGATTGTGCGGTGTGTGATG
*SRP14**	GCAGCACAGTAAAGGGCATA	CAGCACAGACCAATTAGCCAA

SLCO2B1	GCGCACTCACTGATTCCTAC	ACATTATCCACACTGCCCCA
Dloop	CATAAAGCCTAAATAGCCCACACG	CCGTGAGTGGTTAATAGGGTGATA

Dloop[137]

2.16 Statistical Analysis

The results are presented as the mean ± standard deviation (SD) for independent experiments. Significant differences were assessed by one-way ANOVA with significance set at $p<0.05$ (* $p < 0.05$, ** $p < 0.01$, *** $p < 0.001$, **** $p < 0.0001$) unless otherwise specified. Figures were produced and analyses were performed using GraphPad Prism software.

Chapter 3: A novel anti-inflammatory role links the CARS2 locus to protection from coronary artery disease.

3.1 Introduction

The heritability of CAD is well established, with studies estimating heritability between 40-60%[48]. GWAS have identified significant associations between hundreds of loci and CAD, including current drug targets and known genes, as well as many novel genes[138]. Identifying the causal genes that connect genetic variants to disease risk will reveal new mechanisms and therapeutic targets for CAD.

The joint association analysis of the CARDIoGRAMPlusC4D data using the 1000 Genomes Project imputation identified 202 FDR variants (q-value < 0.05) in 129 loci[76]. Seven independent CAD-associated signals are located on chromosome 13q34. Among these, rs61969072(T>G) is located in an intergenic region proximal to *ING1* (inhibitor of growth family member 1), CARKD (NAD(P)HX dehydratase), and *CARS2* (cysteine tRNA synthetase, mitochondrial). The common allele (T) (MAF T = 0.82 (ALFA)[139] is associated with protection from CAD (beta = −0.0584)[76]. eQTL analysis revealed increased *CARS2* expression in carriers of the protective T allele in various human tissues, suggesting that CARS2 is a candidate causal gene.

CARS2 encodes a mitochondrial cysteinyl-tRNA synthetase, which plays a key role in mitochondrial translation by charging tRNA with cysteine. These studies aimed to characterise CARS2 expression in macrophages, a cell type that plays an important role in plaque progression.

3.2 Results

3.2.1 rs61969072 is strongly associated with *CARS2* expression.

To investigate genes influenced by rs61969072 and linked SNPs, expression quantitative trait locus (eQTL) analysis was performed. Data from the Genotype-Tissue Expression (GTEx) project revealed that rs61969072 is associated with *CARS2* expression in various human tissues, including the aorta and subcutaneous tissues (**Table 3.1**). The risk allele (G), which is associated with increased susceptibility to CAD, correlates with lower CARS2 expression. In the Biobank of Karolinska Endarterectomies (BiKE) database, two SNPs linked to rs61969072 were associated with *CARS2* mRNA expression in plaque and PBMC samples from 125 individuals. These risk alleles were associated with lower CARS2 expression (**Figure 3.1**). The proximal genes *ING1* and *CARKD* were not associated with the two linked SNPs in plaques, and only *ING1* was significantly associated with SNPs in the PBMCs. Finally, in the Advanced Study of Aortic Pathology (ASAP), there was a strong association between the SNP and CARS2 expression in liver and heart tissues (**Figure 3.2**). *ING1* and *CARKD* were not significantly associated with SNP in the ASAP data. Taken together, these data suggest that *CARS2* is the causal gene identified in this GWAS CAD-associated locus.

Table 3.1 GTEx eQTL data. eQTL analysis of the top gene associations with rs61969072-G based on the GTEx dataset (release 7). rs61969072-G was significantly associated with decreased *CARS2* gene expression in artery aorta, subcutaneous adipose tissue, and artery tibial. The normalised effect size (NES) of the eQTLs was calculated as the effect of the alternative allele (effect allele) relative to that of the reference allele. Genotype-Tissue Expression (GTEx); Expression quantitative trait loci (eQTL)

rs61969072T>G	***CARS2***		***ING1***		***CARKD***	
Tissue	**P-value**	**NES**	**P-value**	**NES**	**P-value**	**NES**
Artery – Aorta	1.70E-07	-0.31	0.49	-0.047	0.58	0.55
Adipose – Subcutaneous	1.80E-14	-0.35	0.021	-0.13	0.000028	-1.8
Artery – Tibial	1.10E-15	-0.35	0.09	-0.081	0.44	0.025
Artery – Coronary	0.000055	-0.35	0.24	-0.14	0.26	-0.1

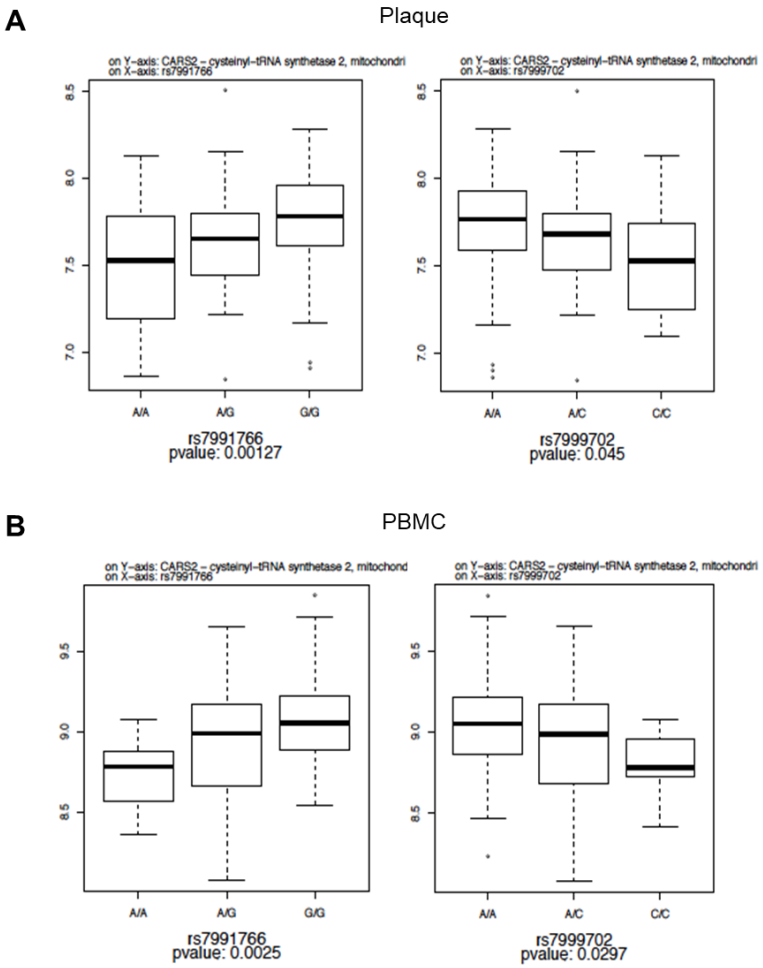

Figure 3.1 The proxy SNPs, rs7991766 and rs7999702, were associated with CARS2 expression. Two SNPs proximal to rs61969072, rs7991766 (LD r^2=0.72) and rs7999702 (LD r^2=0.99), were associated with *CARS2* expression in **(A)** plaque and **(B)** peripheral blood mononuclear cells (PBMC) in samples from the BiKE Database. The alternative allele was associated with decreased *CARS2* expression and increased CAD (rs7991766-A and rs7999702-C). Linkage disequilibrium (LD); Biobank of Karolinska Endarterectomy (BiKE).

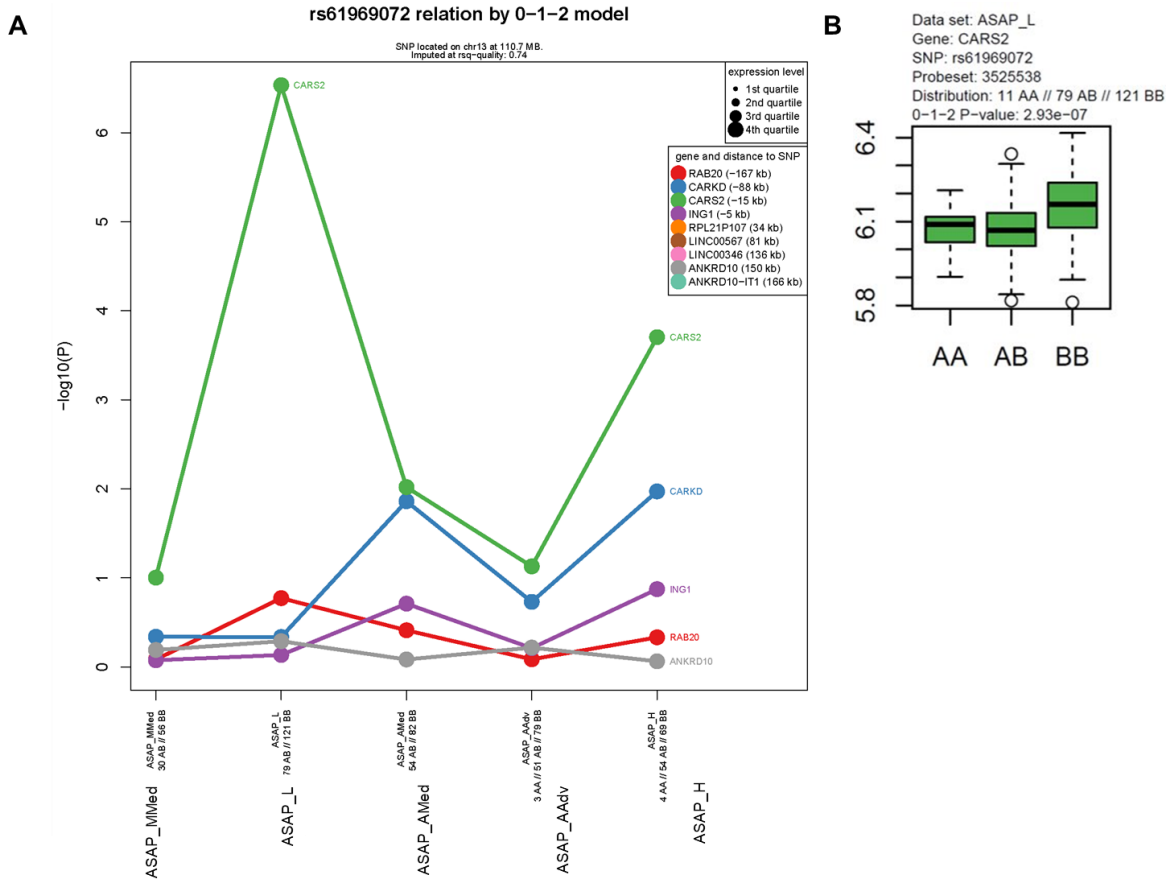

Figure 3.2 Tissue-specific associations between rs61969072 and proximal genes from the ASAP study. (A) The y-axis shows the calculated -log10(P) value for the association between genotype and expression level. The x-axis shows the tissues: medial mammary artery tissue (MMed), liver samples (L), medial aortic tissue (AMed), adventitial aortic tissue (AAdv) and heart tissues (H). The rs6196072 SNP and *CARS2* expression are associated with liver, heart, and medial aortic tissues. **(B)** The BB genotype corresponds to the protective allele (T) and is associated with increased *CARS2* expression. Advanced Study of Aortic Pathology (ASAP).

3.2.2 CARS2 expression is decreased in pro-inflammatory M1 macrophages.

The BioGPS transcriptome database indicated the highest *CARS2* gene expression in monocytes, a precursor of macrophages, which is highly relevant in atherosclerosis (**Figure 3.3**)[140,141]. As shown in **Figure 3.4**, *CARS2* expression was significantly reduced in pro-inflammatory M1 macrophages compared to both naïve THP-1 macrophages (M0) and Human Monocyte-Derived Macrophages (HMDM). CARS2 protein expression was significantly lower in M1 macrophages than that in naïve and M2 macrophages. Next, *CARS2* expression was examined during differentiation (Monocyte to M0) and polarisation (M0 to M1 or M2) (**Figure 3.5**). *CARS2* expression initially decreased and then gradually increased during differentiation into macrophages. A similar initial decreasing trend was observed in protein expression, which continued to decrease gradually. When polarised into M1 macrophages, a rapid and sustained decrease in *CARS2* expression was observed. In contrast, in M2 anti-inflammatory macrophages, *CARS2* expression decreased slightly but then increased. Interestingly, CARS2 protein rapidly increased during M1 polarisation, before consistently decreasing over time. In M2 macrophages, CARS2 expression gradually increased.

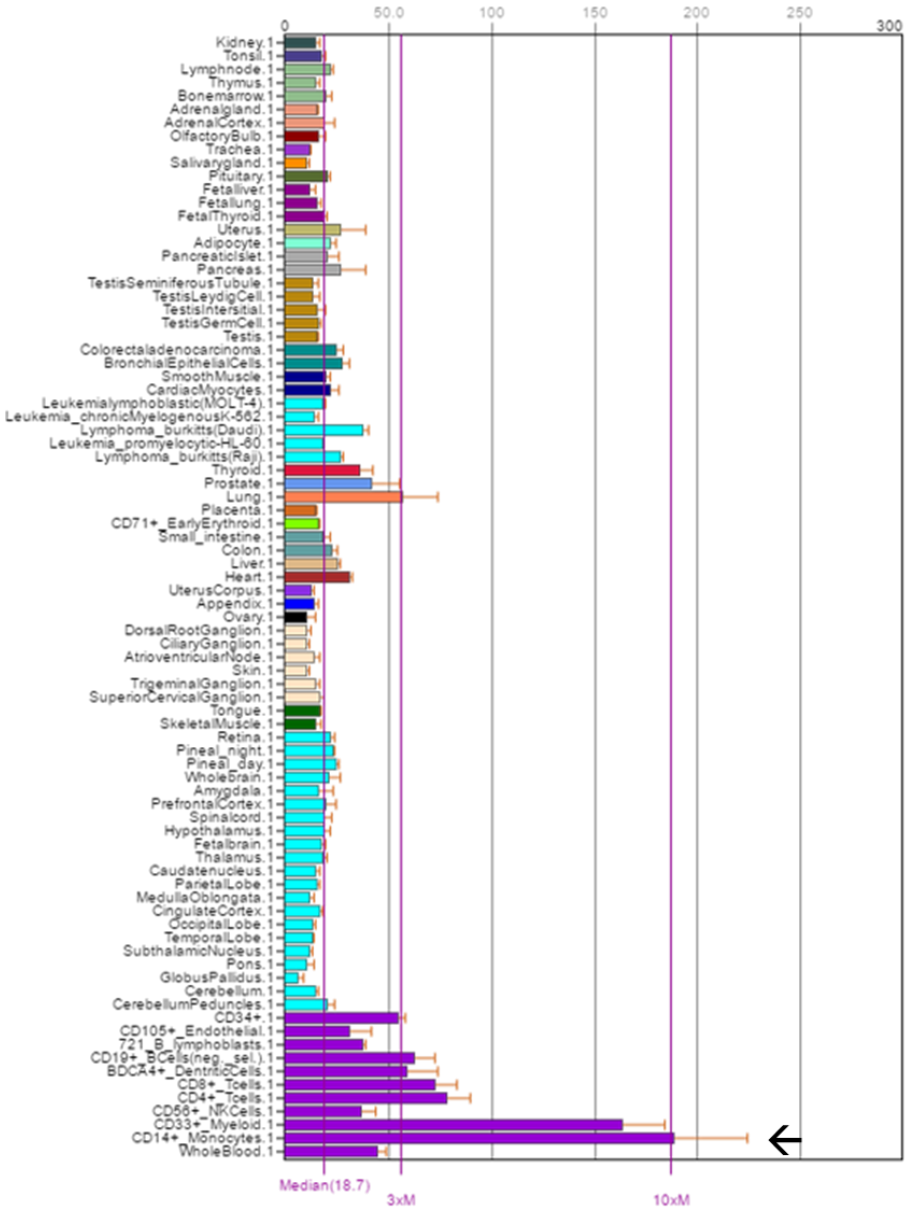

Figure 3.3 Tissue-specific pattern of CARS2 mRNA expression. Gene expression charts were produced in BioGPS (http://biogps.org/downloads/) using the GeneAtlas U133A gcrma dataset. Arrow indicates CD14+ monocytes.

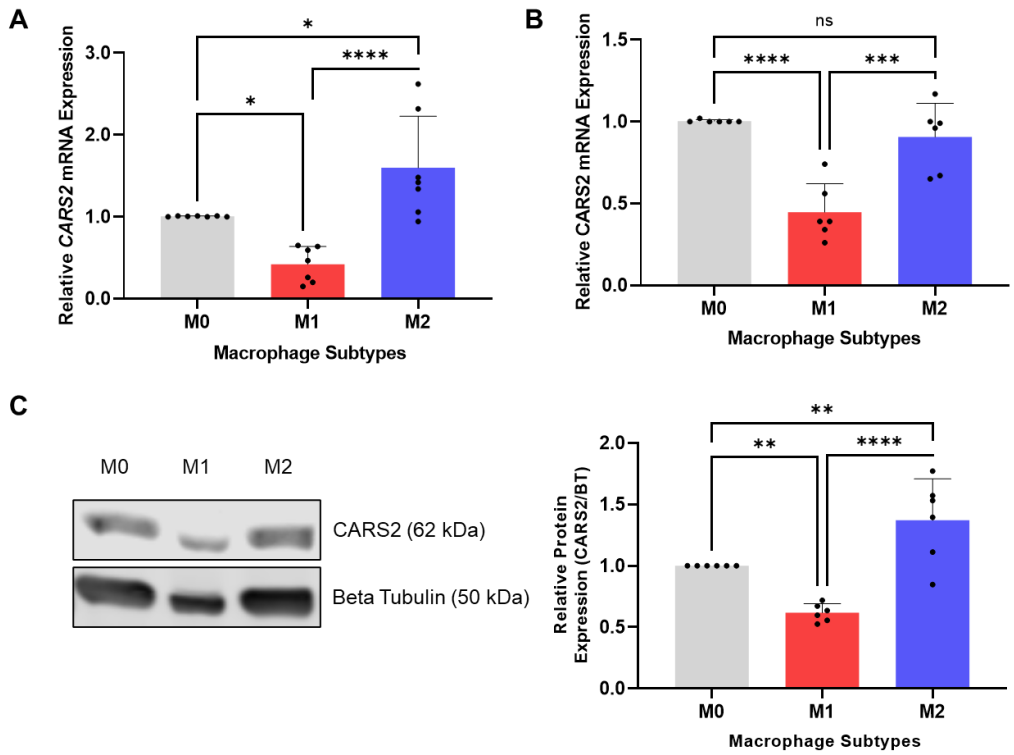

Figure 3.4 Decreased CARS2 expression in pro-inflammatory M1 macrophages. *CARS2* expression, normalised to *SRP14* expression, was plotted as a fold-change in mRNA expression relative to M0 macrophages (M0 = 1) in **(A)** THP-1 macrophages and **(B)** HMDMs. Data are presented as the mean ± SD for n=7 (THP-1) and n=6 (HMDM). **(C)** CARS2/Beta Tubulin protein expression was quantified in macrophage subsets after 72 h of cytokine treatment. Data are presented as the mean ± SD (n=6). (Ordinary one-way ANOVA, uncorrected Fisher's LSD) * $p<0.05$, ** $p< 0.01$, *** $p<0.001$, **** $p < 0.0001$.

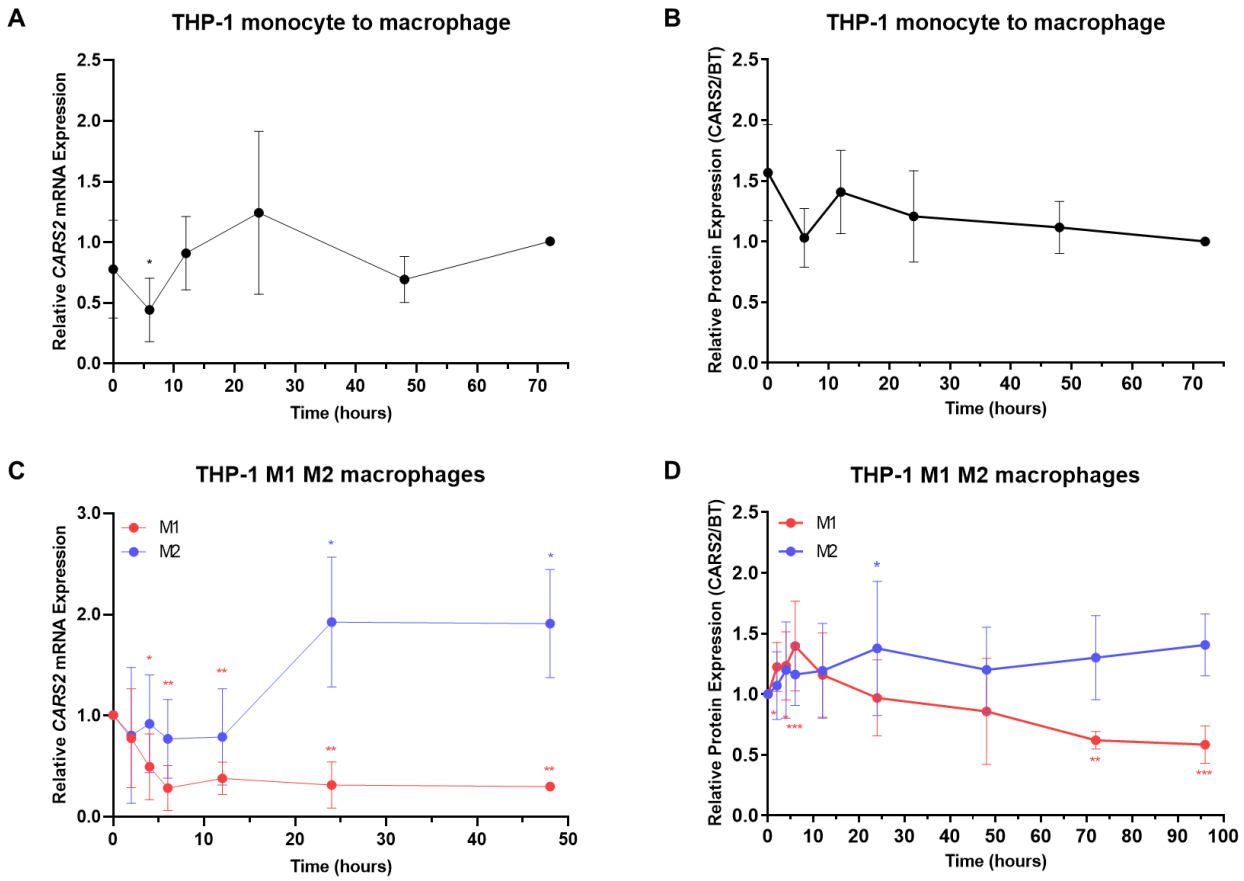

Figure 3.5 Rapid decrease in CARS2 expression following polarisation to M1 macrophages. *CARS2* gene expression during differentiation of **(A)** THP-1 monocytes to macrophages (M0) and further polarisation to **(C)** M1 pro-inflammatory and M2 anti-inflammatory macrophages over 72 h. *CARS2* gene expression was graphed as a fold change in mRNA expression compared to M0 macrophages (M0=1). *SRP14* was used as an internal standard. The data represent the mean ± SD for n=4 (monocyte to M0), n=4 (M1, M2), and n=3 (48 h M1, M2). Protein expression during **(B)** differentiation into macrophages and **(D)** polarisation after 96 h. CARS2/Beta Tubulin protein expression was quantified. Western blotting results are representative of three independent experiments. Data are presented as the mean ± SD for n=3 (monocyte to M0), n=7 (M1, M2), n=6 (48 h M1, M2), and n=3 (96h M1, M2). (Ordinary one-way ANOVA, uncorrected Fisher's LSD) * $p<0.05$; ** $p< 0.01$; *** $p<0.001$ (A, B) vs. 72 h and (C, D) vs. 0 h.

3.2.3 Reduced levels of CARS2 lead to increased pro-inflammatory cytokine expression.

These results suggested that *CARS2* plays contrasting roles in M1 and M2 macrophages, possibly favouring an anti-inflammatory phenotype. This was tested by *CARS2* siRNA-mediated knockdown in THP-1 macrophages and HMDMs before polarisation. This was followed by gene expression analysis of pro-inflammatory (*TNFα*, *IL-1β*, *IL6, and MCSF*) and anti-inflammatory markers (*IL10* and *CCL22*). Compared to the control siRNA, CARS2 suppression significantly increased pro-inflammatory cytokine expression (**Figure 3.6A**). In similarly treated HMDMs, changes in the expression of IL-6 and TNF-α were directionally consistent but did not reach significance. This may be explained, in part, by the reduced knockdown efficiencies of HMDMs (58%) compared to THP-1s (81%). Consistent with the knockdown data, overexpression of CARS2 in THP-1 macrophages via lentiviral delivery resulted in reduced expression of pro-inflammatory cytokine TNFα. In line with the gene expression data, there was a significant increase in the abundance of pro-inflammatory cytokines (TNF-α, IL-1β, IL-6, and M-CSF) in the cell medium of CARS2 knockdown THP-1 macrophages. Taken together, these results were consistent with CARS2 playing an anti-inflammatory role in macrophages.

The inflammatory footprint seemed specific to CARS2, as the suppression of two other structurally related (class I) mitochondrial aminoacyl-tRNA synthetases tested (*YARS2* and *MARS2*) did not result in the increased expression of pro-inflammatory transcripts (**Figure 3.7)**. Interestingly, when the levels of cytoplasmic aminoacyl-tRNA synthetase (*CARS1*) were reduced, there was only an increase in the expression of pro-inflammatory cytokines (*IL1*β and *IL6*). In comparison, lower CARS2 expression led to increased expression of more pro-inflammatory cytokines, suggesting a distinct function for mitochondrial CARS2 in inflammation.

To gain a more global understanding of the role of CARS2 in the anti-inflammatory process, total RNA isolated from *CARS2* and control siRNA-transfected THP-1 macrophages was subjected to expression array analysis followed by Gene Set Enrichment Analysis (GSEA). The analysis revealed multiple Reactome pathways linked to the immune system (**Table 3.2**). Next, we used a qPCR inflammatory cytokine array to validate the inflammatory cytokines and receptor genes affected by CARS2 knockdown, and to aid in prioritising the inflammatory pathways (**Table 3.3**). The cytokine array results were largely consistent with the transcription-array data from GSEA analysis. The qPCR-ranked gene list identified the IL-10 signaling pathway (R-HSA-6783783) (**Table 3.2**). This array focused on inflammation via chemokines, cytokines, and interleukins and did not include interferons, which likely explains why interferon pathways were not identified by GSEA analysis of the data from this platform. Importantly, GSEA of both arrays identified the IL-10 signaling pathway and other immune-related pathways. The NES for the IL-10 signaling pathway was >1, suggesting that the genes affected by CARS2 knockdown were positively correlated with the gene set. However, in this gene set, some IL-10 downregulated genes, namely the extracellular and plasma membrane-associated transcripts, were found to increase with CARS2 knockdown, suggesting that the pathway has decreased activity (**Table 3.4**).

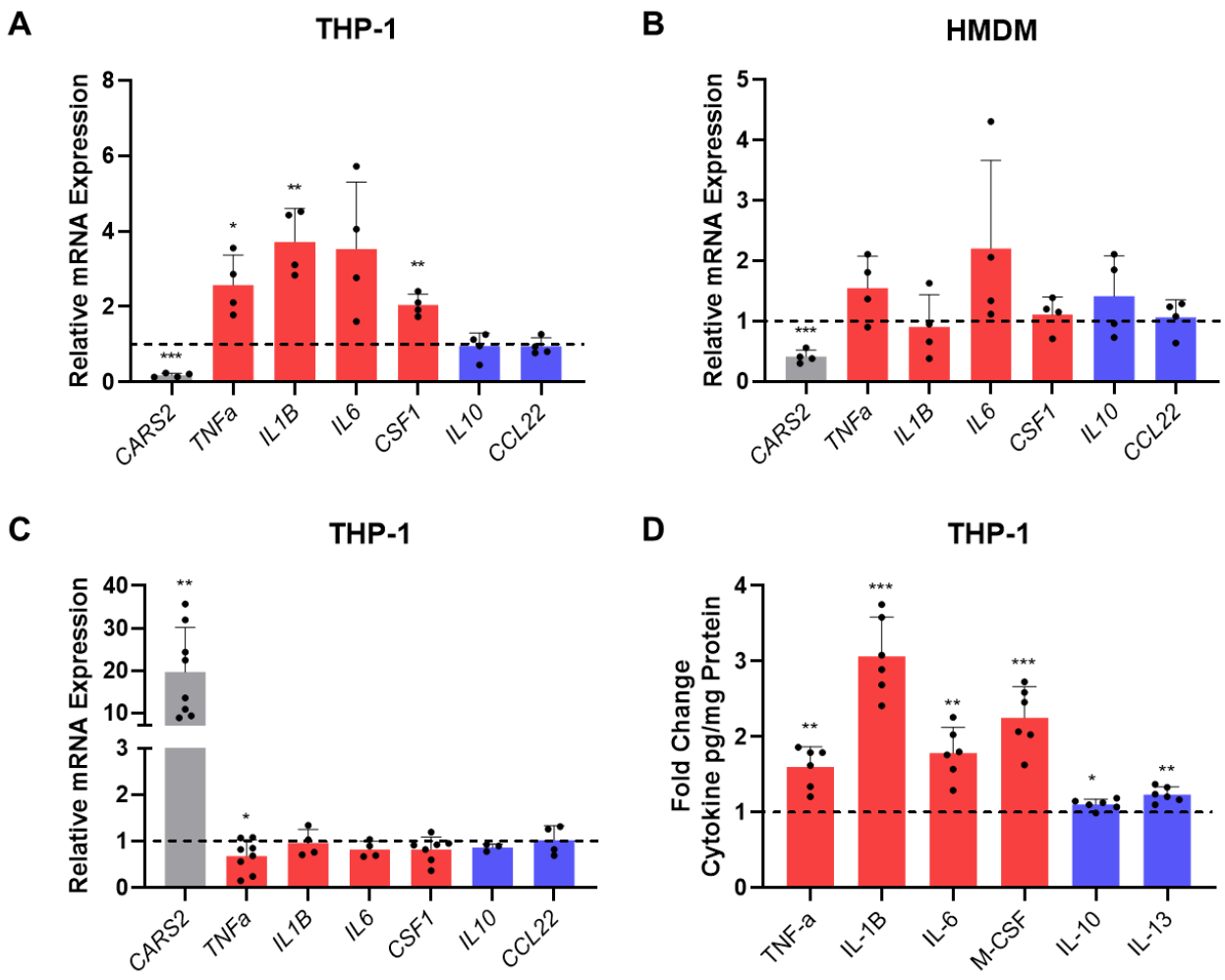

Figure 3.6 Decreased CARS2 expression increases pro-inflammatory cytokine expression in macrophages. Small interfering RNA (siRNA)-mediated knockdown of *CARS2* in macrophages leads to increased expression of pro-inflammatory cytokines. Gene expression of pro-inflammatory cytokines (*TNFα*, *IL1β*, *IL6*, and C*SF1*) in red and anti-inflammatory cytokines (*IL10* and *CCL22*) in blue graphed as a fold change relative to the NT2 siRNA control in **(A)** THP-1 macrophages and **(B)** HMDMs. Data represent the mean ± SD for n=4 (THP-1) and n=5 (HMDM). **(C)** Overexpression of *CARS2* reduces the expression of inflammatory markers in THP-1 macrophages. THP-1 macrophages were transduced with either pLVX-CARS2-HA or the pLVX control. Gene expression was graphed as fold-change relative to the pLVX control in THP-1 macrophages. *SRP14* was used as an internal standard. Data represent the mean ± SD for n = 8 for *CARS2 and TNFα,* n=7 for *CSF1*, and n = 4 for *IL1β*, *IL6, IL10*, and *CCL22*. **(D)** Supernatants were collected 96 h after *CARS2* siRNA transfection in THP-1 macrophages. The concentrations of inflammatory cytokines were determined using the Luminex Human Magnetic Assay. Cytokine levels were normalised to the total protein concentration. The fold-change was calculated by comparison with the NT2 samples. The horizontal lines represent control values (NT2 or pLVX) at 1. Data are presented as the mean ± SD for n = 6. (Unpaired t-test with Welch's correction versus control (NT2 or pLVX)) * $p<0.05$; ** $p<0.01$; *** $p<0.001$.

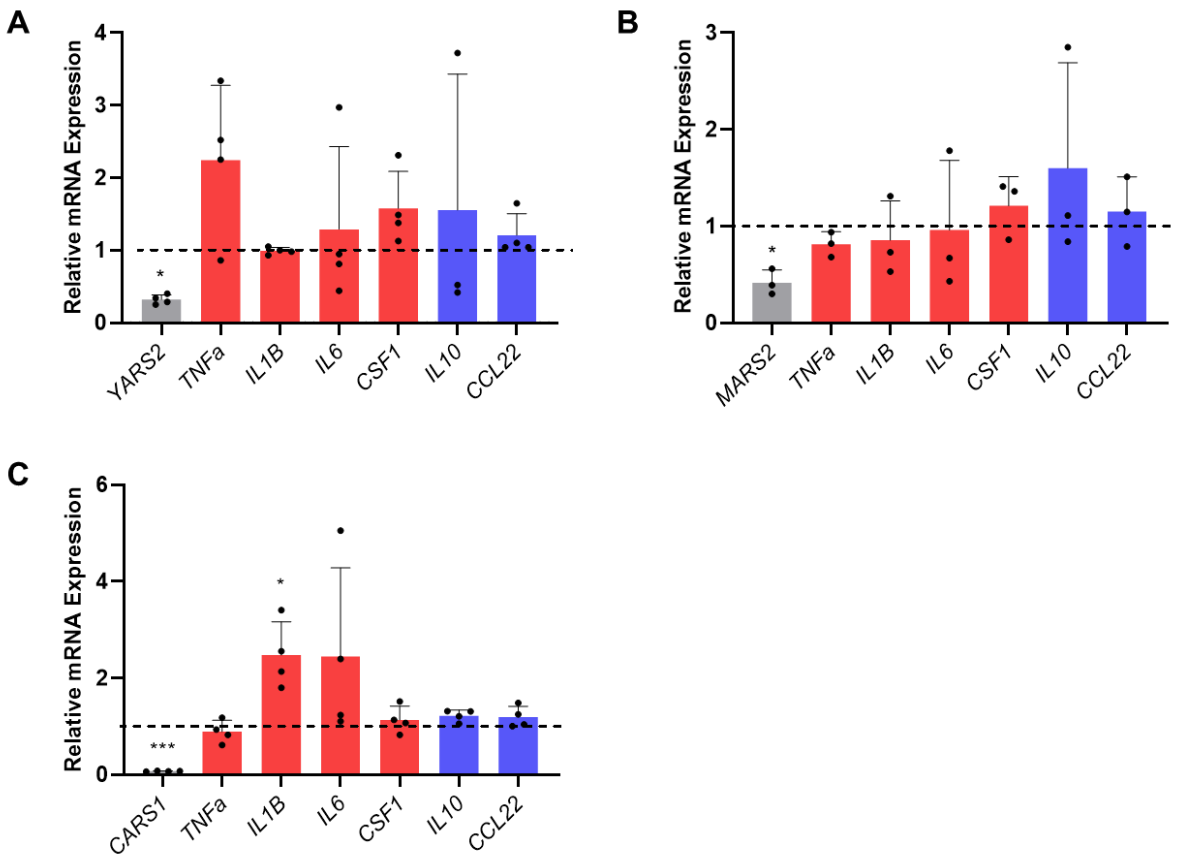

Figure 3.7 Expression of inflammatory cytokines in macrophages following aminoacyl tRNA synthetase knockdown. THP-1 macrophages were transfected with **(A)** *YARS2*, **(B)** *MARS2*, **(C)** *CARS1*, or NT2 siRNA. Gene expression of pro-inflammatory cytokines (*TNFα, IL1β, IL6, and MCSF*) and anti-inflammatory cytokines (*IL10, CCL18, CCL22*) was graphed as a fold-change relative to the NT2 siRNA control. Data are presented as the mean ±SD for n=4 (*CARS1*) and n=3 (*YARS2* and *MARS2*). The horizontal line represents a control value (NT2) of 1. *SRP14* was used as an internal standard. (Unpaired t-test with Welch's correction) * $p<0.05$; ***$p<0.001$.

Microarray							
Gene Set	**Description**	**Size**	**Leading Edge Number**	**ES**	**NES**	**P Value**	**FDR**
R-HSA-909733	Interferon alpha/beta signaling	64	37	0.56153	4.8217	0	0
R-HSA-913531	Interferon Signaling	178	57	0.35128	4.5228	0	0
R-HSA-877300	Interferon gamma signaling	78	38	0.38791	3.5809	0	0
R-HSA-1280215	Cytokine Signaling in Immune system	640	146	0.14601	2.8954	0	0.000249
R-HSA-1169410	Antiviral mechanism by IFN-stimulated genes	72	13	0.30054	2.6842	0	0.003181
R-HSA-6783783	Interleukin-10 signaling	44	19	0.35723	2.65	0	0.003811
R-HSA-168928	DDX58/IFIH1-mediated induction of interferon-alpha/beta	73	25	0.27198	2.4784	0	0.015053
R-HSA-111933	Calmodulin induced events	26	21	-0.416	-2.4003	0	0.040652
R-HSA-111997	CaM pathway	26	21	-0.416	-2.4003	0	0.040652
R-HSA-933541	TRAF6 mediated IRF7 activation	28	13	0.39389	2.3466	0.001988	0.045727
Inflammatory qPCR Array.							
Gene Set	**Description**	**Size**	**Leading Edge Number**	**ES**	**NES**	**P Value**	**FDR**
R-HSA-6783783	Interleukin-10 signaling	17	9	0.7604	1.7666	0.001054	0.001017
R-HSA-372790	Signaling by GPCR	19	8	0.68307	1.6082	0.010417	0.02684
R-HSA-388396	GPCR downstream signalling	19	8	0.68307	1.6082	0.010417	0.02684
R-HSA-418594	G alpha (i) signalling events	19	8	0.68307	1.6082	0.010417	0.02684
R-HSA-449147	Signaling by Interleukins	24	12	0.71079	1.6501	0.004111	0.035584
R-HSA-162582	Signal Transduction	25	9	0.65118	1.5458	0.015385	0.043548
R-HSA-1280215	Cytokine Signaling in Immune system	31	13	0.60373	1.3762	0.070769	0.10523
R-HSA-373076	Class A/1 (Rhodopsin-like receptors)	18	7	0.58725	1.381	0.084463	0.10971
R-HSA-375276	Peptide ligand-binding receptors	18	7	0.58725	1.381	0.084463	0.10971
R-HSA-500792	GPCR ligand binding	18	7	0.58725	1.381	0.084463	0.10971
R-HSA-5669034	TNFs bind their physiological receptors	5	5	-0.34146	-0.85629	0.65766	0.63884

Table 3.2 Gene Set Enrichment Analysis identifies IL-10 signaling as a positively related category.

THP-1 macrophages were transfected with either *CARS2* or control siRNA. RNA samples were processed using the Inflammatory Cytokine and Receptor RT2 Profiler Array (PAHS-011ZA) or Affymetrix Human Gene 2.0 ST expression array. Ranked gene lists were produced and were submitted to WebGestalt (http://www.webgestalt.org/) for Gene Set Enrichment Analysis (GSEA) using the Reactome database for pathway analysis. This table lists the enriched Reactome categories (Gene Set), the number of Entrez genes in the user gene list (Size), Leading Edge Number, Enrichment Score (ES), Normalized Enrichment Score (NES), p-values and FDR. GSEA interprets gene expression data to determine whether genes in a set occur at the top or bottom of a ranked list, or are randomly distributed. Size indicates the number of genes in the uploaded ranked gene list and category. The leading-edge number describes a subset of the genes in a gene set. The enrichment score (ES) was calculated to reflect the degree to which a gene set was overrepresented at the top (positive) or bottom (negative) of the entire ranked gene list. The normalised enrichment score (NES) accounted for the differences in gene set sizes. The False Discovery Rate was calculated using the Benjamini-Hochberg method.

Gene	Fold Change	P value	Adjusted P Value	Description
CCR4	0.6325	**0.002806**	0.129063	C-C motif chemokine receptor 4
IL13	0.6825	**0.038455**	>0.999999	interleukin 13
CD40LG	0.7075	**0.017658**	0.812271	CD40 ligand
CCL22	0.735	**0.024817**	>0.999999	C-C motif chemokine receptor 22
NAMPT	1.32	0.414206	>0.999999	Nicotinamide phosphoribosyltransferase
VEGFA	1.345	0.115066	>0.999999	vascular endothelial growth factor A
CCL1	1.388	0.37983	>0.999999	C-C motif chemokine ligand 1
TNFRSF11B	1.498	0.373434	>0.999999	TNF receptor superfamily member 11b
CCL5	1.855	0.26572	>0.999999	C-C motif chemokine ligand 5
IL7	1.925	0.121752	>0.999999	interleukin 7
IL33	2.103	0.265111	>0.999999	interleukin 33
CSF1	2.26	0.072553	>0.999999	colony stimulating factor 1
CXCL10	2.915	0.259504	>0.999999	C-X-C motif chemokine ligand 10
CXCL2	3.328	0.372043	>0.999999	C-X-C motif chemokine ligand 2
CCL3	3.37	0.357661	>0.999999	C-C motif chemokine ligand 3
CXCL1	3.403	0.345304	>0.999999	C-X-C motif chemokine ligand 1
CXCL11	3.68	0.153336	>0.999999	C-X-C motif chemokine ligand 11
CCL20	4.01	0.20844	>0.999999	C-C motif chemokine ligand 20
CXCL8	4.125	0.259608	>0.999999	C-X-C motif chemokine ligand 8
CXCL3	4.41	0.320622	>0.999999	C-X-C motif chemokine ligand 3
TNF	5.298	0.295632	>0.999999	tumor necrosis factor
CCL4	9.63	0.362185	>0.999999	C-C motif chemokine ligand 4

Table 3.3 Summary of qPCR array results from the CARS2 siRNA-mediated knockdown in M0 macrophages. Comparisons between *CARS2* knockdown and control samples identified 18 upregulated and four downregulated genes with fold difference ≥1.25 or ≤ 0.75, ranked by fold change. The red values indicate significant q values. The data represents the fold-change relative to the control for the mean ± SD for n = 4. (Unpaired t test with Welch's correction, Bonferroni-Dunn's multiple comparisons test)

3.2.4 CARS2 silencing reduced STAT3 activation in the IL-10 signaling pathway.

IL-10 plays an important role in immunoregulation and inflammation and has been reported to be atheroprotective[35]. By binding to its cognate receptor (IL10R), IL-10 activates the JAK1/STAT3 cascade. Once phosphorylated by receptor-associated JAKs, STAT3 homodimerizes and translocates to the nucleus to activate the expression of transcriptional repressors which, in turn, suppresses pro-inflammatory genes[142]. To examine the role of CARS2 in the IL-10 signaling pathway, macrophages transfected with *CARS2,* or control siRNA, were briefly exposed to IL-10 to activate STAT3 tyrosine phosphorylation (Tyr705). An approximately 40% reduction in CARS2 protein levels (**Figure 3.8**) reduced the relative ratio of phosphorylated STAT3 to total STAT3 by 30% in response to IL-10. These data demonstrate that CARS2 is necessary for optimal IL-10 signaling in THP-1 macrophages.

IL10-downregulated extracellular & plasma membrane associated genes	QPCR Array Fold Change	p-value	FDR p-value	Micro Array Fold Change	p-value	FDR p-value
IL1A				-1.03	0.7136	0.9956
IL1B				1.17	0.4486	0.9944
IL6				-1.12	0.9353	0.9985
IL12A				1.03	0.6906	0.9956
IL12B				1.09	0.8438	0.9964
IL18				1.2	0.1206	0.9773
CSF2				-1.06	0.7392	0.9956
CSF3				1.34	0.1658	0.9882
CSF1	2.26	0.0345	0.1321	1.15	0.192	0.9912
TNF	5.30	0.2532	0.4313	1.59	0.021	0.9058
LIF				1.96	0.0716	0.9678
CCL2				1.01	0.5995	0.9956
CCL3	3.37	0.3198	0.4392	1.47	0.0193	0.9058
CCL3L1				1.53	0.0337	0.9485
CCL4	9.63	0.3246	0.4392	2.26	0.0022	0.8419
CCL20	4.01	0.1616	0.3717	1.16	0.09	0.9754
CCL19				-1.33	0.2886	0.9912
CCL5	1.85	0.2236	0.3956	1.41	0.035	0.9526
IL8/CXCL8	4.13	0.215	0.3956	1.05	0.307	0.9912
CXCL10	2.92	0.2144	0.3956	2.53	0.0387	0.9534
CXCL2	3.33	0.3358	0.4392	1.19	0.0573	0.963
CXCL1	3.4	0.3068	0.4392	1.13	0.0403	0.9598
IL1R1	0.83	0.024	0.1103	1.25	0.3098	0.9912
IL1R2				1.38	0.0633	0.9642
PTGS2				1.55	0.5936	0.9956
ICAM1				-1.05	0.6678	0.9956
CD80				1.19	0.2109	0.9912
CD86				-1.04	0.8282	0.9964
FCER2(1-321)				-1.18	0.5019	0.9953
IL10-upregulated plasma membrane genes	QPCR Array Fold Change	p-value	FDR p-value	Micro Array Fold Change	p-value	FDR p-value
FPR1				-1.35	0.0949	0.9754
PTAFR				1.06	0.5313	0.9953
CCR1	0.84	0.2159	0.3956	1.32	0.1863	0.9912
CCR2	0.79	0.309	0.4392	-1.11	0.2787	0.9912
CCR5				-1.32	0.3349	0.9912
IL1RN	0.95	0.5533	0.6247	1.21	0.0934	0.9754
TNFRSF1B				1.08	0.4084	0.9918
TIMP1				1.12	0.2774	0.9912

Table 3.4 IL-10-downregulated/upregulated extracellular and plasma membrane genes. The list of IL-10 downregulated and upregulated genes was obtained from Reactome (R-HSA-6783783). Fold changes, p-values, and FDR p-values were obtained from both qPCR (Table 2) and microarray results (Transcriptome Analysis Console).

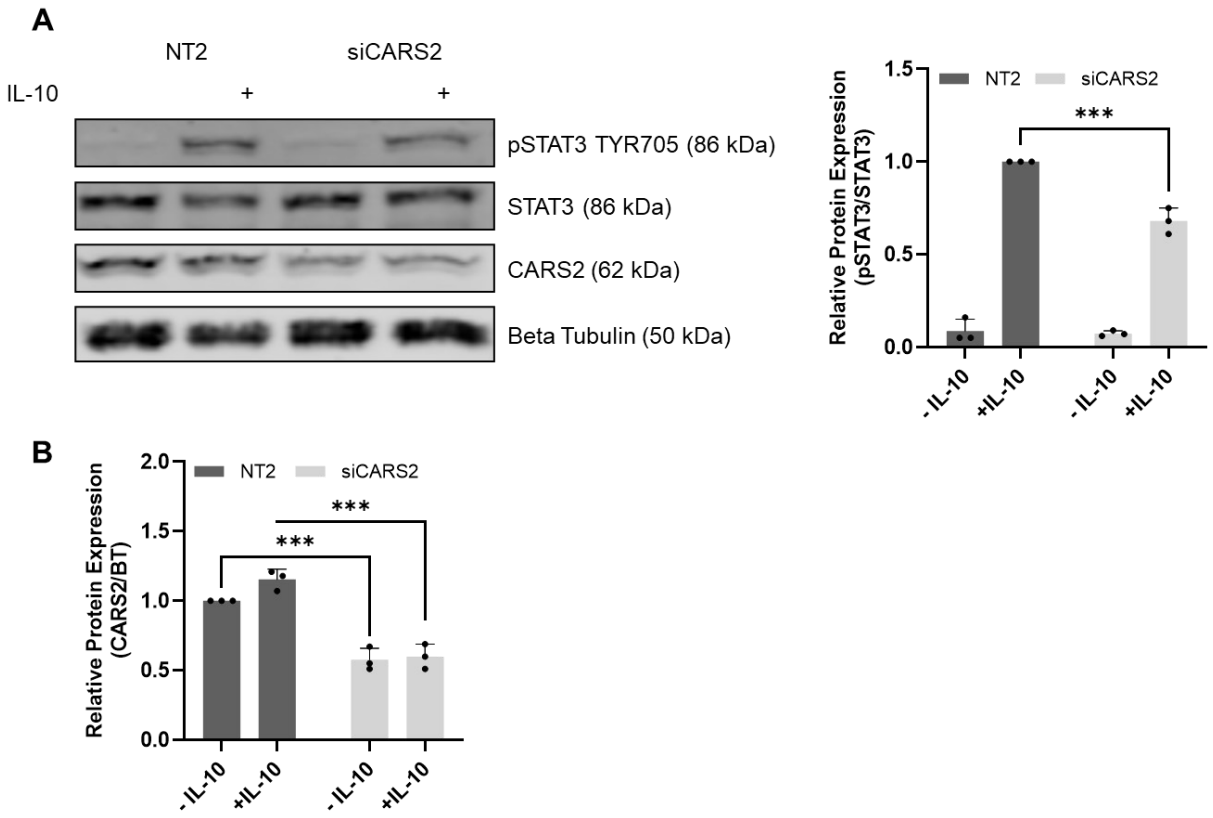

Figure 3.8 CARS2 silencing in M0 macrophages reduced STAT3 phosphorylation in response to IL-10. Following siRNA silencing of CARS2 in M0 macrophages, cells were treated with IL-10 (30 ng/mL) for 15 min. Western blot and protein quantification of **(A)** pSTAT3/STAT3 and **(B)** CARS2/BT expression. Data are presented as the mean ± SD, n=3. (2-way ANOVA) ** $p<0.01$; *** $p<0.001$.

3.2.5 *CARS2* knockdown in macrophages altered the expression of SMC markers in co-culture.

In advanced atherosclerotic lesions, macrophages are major contributors to the inflammatory response, promoting the recruitment of SMCs to the lesion area[143]. SMCs play a key role in plaque stability but have also been shown to generate lipid-laden foam cells that produce pro-inflammatory cytokines[144]. The effect of reduced CARS2 levels in macrophages on SMC gene expression was examined using a co-culture approach (**Figure 3.9A**). *CARS2* silencing reduced the expression of contractile genes *ACTA2* and *TAGLN*. The structural gene *COL3A1* displayed a slight reduction, whereas *FN1* expression remained unchanged. Inflammatory cytokine expression was modestly increased compared to control. Overall, SMCs co-cultured with *CARS2* silenced macrophages, displayed a decreased contractile phenotype with a concomitant increase in inflammatory markers.

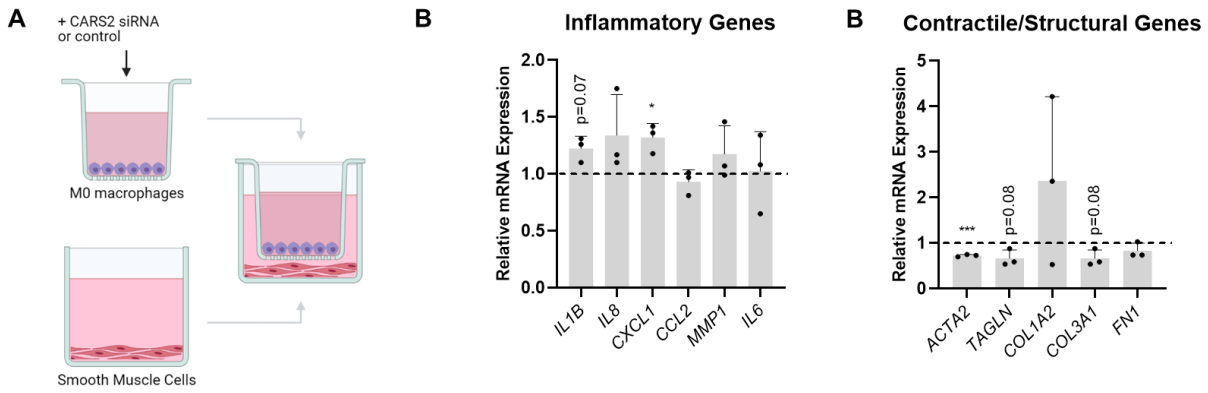

Figure 3.9 CARS2 knockdown in macrophages altered the expression of major smooth muscle cell markers in co-culture experiments. (A) Experimental co-culture diagram. Gene expression of **(B)** inflammatory, **(C)** contractile, and structural mRNAs in smooth muscle cells (SMCs) after co-culture with M0 macrophages with or without *CARS2* knockdown. *SRP14* was used as an internal standard. The horizontal line represents the control value (NT2) of 1. Data are presented as the mean ± SD for n = 3. (Unpaired t-test with Welch's correction) * $p<0.05$; ** $p<0.01$. Schematic was created with BioRender.com.

3.2 Discussion

GWAS has provided new insights into CAD disease biology and led to the discovery of unexpected gene functions[145,146]. Recent GWAS have identified two genetic variants associated with CAD: rs61969072 and rs9583531, proximal to the CARS2 locus[76,147]. Through eQTL analysis, we demonstrated that the protective allele of the index GWAS SNP rs61969072 is associated with increased expression of CARS2 in tissues relevant to atherosclerosis. Using a siRNA-mediated knockdown model in macrophages to reduce CARS2 levels, we showed a novel protective anti-inflammatory role of CARS2 in THP-1 macrophages through the IL-10 signaling pathway. These findings have added CARS2 to the list of CAD risk loci that are directly linked to inflammation and immunity[148].

In support of its role in inflammation, siRNA-mediated CARS2 knockdown increased the expression of pro-inflammatory cytokines in THP-1 macrophages and HMDMs. A reciprocal effect was observed in response to *CARS2* overexpression in THP-1 macrophages, as evidenced by a significant decrease in *TNFα* expression. These effects were propagated in a co-culture with SMCs. When macrophages were co-cultured with SMCs, reduced CARS2 levels in macrophages elicited a local inflammatory response, characterised by increased inflammatory cytokine gene expression. This was accompanied by the decreased expression of genes associated with a contractile SMC phenotype, a key feature of pro-inflammatory (synthetic) SMCs[149]. SMCs can undergo phenotype differentiation in response to various extracellular stimuli, including pro-inflammatory cytokines, in this case, due to lower CARS2 levels in macrophages, leading to a synthetic phenotype[150–152]. These data are consistent with the paracrine role of macrophage CARS2 in the crosstalk with vascular SMCs.

In contrast to CARS2, suppression of two other mitochondrial ARS and cytoplasmic CARS1 did not result in pro-inflammatory profiles. These results suggest that mitochondrial perturbations do not play a major role in promoting inflammation. Other aminoacyl-tRNA synthetases have been shown to have pro-inflammatory functions. Tryptophanyl-tRNA synthetase (WARS) is a regulator of angiogenesis that is secreted in response to IFN-γ and signals through Toll-like receptor 2 (TLR2) in macrophages to increase the secretion of TNF-α and CXCL8 in macrophages[113,153]. Tyrosyl-tRNA synthetase (YARS) can be divided into two fragments with distinct cytokine activities that stimulate the production of TNF-α and function as an IL-8 cytokine[111].

CARS2 expression observed during monocyte-to-macrophage differentiation follows a pattern consistent with processes including cytokine- and chemokine-mediated signaling pathways, cell structure and motility[154]. This expression pattern is characterised by increased expression at 16 H and a return to baseline by 168 H. CSF1, which promotes monocyte differentiation into macrophages, is one of the many genes involved in this pattern[155]. Increased CARS2 expression following this pattern suggests a role in enhancing differentiation. In fact, other chemokines included in this pattern (*CCL3, CCL4, CCL5, CXCL7, CCR1, and IL6R)* were upregulated with reduced CARS2 levels. Consistent with a previous study investigating monocyte-macrophage differentiation and further polarisation to pro- or anti-inflammatory macrophages[156], we observed decreased *CARS2* expression in M1 macrophages following treatment with LPS and IFN-γ.

The interleukin-10 (IL-10) signaling pathway was identified as the top hit by GSEA analysis of both the microarray and qPCR arrays. IL-10 is secreted by macrophages and is considered anti-atherosclerotic[35]. Il-10 inhibits the production of LPS-induced inflammatory genes[157,158]. In the presence of IL-10, reduced *CARS2* levels in macrophages result in increased pro-inflammatory

cytokine expression. IL-10 suppression of genes induced by LPS was also affected by *CARS2* knockdown, with a trend towards increased pro-inflammatory cytokine expression (*IL6*, *CXCL8*, *and CSF1*). In summary, we showed that loss of CARS2 affects IL-10 activation through STAT3 phosphorylation and hinders the repression of its downstream targets, highlighting its novel role in the anti-inflammatory pathway. Other pathways involving STAT3 phosphorylation may also play a role in the anti-inflammatory effects of CARS2[159]. For example, IFN-α/β-induced STAT3 expression can negatively regulate type I IFN signaling by suppressing STAT1 monomers[159,160]. There are limitations to the cell model; the THP-1 monocyte-like cell line, from which most of the presented data were derived, only approximates the phenotype of primary human macrophages. Although the HMDM data presented were largely consistent with the THP-1 model, they differed both qualitatively and quantitatively. This may be related to the greater inherent biological variability and reduced knockdown efficiency achieved in HMDMs (58%) vs. THP1s (81%). The sample sizes between the experiments were not consistent, and there were unequal sample sizes. This is because of the inconsistent measurements of data points before combining them into a final dataset. We used Welch's t-test or an unequal variances t-test to correct for the varying sample sizes. Of the arrays used, the qPCR inflammatory array did not demonstrate significant increases in pro-inflammatory genes of interest. This was because of the small sample size. However, overall, the increased expression of pro-inflammatory genes was largely consistent in qPCR and transcription arrays. Finally, we did not directly examine the role of CARS2 in an animal atherosclerosis model. *Cars2*$^{-/-}$ mice are embryonic lethal[127]; hence, a heterozygous *Cars2*$^{+/-}$ model, demonstrating reduced CARS2 levels[127], is required. The heterozygous *Cars2*$^{+/-}$ mice can be fed either a normal or atherogenic diet for 12 weeks[161]. At 16

weeks, the following can be measured: plasma lipid profile, blood pressure, oxidative stress, atherosclerotic lesion size in aortic roots and inflammation[161,162].

In summary, in the experimental validation of a GWAS-identified locus for CAD, we identified a novel atheroprotective role of CARS2. *CARS2* silencing in human macrophages elicits increased expression of pro-inflammatory genes and secretion of pro-inflammatory cytokines. Crosstalk with adjacent SMCs, in turn, leads to altered SMC gene expression, indicative of a less contractile and more inflammatory state.

Chapter 4: CARS2 knockdown alters NF-κB activity and expression in macrophages.

4.1 Introduction

As discussed in the previous chapter, CARS2 was shown to affect inflammation through the IL-10 signaling pathway. However, the wider role of CARS2 in inflammation is unknown. Here, we conducted gene expression profiling microarray analysis to determine the response of macrophages to reduced CARS2 levels. Identifying key pathways and upstream regulators could provide important clues to mechanisms leading to increased inflammation from altered CARS2 expression.

Consistent with our results, genes and pathways associated with inflammation and immune responses were enriched. Pathway analysis also identified the NF-κB signaling pathway as affected by CARS2. Transcription factor NF-κB contributes to atherosclerotic plaque progression at every stage[29]. Due to its role in controlling inflammation, we assessed NF-κB protein expression and activation through western blotting. While NF-κB protein expression is increased with CARS2 knockdown, a luciferase NF-κB reporter THP-1 cell line showed significantly decreased activation.

4.2 Results

4.2.1 IPA Analysis revealed inflammatory pathways relevant to genes differentially regulated in reduced *CARS2* macrophages.

Differentially expressed genes were categorised into related canonical pathways using Core Analysis in the Ingenuity IPA Software (Ingenuity Systems, Stanford, USA). By applying a threshold of -log(p-value) >1.3, 42 enriched canonical pathways were identified and ranked according to their significance (**Figure 4.1**). The top pathways were related to inflammation and innate immunity. The top three ranking pathways were the “Role of

Hypercytokinemia/hyperchemokinemia in the Pathogenesis of Influenza" (-log(p-value) = 19.7), "Interferon Signaling" (-log(p-value) = 11.3), and "Activation of IRF by Cytosolic Pattern Recognition Receptors" (-log(p-value) = 8.72). Based on a z-score of >2 as the threshold for significant activation, the most enriched pathways were activated. Only one pathway had a z-score <-2, indicating inhibition of the "Coronavirus Pathogenesis Pathway" (z-score = -3.162). Upstream Regulator Analysis identified the key regulators that could explain the observed changes in gene expression in the dataset. Various molecules, including transcription factors, cytokines, microRNAs, receptors, kinases, chemicals, and drugs, have been identified. By applying a p-value of overlap of <0.05, 1718 enriched upstream regulators were identified. Among these regulators, 191 had z-scores >2, and 79 had z-scores <-2, indicating activation and inhibition, respectively. Several predicted transcription regulators have been identified to be involved in inflammation, including Interferon Regulatory Factors due to *CARS2* suppression: IRF7, IRF9, STAT transcription factors STAT1 and STAT2, and pro-inflammatory cytokines TNFSF10 and TNF (**Table 4.1**). The most significant activator was non-POU domain-containing octamer binding (NONO) (z-score = 6.718, p-value of overlap = $1.61x10^{-60}$). When considering the experimental fold change, interferon regulatory factor 7 (IRF7) (z-score = 6.231, p-value of overlap = 4.0 × 10–47, fold change = 1.55) was the top activator. The top inhibitor was Mitogen-Activated Protein Kinase 1 (MAPK1) (z-score = -5.379, p-value of overlap = $2.04x10^{-27}$). Differentially expressed genes were categorised into related diseases and cellular functions. By setting the -log(p-value) threshold to >1.3, 30 disease processes and gene functions were ranked based on their significance (**Figure 4.2**). Consistent with the canonical pathway analysis, most functions were linked to inflammation e.g., Inflammatory Response, Immunological Disease,

Inflammatory Diseases, Infectious Disease and Metabolic Disease. These data indicate that CARS2 is involved in many inflammatory processes.

Next, the association between differentially expressed genes and toxicity (tox) functions was determined using IPA software. A total of 12 Tox functions were identified ($p < 0.05$) (**Figure 4.3**). The top enriched function, "Increased Depolarization of Mitochondria and Mitochondrial Membrane", was the most significant, with a p-value of = $2.51x10^{-5}$. Since CARS2 is a mitochondrial protein, it is relevant that the majority of the top five tox functions are linked to the mitochondria such as "Increases Permeability Transition of Mitochondria and Mitochondrial Membrane" and "Increases Damage of Mitochondria". Interestingly, there were also several significant tox functions related to the liver, such as "Liver Necrosis/Cell Death", "Increases Liver Hepatitis", "Liver proliferation" and "Increases Liver Damage". Notably, NF-κB signaling, which plays an important role in atherosclerosis as a regulator of inflammation, has also been identified.

Finally, the IPA software built interacting molecular networks to connect key genes and enriched categories of diseases and functions based on the correlation between differentially expressed genes. The networks displayed interactions between the molecules in the dataset. A total of 25 interacting networks were identified and ranked based on their scores. The highest-ranked network (score = 35) was found to affect 'antimicrobial response, infectious diseases and inflammatory response' involving 20 molecules (**Figure 4.4**). The top two interaction networks showed molecules involved in the antimicrobial response, infectious disease, and inflammatory response (**Table 4.2**), with a score of >30. In IPA network 1, the highest-ranked network, most genes were linked to IRF9, STAT2, and TNF-α, whereas in network 2, most genes were linked

to STAT1, IRF7, and IFN-α (**Figure 4.4**). Again, these data demonstrate strong associations between CARS2 and the inflammatory pathways.

To validate the target genes for the array, seven genes (*EIF2AK2*, *IRF7*, *IRF9*, *STAT2*, *STAT1*, and *CCN1*) were selected for qPCR analysis (**Figure 4.5**). Consistent with the microarray results, the expression levels of *EIF2AK2, IRF7, and CCN1 were* upregulated after the *CARS2* siRNA-mediated knockdown in macrophages. The other genes, which were not significantly different, showed an increasing trend with reduced CARS2 levels.

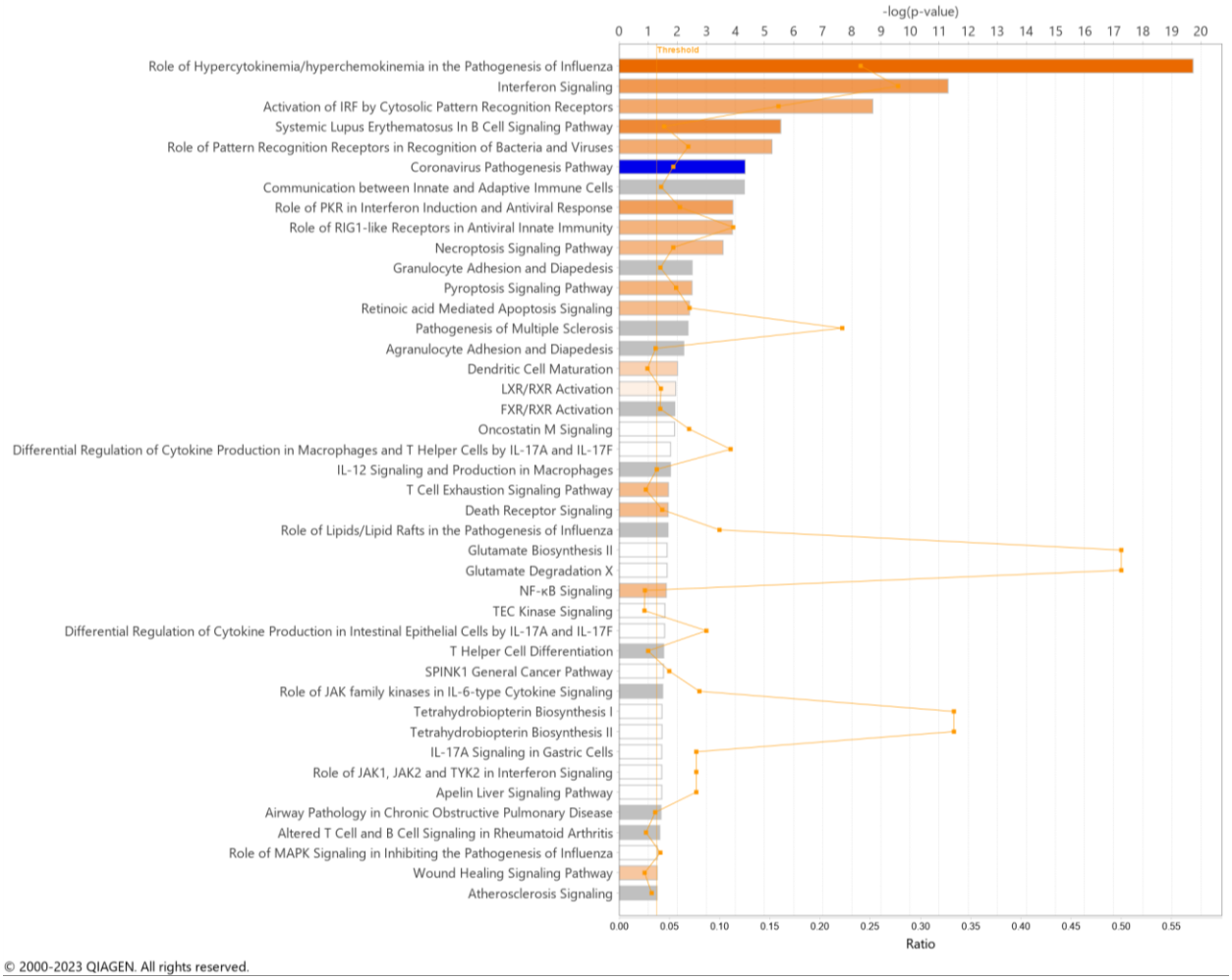

Figure 4.1 Canonical pathways from the Ingenuity Pathway Analysis (IPA). The transcriptome of THP-1 macrophages transfected with *CARS2* or control siRNA was subjected to IPA to identify the canonical pathways. The canonical pathway names are listed along the y-axis. The top x-axis indicates the significant values (p-value of overlap) which were calculated using right-tailed Fisher's Exact Test. The bars indicate the most significant pathways at the top. The threshold line represents the statistical significance cut-off, with a -log(p-value) > 1.3, corresponding to a p-value < 0.05. The colour of the bar indicates the predicted pathway activation based on the z-score. A z-score was used to determine the statistical significance of the pathway activation state. The orange and blue bars indicate predicted pathway activation and inhibition, respectively. The gray bars indicate that no activity prediction could be made. The white bars indicate pathways with z-scores at or very close to zero or with fewer than 4-analysis ready molecules in the dataset associated with the pathway that cannot be analysed. The ratio (orange dots connected by an orange line) was calculated based on the extent of overlap between the dataset molecules and Canonical Pathway. This figure was generated through the use of QIAGEN IPA (QIAGEN Inc., https://digitalinsights.qiagen.com/IPA).

Upstream Regulator	Expr Fold Change	Molecule Type	Predicted Activation State	Activation z-score	Flags	p-value of overlap	Target Molecules in Dataset	Mechanistic Network
NONO	1.04	transcription regulator	Activated	6.718	bias	1.61E-60	CCL4L1/CCL4L2,CMPK2,CXCL	84 (17)
IFNL1	1.14	cytokine	Activated	5.968	bias	2.01E-52	CMPK2,CXCL10,EIF2AK2,GBP	79 (15)
IRF7	1.55	transcription regulator	Activated	6.231	bias	4.81E-47	CMPK2,CXCL10,GBP1,GBP5,H	75 (14)
IFNA2	1.19	cytokine	Activated	6.503	bias	2.18E-44	CMPK2,CXCL10,EIF2AK2,GBP	84 (14)
PRL	-1.03	cytokine	Activated	6.152	bias	1.5E-37	CMPK2,CXCL10,DTX3L,EIF2AK	77 (12)
IRF3	1.17	transcription regulator	Activated	5.554	bias	1.19E-36	CCL3L3,CCL4,CMPK2,CXCL10	72 (14)
IRGM	-1.1	enzyme	Inhibited	-4.83	bias	2.08E-34	GBP1,HERC5,IFI16,IFI35,IFI44,	64 (13)
STAT1	1.53	transcription regulator	Activated	4.944	bias	2E-32	CCL3L3,CCL4,CMPK2,CXCL10	85 (15)
IRF1	1	transcription regulator	Activated	5.453	bias	4.15E-32	CMPK2,CXCL10,EIF2AK2,HEL2	82 (15)
IFNB1	1.02	cytokine	Activated	5.24		6.87E-32	APOL1,CCL4,CMPK2,CXCL10,I	86 (12)
TREX1	1.27	enzyme	Inhibited	-3.911	bias	3.81E-30	CXCL10,IFI16,IFI44,IFI44L,IFIT	66 (16)
RC3H1	-1.05	enzyme	Inhibited	-4.796	bias	4E-30	CCL4,IFI16,IFI27,IFI44,IFI44L,II	85 (15)
RIGI	2.29	enzyme	Activated	4.171	bias	1.89E-29	CCL4,CXCL10,EIF2AK2,HERC5	68 (12)
IFNAR1	-1.17	transmembrane receptor	Activated	3.613	bias	6.16E-29	CCL3L3,CCL4,CMPK2,CXCL10	83 (13)
IL1RN	1.22	cytokine	Inhibited	-5.188	bias	1.04E-28	BTN3A1,GBP1,HERC6,IFI27,IFI	75 (13)
ACKR2	1.13	G-protein coupled receptor	Inhibited	-4.347	bias	2.16E-28	CCL3L3,CXCL10,EIF2AK2,IFI16	76 (13)
MAPK1	1.05	kinase	Inhibited	-5.379		2.04E-27	CCL3L3,CCL4,EIF2AK2,GBP1,(	71 (13)
PNPT1	1.87	enzyme	Inhibited	-4.333	bias	5.2E-27	CMPK2,CXCL10,EIF2AK2,IFI16	68 (14)
RNASEH2B	-1.15	other	Inhibited	-3.988	bias	5.74E-27	CMPK2,CXCL10,EIF2AK2,HERC	62 (14)
STAT2	1.5	transcription regulator	Activated	3.373	bias	1.31E-26	CXCL10,GBP1,IFI27,IFI35,IFIT1	67 (11)
TLR3	1.88	transmembrane receptor	Activated	4.346	bias	9.23E-25	AIM2,CCL3L3,CCL4,CMPK2,CX	63 (13)
IFNA1/IFNA13	1.34	cytokine	Activated	4.123	bias	1.28E-23	CXCL10,EIF2AK2,IFI27,IFIH1,IF	73 (13)
CITED2	1.18	transcription regulator	Inhibited	-4.792	bias	1.98E-23	CMPK2,CXCL10,DTX3L,GBP5,I	76 (15)
TRIM24	1.08	transcription regulator	Inhibited	-4.239	bias	2.85E-23	CCL4,CMPK2,CXCL10,EPSTI1,	71 (14)
IRF5	1.14	transcription regulator	Activated	4.237	bias	4.99E-23	CCL4,CMPK2,CXCL10,IFI44,IFI	67 (12)
CGAS	1.02	enzyme	Activated	3.574	bias	5.17E-23	CXCL10,HERC5,IFI44,IFI44L,IF	62 (12)
IFNG	-1.01	cytokine	Activated	7.31		5.44E-23	AIM2,APOL1,BTN3A1,CCL3L3,(	84 (14)
STAT3	-1.14	transcription regulator	Inhibited	-2.726		1.02E-22	CCL3L3,CCL4,CMPK2,CXCL10	79 (13)
TLR9	-1.08	transmembrane receptor	Activated	4.943	bias	1.97E-22	AIM2,CCL3L3,CCL4,CXCL10,GI	70 (13)
IRF9	1.51	transcription regulator	Activated	2.419		7.75E-22	CXCL10,GBP1,IFI27,IFIT1,IFIT2	78 (12)

Table 4.1 Top 30 Upstream Regulators from Ingenuity Pathway Analysis (IPA). Filter criteria: significant z-scores (≥2 for predicted activation and ≤ -2 for predicted inhibition) and a p-value <0.05 and Fold Change (≥1.5, or ≤ -1.5).

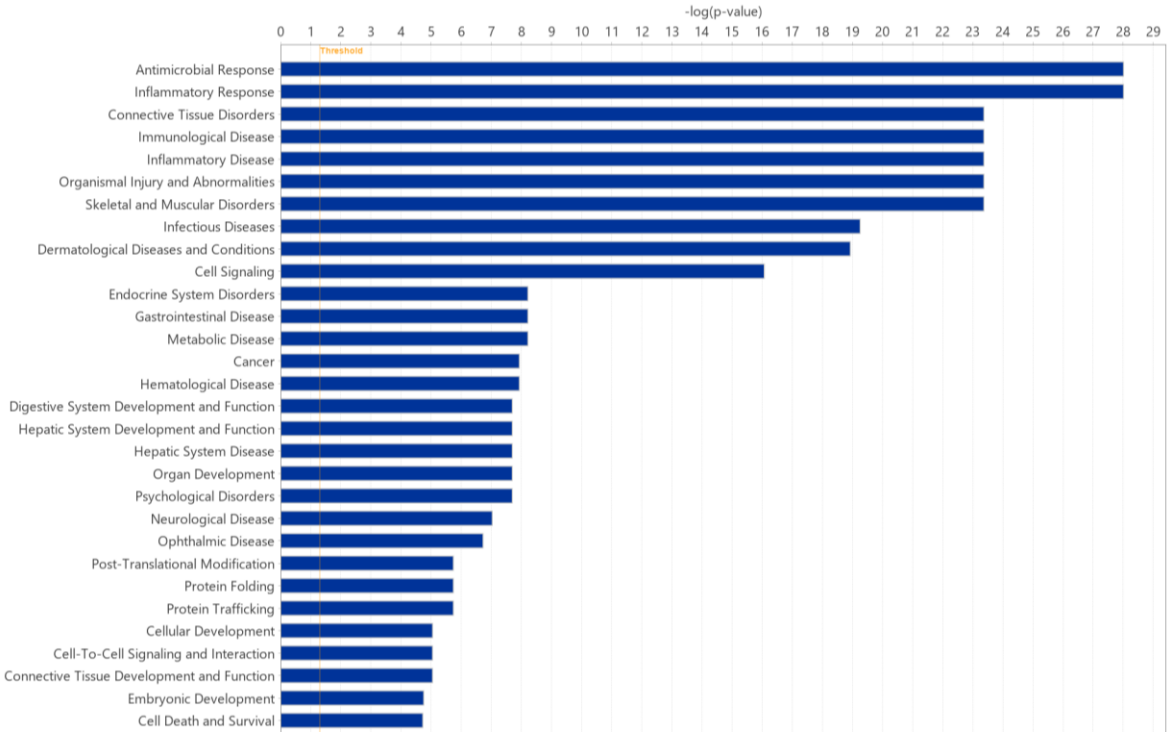

Figure 4.2 Diseases and Biological functions enriched by IPA. The analysis identified diseases and/or biological functions that were most significant in the differential gene expression dataset. The x-axis displays the -log(p-value) significance. The functions are listed from the most to the least significant. The threshold line represents the statistical significance cut-off, with a -log(p-value) > 1.3, corresponding to a p-value < 0.05. This figure was generated through the use of QIAGEN IPA (QIAGEN Inc., https://digitalinsights.qiagen.com/IPA).

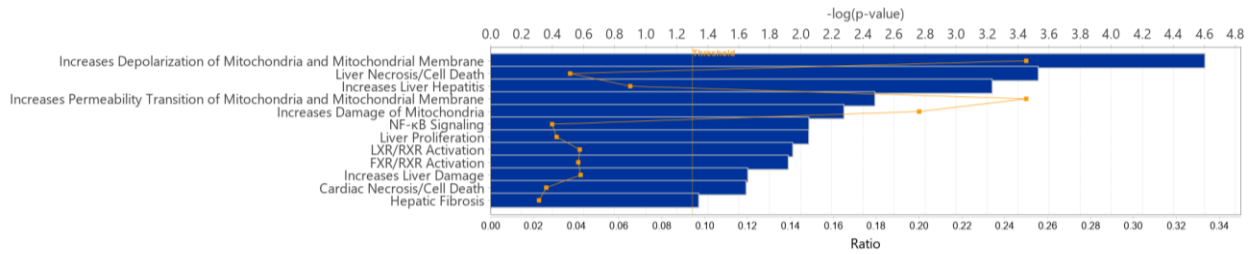

Figure 4.3 Toxicology pathway list from IPA. Toxicology lists are molecules that are known to be involved in toxicology. The top toxicological functions are listed along the y-axis. The top axis indicates the significant values (p-value of overlap) which were calculated using the right-tailed Fisher's Exact Test. The threshold line represents the statistical significance cut-off, with a -log(p-value) > 1.3, corresponding to a p-value < 0.05. The bottom x-axis represents the ratio of the number of genes from the dataset that mapped to the pathway to all known genes in that pathway. The ratio (orange dots connected by an orange line) was calculated based on the extent of overlap of the dataset molecules with the Tox List. This figure was generated through the use of QIAGEN IPA (QIAGEN Inc., https://digitalinsights.qiagen.com/IPA).

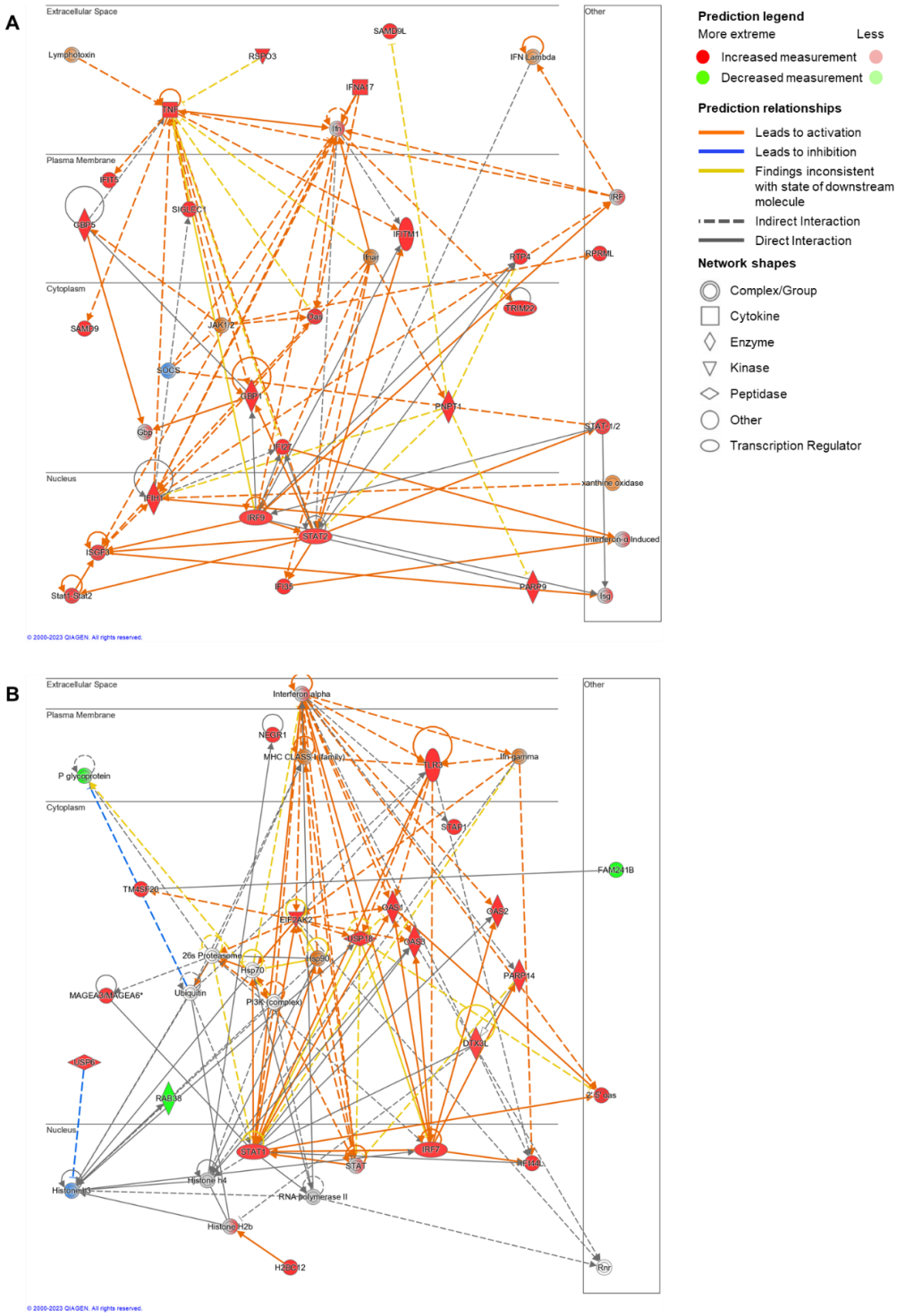

Figure 4.4 Network analysis using IPA. Annotated interactions between genes affected by CARS2 siRNA-mediated knockdown. (**A**, **B**) Top two ranked enriched networks based on differential gene expression. Upregulated (red) and downregulated (green) genes are shown in the network. Nodes representing gene products are displayed by cellular localisation (extracellular space, plasma membrane, cytoplasm, or nucleus). The prediction legend is located on the right side of the figure. The figure was generated through the use of QIAGEN IPA (QIAGEN Inc., https://digitalinsights.qiagen.com/IPA).

ID	Molecules in Network	Score	Focus Molecules	Top Diseases and Functions
1	Gbp,GBP1,GBP5,IFI27,IFI35,IFIH1,IFIT5,IFITM1,Ifn,IFN Lambda,IFNA17,Ifnar,Interferon-α Induced,IRF,IRF9,Isg,ISGF3,JAK1/2,Lymphotoxin,Oas,PARP9,PNPT1,RPRML,RSPO3,RTP4,SAMD9, SAMD9L,SIGLEC1,SOCS,STAT-1/2,Stat1-Stat2,STAT2,TNF,TRIM22,xanthine oxidase	35	20	[Antimicrobial Response, Infectious Diseases, Inflammatory Response]
2	2' 5' oas,26s Proteasome,DTX3L,EIF2AK2,FAM241B,H2BC12,Histone H2b,Histone h3,Histone h4,Hsp70,Hsp90,IFI44L,Ifn gamma,Interferon alpha,IRF7,MAGEA3/MAGEA6,MHC CLASS I (family),NEGR1,OAS1,OAS2,OAS3,P glycoprotein,PARP14,PI3K (complex),RAB38,RNA polymerase II	33	19	[Antimicrobial Response, Infectious Diseases, Inflammatory Response]
3	Alpha catenin,AMPK,BEAN1,Calmodulin,Ck2,CKAP4,DDX58,F Actin,FAM133B,Fibrinogen,GLUD1,Gsk3,HELZ2,hemoglobin,IFI16,IgG2b,IKK (complex),IL13RA2,IMP3,Insulin,ISG15,KLHL22,LOXL4,LYPLA2,Mapk,MTORC1,Notch,NPAS2,PDK4, PGK1,Proinsulin,SLC2A3,SQOR,SRC (family),STAT5	30	18	[Cellular Compromise, Developmental Disorder, Hereditary Disorder]
4	ABCB4,Alp,CCN1,COL10A1,COL6A3,collagen,Collagen type II,Collagen type IV,Collagen(s),collagenase,creatine kinase,DDAH1,DDR1,ERK1/2,Growth hormone,Hat,histone deacetylase,HS2ST1,Hsp27,Ikk (family),IL-1R,LAIR2,LATS,LOC100288798,MMP8,OSMR,Pdgf (complex),PDGF	28	17	[Cancer, Organismal Injury and Abnormalities, Tissue Development]
5	AGO2,AIM2,C2orf78,CALHM5,CAMTA1,EIF3,ELK4,FAM168A,HNRNPCL1/HNRNPCL2,IFI27,IFIT1,IFIT2,IFIT3,IFNL4,IKZF3,Interferon-α Induced,KRTAP10-4,mir-548,miR-548o-3p (and other miRNAs w/seed CAAAACU),miR-579-3p (and other miRNAs w/seed UCAUUUG),NLRP11,OASL,OR10J5,PC	28	17	[Dermatological Diseases and Conditions, Immunological Disease, Inflammatory Disease]
6	ARMCX2,CD200,CD3-TCR,CLDN24,DISC,EGR2,HERC5,IFI44,IFIT1,IL2RG,Leukocyte Extravasation Signaling,LINC01139,MAPK1,MHC Class II (complex),mir-583,MR1,MX2,NCMAP,OAS1,PRKCD,SEMA3D,SLAMF6,Spectrin,T cell receptor alpha joining,T-cell alpha/beta receptor,TEC,TRA	26	16	[Connective Tissue Disorders, Immunological Disease, Inflammatory Disease]
7	ADRB,Angiotensin II receptor type 1,Cbp/p300,CG,Ck2 alpha,collagen type i (family),COX7A1,Creb,CXCL10,elastase,EPSTI1,estrogen receptor,FHDC1,GCH1,Hdac,HERC6,JAK,N-cor,NFkB (complex),NFkB (family),Nr1h,NR1H3,PADI2,PEPCK,PML,Ppar,PRC2,PRKD,RASGRF1,Rxr,SEMA	24	15	[Cancer, Organismal Injury and Abnormalities, Reproductive System Disease]
8	ADCY,APOL1,Caspase 3/7,DACT1,FSH,G protein,G protein alphai,Gpcr,GSTA2,HCG11,HDL,IL23,Jnk,LCLAT1,Ldh (complex),LDL,Lh,Nos,NPY,ORM1,Pkc(s),PLC,PPY,PRKAA,PTPase,RXFP1,RXFP2,SLC13A1,Sod,SST,SSTR2,TDRD7,TSH,TSPAN2,voltage-gated calcium channel	24	15	[Cell Signaling, Nucleic Acid Metabolism, Small Molecule Biochemistry]
9	ADGRF3,ALG10B,ANKRD26,ANLN,ATP5F1B,Ca2 ,CASR,CIT,CUL5,EFTUD2,G2E3,H2AC4,H4C1,HNRNPCL3/HNRNPCL4,KIF20A,KLK13,KRTAP6-3,LRRC46,MAN1B1,MLN,MLNR,MPLKIP,NANOS3,NKAIN1,PABPC1L,phospholipase,POTEM (includes others),RNF208,SLC35A5,TCF7L2,ZNF320,ZNF395,ZNF525,ZNF79	24	15	[Cell-To-Cell Signaling and Interaction, Cellular Assembly and Organization, Hair and Skin Development and Function]
10	Apol9a/Apol9b,ARRDC2,BC147527,C17orf99,CARS2,CYP4F11,CYTOR,FAHD2B,FAM153A/FAM153B ,GALM,H3C10,HSPD1,IFI44,IGHV3-49,IGKV1-12,IGKV1D-17,IGKV2-40,IGKV2D-28,IGKV2D-40,Igkv8-30,IGLV5-37,IGLV6-57,Immunoglobulin,KIF6,LST1,MESD,PDHA1,PHF11,PMPCA,PPM1K,PRC1,SLC25A4	22	14	[Cancer, Humoral Immune Response, Inflammatory Response]
11	ABRA,Akt,Ap2,C/EBP,Calcineurin protein(s),calpain,caspase,CCL4L1/CCL4L2,Ciap,CREG1,CSF,Cyclin A,Cyclin E,cytochrome C,E2f,EBF1,Fcgr3,GXYLT2,Igm,IL1,Inflammasome,mir-154,mir-320,Mt,MT1G,MT1X,MT2A,Ppp2c,Pro-inflammatory Cytokine,Rb,SAA,Smad2/3,Srebp,Tnf rec	16	11	[Developmental Disorder, Hereditary Disorder, Organismal Injury and Abnormalities]
12	AGFG2,APP,CAPNS2,CIAO1,CLEC12A,CMPK2,CPED1,EGOT,GMEB1,HNRNPH1,ILRUN,ISGF3,KLF7,LMNTD1,MHC Class I (complex),mir-550,miR-550a-3p (and other miRNAs w/seed GUCUUAC),miR-550a-5p (and other miRNAs w/seed GUGCCUG),MX1,nucleoside diphosphates,OR5P2,PAX6,PRMT1,PT	16	11	[Cell Cycle, Embryonic Development, Nervous System Development and Function]
13	AMMECR1,Ap1,BTN3A1,CD3,CFL2,Cofilin,Collagen Alpha1,Collagen type I (complex),Cyclin B,cytokine,DIAPH2,EGLN,Focal adhesion kinase,HERC5,Ikb,INHBA,Laminin (complex),MAP2K1/2,Mek,Mmp,NAV3,P38 MAPK,p70 S6k,PARP,Pka,PP2A,RAS,Ras homolog,SERPING1,TCR,Tgf beta,	12	9	[Cell-To-Cell Signaling and Interaction, Cellular Growth and Proliferation, Hematological System Development and Function]
14	ALT,B-cell receptor,BCR (complex),C1q,CCL3L3,CCL4,chemokine,DKK3,ERK,Fcer1,GOT,HISTONE,IFN alpha/beta,IFN Beta,IFN type 1,Iga,Ige,IgG,IgG1,IgG2a,Igg3,IL12 (complex),IL12 (family),Immunoglobulin,MHC II,Nfat (family),PI3K (family),PLSCR1,Rac,Shc,TAGAP,TCP11	10	8	[Gastrointestinal Disease, Immunological Disease, Ophthalmic Disease]
15	ADO,ALAD,ANKRD20A4P (includes others),ATP1A2,ATP6V1G1,BTBD2,CDY1 (includes others),DDI2,DIP2A,EIF5,FAM171A2,HSPA8,HUWE1,KCNJ10,KIAA1191,MCCC1,MCCC2,MINDY1,MLLT11,MROH9,OLA1,PCCB,PCDHB12,PPIH,RIOK3,RNF123,RNF25,SGPP2,TNR,TPTE2,TRIM16L,UBC,UBE2G1,USP50,YOD1	7	6	[Developmental Disorder, Small Molecule Biochemistry, Vitamin and Mineral Metabolism]
16	CARD10,ZNF285	2	1	[Developmental Disorder, Neurological Disease, Organismal Injury and Abnormalities]
17	mir-1302,miR-1302 (and other miRNAs w/seed UGGGACA)	2	1	[]
18	miR-4279 (miRNAs w/seed UCUCCUC),MIR4279	2	1	[]
19	miR-4310 (and other miRNAs w/seed CAGCAUU),MIR4310	2	1	[]
20	miR-4432 (miRNAs w/seed AAGACUC),MIR4432	2	1	[]
21	miR-3147 (miRNAs w/seed GUUGGGC),MIR3147	2	1	[]
22	mir-3193,miR-3193 (miRNAs w/seed CCUGCGU)	2	1	[]
23	miR-3123 (miRNAs w/seed AGAGAAU),MIR3123	2	1	[]
24	miR-2681-3p (miRNAs w/seed AUCAUGG),miR-2681-5p (miRNAs w/seed UUUUACC),MIR2681	2	1	[]
25	miR-4746-3p (miRNAs w/seed GCGGUGC),miR-4746-5p (miRNAs w/seed CGGUCCC),MIR4746	2	1	[]

Table 4.2 Network analysis. The score is based on a p-value, which calculates the likelihood that the network-eligible molecules that are part of a network are found by random chance alone. The score is the negative exponent of the right-tailed Fisher's exact test results. The greater the number of network-eligible molecules, the higher the score (lower the p-value). The focused molecule indicates the number of network-eligible molecules per network. The default number of molecules per network was 35. The top diseases and functions list the three most significant functions for each network.

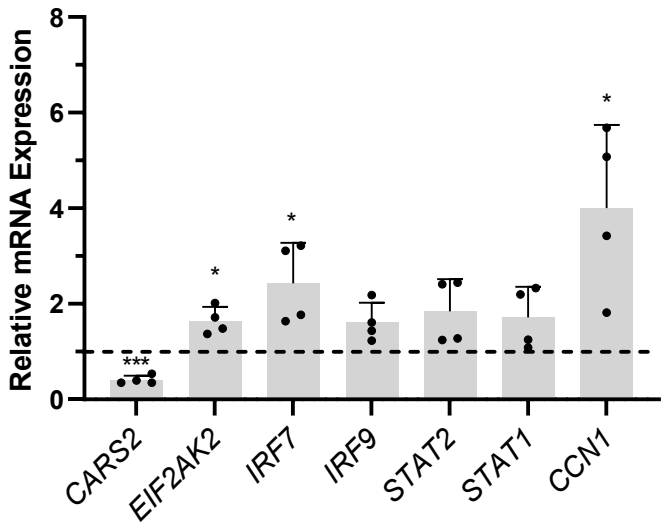

Figure 4.5 Validation of QPCR array data. Six additional genes were selected for the validation of the microarray data. Twelve additional genes were selected to validate the inflammatory array data. SRP14 was used as the internal standard. Data are presented as the mean ± SD for n = 4. (Unpaired t-test with Welch's correction) * $p < 0.05$; *** $p < 0.001$.

4.2.2 Reduced CARS2 levels increased NFKB protein expression.

Previously, the IL-10 signaling pathway was identified as a top hit by GSEA analysis of both microarray and qPCR arrays. These data indicate that CARS2 is required for optimal IL-10 signaling, consistent with its direct anti-inflammatory role. However, given that increased pro-inflammatory cytokine expression was observed in the absence of IL-10 supplementation, other pathways involving STAT3 phosphorylation are likely to be involved. The Protein Kinase R (PKR) signaling pathway was another hit identified by IPA Pathway analysis (**Figure 4.6**). Many upstream regulators identified in the microarray analysis are part of the PKR signaling pathway. PKR is required for inflammasome activation, which triggers the release of various cytokines including IL-1β[163]. Transcription factor NF-κB, a protein involved in the PKR pathway, regulates the expression of inflammatory cytokines[164]. We used western blot analysis to characterise protein expression downstream of the PKR pathway (STAT1, STAT3, NF-κB, ERK1/2, and pERK1/2 (Thr202 and Tyr204)) (**Figure 4.7**). The results showed that NF-κB protein expression significantly increased in response to *CARS2* knockdown. In addition, STAT1 levels increased albeit not significantly, consistent with the mRNA levels measured during validation (**Figure 4.5**).

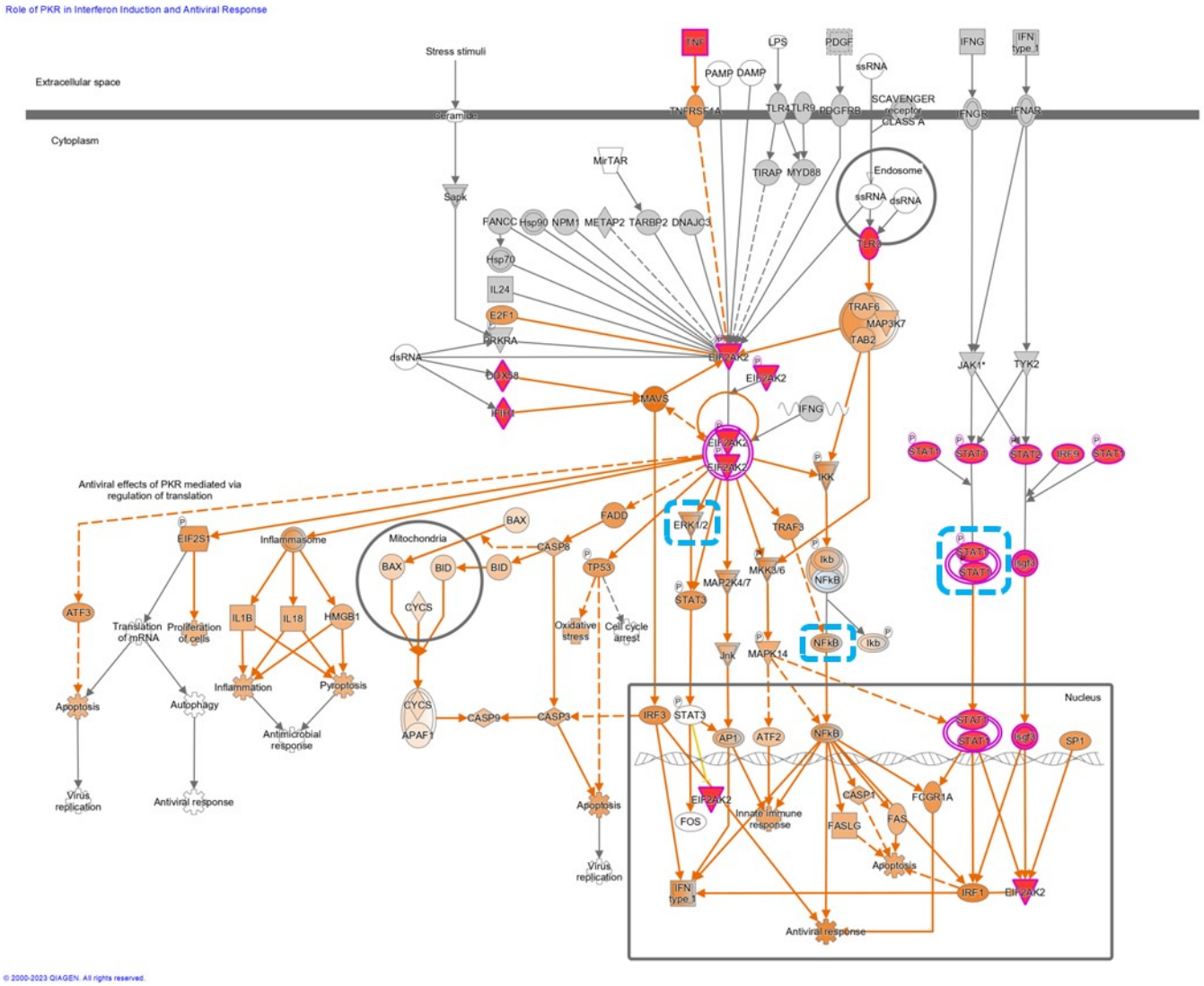

Figure 4.6 Schematic overview of the Role of PKR in Interferon Induction and Antiviral Response. Proteins of interest are highlighted by blue squares. The Canonical Pathway figure was generated through the use of QIAGEN IPA (QIAGEN Inc., https://digitalinsights.qiagen.com/IPA).

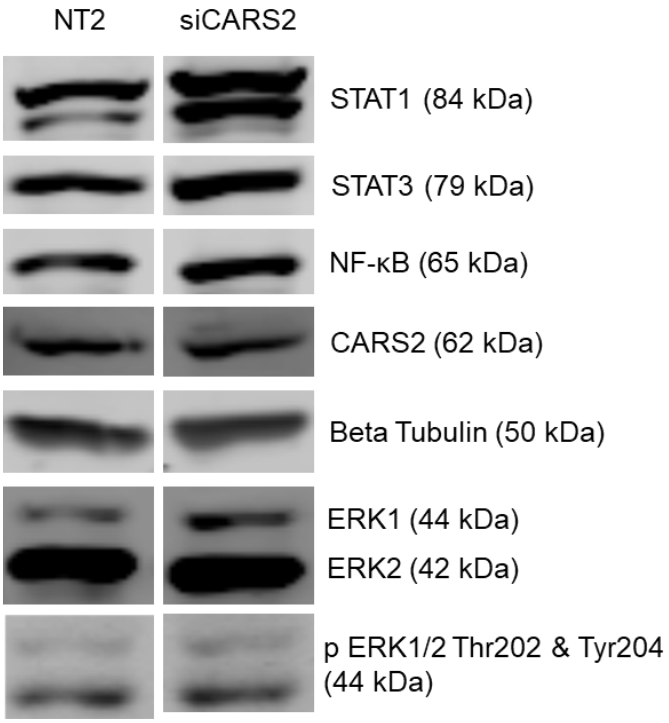

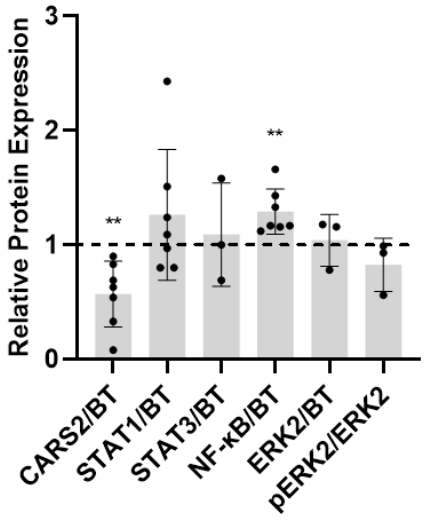

Figure 4.7 CARS2 affects protein expression in the PKR pathway. THP-1 macrophages were transfected with either *CARS2* or a control siRNA. The protein expression of STAT1, STAT3, NF-κB, CARS2, Beta Tubulin (BT), ERK1/2, and phosphorylated ERK1/2 (Thr 202 and Thr 204) was determined by western blotting. The ratio of phosphorylated protein/total protein in control-treated cells and the normalised protein expression to BT were represented as 1. Data are presented as the mean ± SD, n=3 for all proteins and n=6 for STAT1, NF-κB, and CARS2. (Unpaired t-test with Welch correction). ** $p<0.01$.

4.2.3 NF-κB translocation is not affected by lower CARS2 expression.

NF-κB translocates from the cytoplasm to the nucleus when activated by inflammatory stimuli, such as LPS[165]. Upstream, IκBα, an inhibitor of NF-κB, is phosphorylated and degraded. To better understand the increase in NF-κB expression, we investigated NF-κB protein translocation. Following *CARS2* or control siRNA transfection, the cells were fractionated to obtain cytoplasmic and nuclear fractions. Interestingly, while NF-κB increased in response to a 40% CARS2 knockdown (**Figure 4.7**), there was no change in whole cell extracts when treated with LPS (**Figure 4.8**). There was no change in phosphorylation activation in either the whole-cell or the cytoplasmic extracts. In the nuclear fraction of macrophages treated with LPS, while there was no significant change, the overall trend was increased NF-κB in reduced CARS2 macrophages compared to the control. To confirm the degradation, whole-cell samples were probed with IκBα. Following LPS treatment, IκBα protein expression significantly decreased. However, with reduced CARS2 levels, IκBα protein expression did not change (**Figure 4.9**).

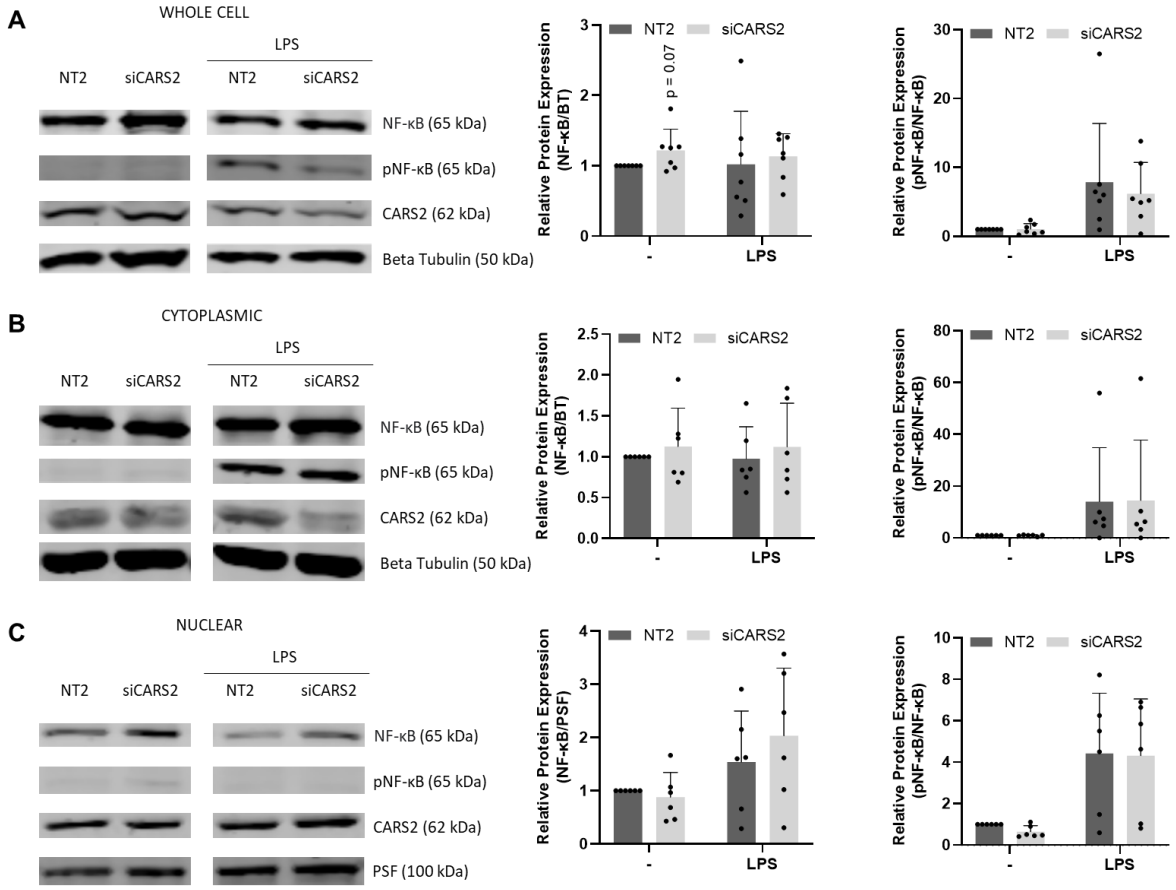

Figure 4.8 NF-κB translocation was examined by protein fractionation. NF-κB p65 nuclear translocation in THP-1 macrophages transfected with either *CARS2* or control siRNA and treated with 100 ng/mL LPS for 15 min. Cellular fractions **(A)** whole cells, **(B)** cytoplasmic fractions, and **(C)** nuclear fractions were analysed by western blotting using PSF to identify nuclear proteins and Beta-tubulin in the cytosol. WCE, whole-cell extract; CYTO, cytosolic extract; NUC, nuclear extract. Protein quantification was normalised to that of the NT2 control. Data are presented as the mean ± SD, n=6 for CYTO, NUC, and n=7 for WCE.

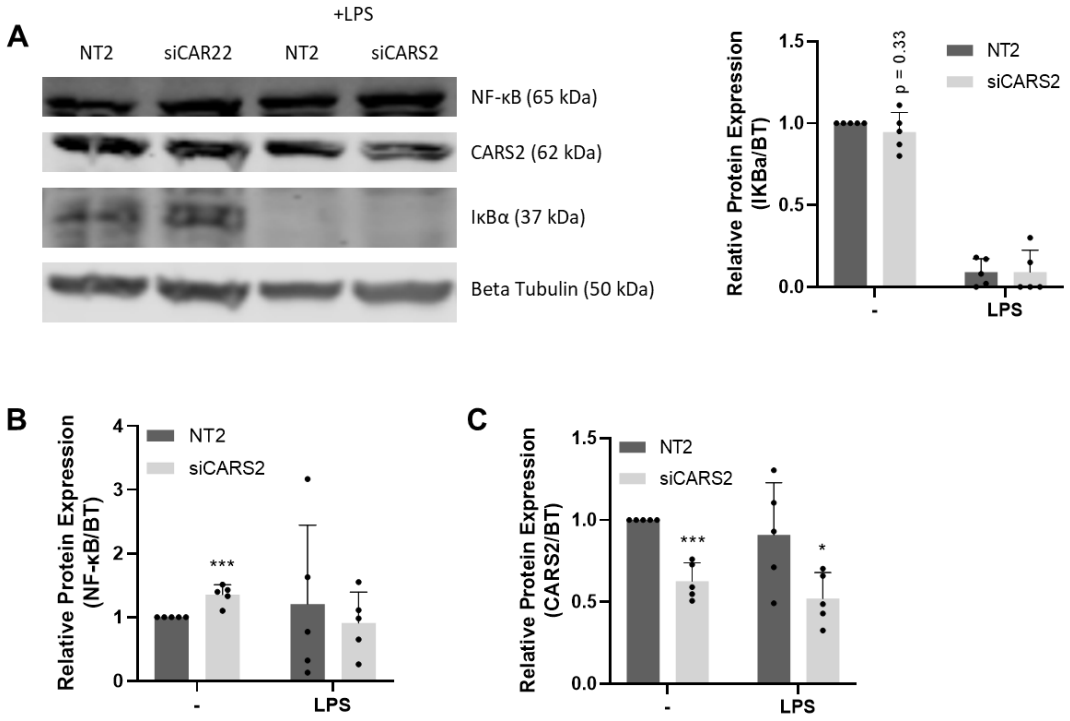

Figure 4.9 Reduced CARS2 levels may reduce NF-κB inhibitor alpha (IKB-α) expression. THP-1 macrophages were transfected with either *CARS2* or control siRNA, treated with 100 ng/mL LPS for 15 min, and the protein was harvested. Quantification of western blots for **(A)** IKB-α, **(B)** NF-κB, and **(C)** CARS2. Protein quantification was normalised to that of the NT2 control. Data are presented as the mean ± SD, n=5 (Unpaired t-test) * $p<0.05$; ** $p<0.01$.

4.2.4 NF-κB activation is decreased following reduced CARS2 levels.

Given the increase in NF-κB protein expression and translocation, we next used a luciferase NF-KB reporter THP-1 cell line to investigate NF-κB activation. Surprisingly, the reduced levels of *CARS2* significantly decreased the activation of basal NF-κB. Even after TNF-α and LPS stimulation for 6 H, NF-κB activity decreased (**Figure 4.10**). Conversely, when luciferase reporter cells were stimulated with IL-10, the NF-κB activity increased. In these cells, treatment with TNF-α and LPS dramatically increased luciferase activation (**Figure 4.10B**). Consistent with previous results, in this cell line, NF-κB protein expression was also significantly increased with CARS2 knockdown (**Figure 4.10C**). The increase in inflammatory cytokine gene expression was significant for *IL1β* and *CSF1* and trending up for *TNFα* and *IL6* (**Figure 4.10D**).

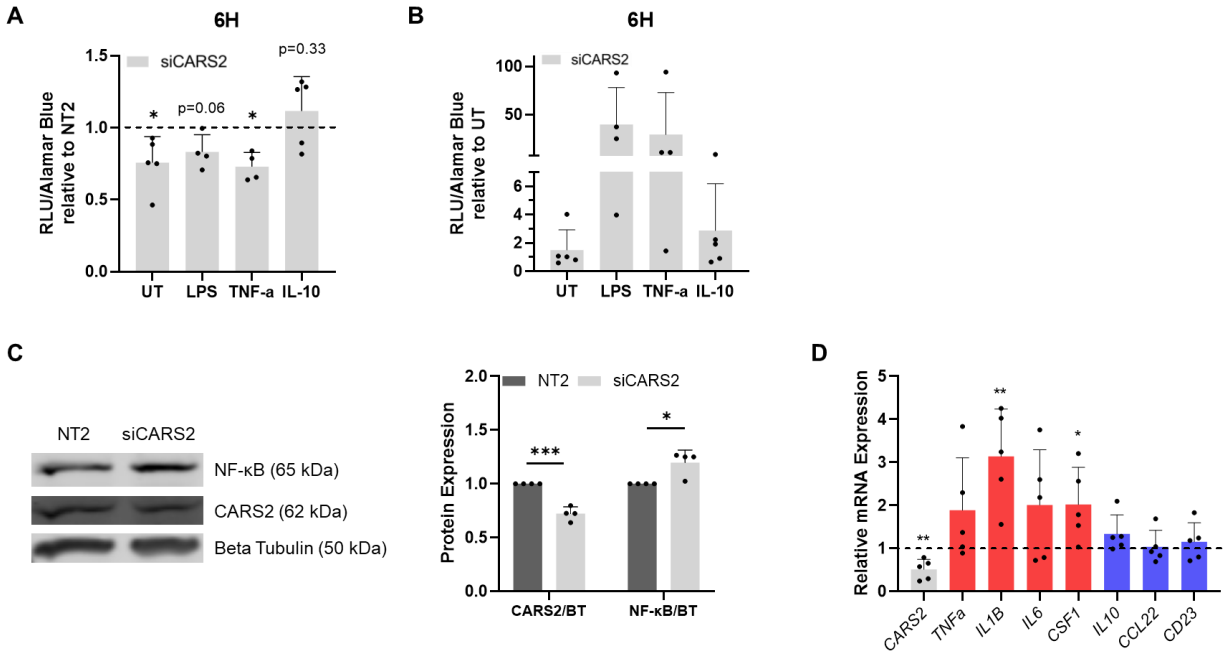

Figure 4.10 CARS2 decreased NF-κB activation after LPS treatment. THP-1 NF-κB reporter cells were transfected with *CARS2* siRNA for 96H and then treated with 100 ng/mL LPS, 20 ng/mL TNF-α, or 30 ng/mL IL-10 for 6 h. **(A)** Luciferase luminescence was measured to quantify NF-κB activation relative to alamarBlue staining. Data are shown as relative light units (RLUs) relative to respective NT2 controls. The horizontal line represents the control value (NT2) at 1. **(B)** Luciferase luminescence of *CARS2* siRNA treated macrophages relative to untreated THP-1 NF-κB reporter cells (UT). **(C)** Western blot quantification of CARS2 and NFKB protein levels in transfected THP-1 NF-κB reporter cells. Data are presented as the mean ± SD, n=4. **(D)** Inflammatory QPCR results in *CARS2* siRNA transfected THP-1 NF-κB reporter cells graphed as a fold change relative to the NT2 control. Data are presented as the mean ± SD, n=5. (Unpaired t-test) * $p<0.05$; ** $p<0.01$; *** $p<0.001$.

4.3 Discussion

We previously demonstrated that reduced levels of CARS2 in macrophages led to increased expression of inflammatory markers and in co-culture with ECs, altered SMC gene expression, indicative of a less contractile and more inflammatory state. Atherosclerosis is a chronic inflammatory disease, in which inflammation plays a role in every stage of plaque progression[24], and involves numerous signaling pathways. To investigate changes in the global gene expression profile in response to reduced CARS2 levels in macrophages, we used microarray and bioinformatic analyses to identify the potential underlying signaling pathways. IPA revealed various inflammatory pathways and regulators that were significantly affected by decreased CARS2 expression, further implicating its role in inflammation.

Canonical pathway analysis identified 42 significant pathways, the majority of which were immune- and inflammation-related. The highest-ranking pathway, "Role of hypercytokinemia/hyperchemokinemia in the pathogenesis of influenza" is characterised by cytokine dysregulation and extreme production and secretion of pro-inflammatory cytokines and chemokines. This is relevant for atherosclerosis, in which inflammation plays an important role in plaque progression[166,167]. Many of these pathways, including NF-κB and interferon signaling, are linked to atherosclerosis[29,168]. A previous study examined the transcriptomes of classically (M1) or alternatively (M2) activated mouse bone marrow-derived macrophages (BMDMs) [169]. The top pathways identified in the M1 (LPS and IFN-γ) treated macrophages were also identified in the CARS2 reduced macrophages pathways such as "Role of Hypercytokinemia/hyperchemokinemia in the Pathogenesis of Influenza", "Differential Regulation of Cytokine Production in Macrophages and T Helper Cells by IL-17A and IL-17F", Role of MAPK Signaling in Inhibiting the Pathogenesis of Influenza" and "IL-17A Signaling in

Gastric Cells" suggesting that silencing CARS2 leads to a more inflammatory, M1 like phenotype.

The top identified upstream regulators include various transcription factors linked to macrophage function and subsequent atherosclerosis. Previous studies have shown that IRF7 and IRF3 are central mediators of type I interferon-dependent (IFN-α and IFN-β) immune responses[170–172], and drive the differentiation of monocytes into macrophages[173]. *STAT1* and *STAT2* expression increased 1.5-fold when CARS2 was knocked down and was shown to be an activated upstream regulator. These STAT transcription factors are key mediators of type I and type III IFN signaling, and play important roles in cellular antiviral responses and adaptive immunity[174]. They associate with IRF9, also listed as an upstream regulator, to form a transcription factor complex known as ISGF3 that drives IFN-β stimulated gene expression[174]. STAT3 is an inhibited upstream regulator which is consistent with decreased phosphorylation when activated with IL-10 in CARS2 reduced macrophages as seen in Chapter 2. *EIF2AK2*, which encodes PKR, affects transcription factors, such as IRF3 and NF-κB, leading to increased expression of pro-inflammatory cytokines and IFNs[175–177]. These findings are consistent with the hypothesis that the atheroprotective contribution of CARS2 involves repression of various transcription factors linked to increased inflammation.

Disease and biological function analyses further supported a role for CARS2 in inflammation. The most significant functions were found to be inflammatory and immune responses, such as the "Inflammatory Response"," Immunological Disease" and "Inflammatory Disease", consistent with atherosclerosis as a chronic inflammatory disease. Of note, none of these functions are linked to epilepsy or encephalopathy, phenotypes previously linked to CARS2[123] or cysteine persulfide synthase function[127].

Toxicological analyses identified several mitochondrial-linked pathways. As a mitochondrial protein, this is consistent with mitochondrial dysfunction, such as decreased mitochondrial membrane potential and oxygen consumption rate in the absence of CARS2[127]. However, further investigations are required to determine the link between mitochondrial dysfunction and inflammation in macrophages in the context of reduced *CARS2* expression. Interestingly, many liver-linked tox functions have been identified, which are described as features of non-alcoholic fatty liver disease (NAFLD) and liver inflammation such as "Increases liver hepatitis", "LXR/RXR Activation" and "Hepatic Fibrosis" [178–180]. NAFLD represents a chronic inflammatory state and is strongly associated with atherosclerosis [181]. Previous research showed that the CAD-associated SNP rs61969072 is linked to *CARS2* expression in liver (Chapter 2), relevant to its role in inflammation. Further investigation into the role of *CARS2* in the liver should shed light on the mechanisms linking NAFLD to cardiovascular risk.

The "Role of Protein Kinase R (PKR) in Interferon Induction and Antiviral Response" pathway was identified as a significantly affected canonical pathway. PKR, a serine/threonine kinase, is activated by various signals, including interferons and cytokines[182]. PKR contributes to inflammation and immune regulation by activating downstream effectors such as inhibitor of κB (IκB) kinase (IKK) and NF-κB[176,183].

Activation of NF-κB in atherosclerotic plaques plays a role in disease progression, leading to increased levels of pro-inflammatory mediators[184]. The above findings demonstrate increased protein expression of the transcription factor NF-κB and reduced CARS2 levels in macrophages, suggesting inflammation may involve this signaling pathway. NF-κB signaling was also identified using Tox Analysis. Despite the increased expression and translocation of NF-κB under LPS-treated conditions, there was no increase in activation, as measured by p65- NF-κB

phosphorylation and luciferase assays. Using a luciferase NF-κB reporter THP-1 cell line, even under basal conditions, decreased activity was observed with lower CARS2 levels. IL-10 treatment decreased NF-κB activation, suggesting a specific role for CARS2 in an anti-inflammatory mechanism, consistent with previous lowered STAT3 activation results. An important limitation of this cell line is that we were unable to obtain any information from the vendor regarding the promoter sequence. However, the cell line does appropriately reflect NF-κB activation in response to LPS and TNF-α. This limits the interpretation of the data, as the promoter sequence may not fully reflect the NF-κB binding sequences.

Further investigation of this pathway will be required to unravel the molecular mechanism.

Chapter 5: Effects of CARS2 on mitochondrial bioenergetics and function

5.1 Introduction

Mitochondrial dysfunction can contribute to atherosclerosis by affecting major cell types in arterial walls[42,43]. Mitochondria may influence inflammation through overproduction of ROS which leads to oxidation of lipids and proteins and cellular damage[42] and by releasing mtDNA to activate innate immune receptors[44].

Mutations in *CARS2* have been shown to result in defects in mitochondrial translation, leading to mitochondrial epileptic encephalopathy and progressive myoclonic epilepsy[118,119]. Mutations affecting the highly conserved residues in the conserved functional ligase domain have been reported to cause structural changes, including incomplete assembly of complex V and deficiency of mitochondrial complexes I, III, and IV[119]. We hypothesized that mitochondrial dysfunction due to reduced CARS2 levels may be linked to increased inflammation in macrophages. To assess mitochondrial function, we used a variety of assays to measure mitochondrial bioenergetics, mitochondrial membrane potential, mtDNA levels, and ROS levels.

5.2 Results

CARS2 is encoded by the nuclear genome and is then imported into the mitochondria. Previous studies have indicated that homozygous or compound heterozygous carriers of damaging mutations in *CARS2* exhibit defects in mitochondrial translation, leading to mitochondrial epileptic encephalopathy and progressive myoclonic epilepsy[118,185]. Mutations affecting highly conserved residues in the conserved functional ligase domain have been linked to structural changes resulting in incomplete assembly of complex V and deficiency of mitochondrial

complexes I, III, and IV[185]. Here, we have further investigated the role of CARS2 in macrophage mitochondria.

5.2.1 Mitochondrial mass is unchanged by reduced CARS2 levels.

Translocase of outer mitochondrial membrane 20 (TOMM20) is a receptor subunit of the mitochondrial membrane import core and a reliable marker of mitochondrial mass. Whole protein lysates of THP-1 macrophages transfected with *CARS2* or control siRNA were analysed by western blotting and probed for TOMM20. We found no change in TOMM20 protein expression after partial CARS2 knockdown, suggesting no changes in mitochondrial mass (**Figure 5.1**).

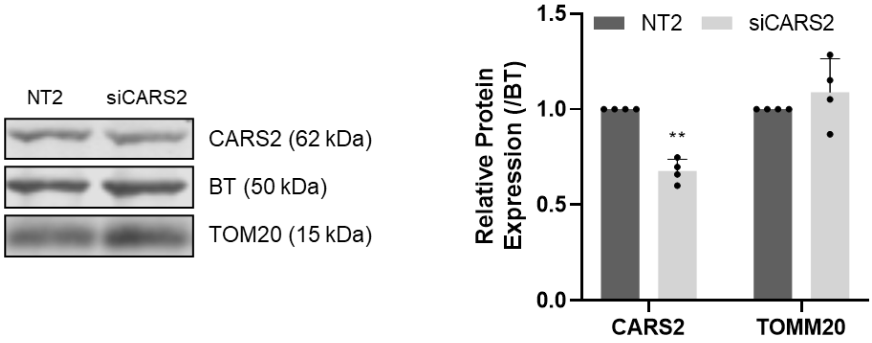

Figure 5.1 TOMM20, a marker of mitochondrial mass, remained unchanged under conditions of reduced CARS2 levels. Western blot analysis and quantification of TOMM20 protein levels in THP-1 macrophages transfected with CARS2 or control siRNA. Data represent the mean ± SD for n=4. (Student's t-Test) ** $p < 0.01$.

5.2.2 Decreasing CARS2 expression did not affect the oxygen consumption rate.

CARS2 has been shown to affect mitochondrial biogenesis and bioenergetics in HEK293T cells[186]. In *CARS2* knockout 293T cells, there was a significant decrease in the oxygen consumption rate (OCR). To characterize the metabolic energy profile in THP-1 macrophages, the Cell Energy Phenotype test was performed using a Seahorse XF96 Analyzer. The analysis examined OCR, the rate of decrease of oxygen concentration in the assay medium, a measure of mitochondrial respiration, extracellular acidification rates (ECAR), the rate of increase in proton concentration (or decrease in pH) in the assay medium, and a measure of glycolysis. Naïve THP-1 and *CARS2* or control siRNA-transfected macrophages displayed a similar metabolic phenotype, with an increase in metabolic response to Oligomycin A and FCCP compared to baseline (**Figure 5.2**). Based on the metabolic phenotype, macrophages, regardless of treatment, can be classified as "quiescent", with a relatively low glycolytic and oxidative metabolism. Metabolic potential is a measure of the ability of cells to meet their energy demands via respiration and glycolysis. The macrophages showed an increase in metabolic potential via both respiration and glycolysis when exposed to metabolic stressors. Of note, we found a slightly higher stressed ECAR compared to OCR, suggesting that they may be more dependent on glycolysis. There were no significant changes across transfections for either OCR or ECAR at baseline. When exposed to the stressors, oligomycin and FCCP, all macrophages displayed a similar response. Overall, these data suggest that moderately reduced levels of CARS2 in macrophages do not affect mitochondrial metabolism, in contrast to a previous report in *CARS2* knockout 293T cells.

The toxicity function analysis revealed various effects related to the mitochondria, one of which was "Increased Depolarization of Mitochondria and Mitochondrial Membrane".

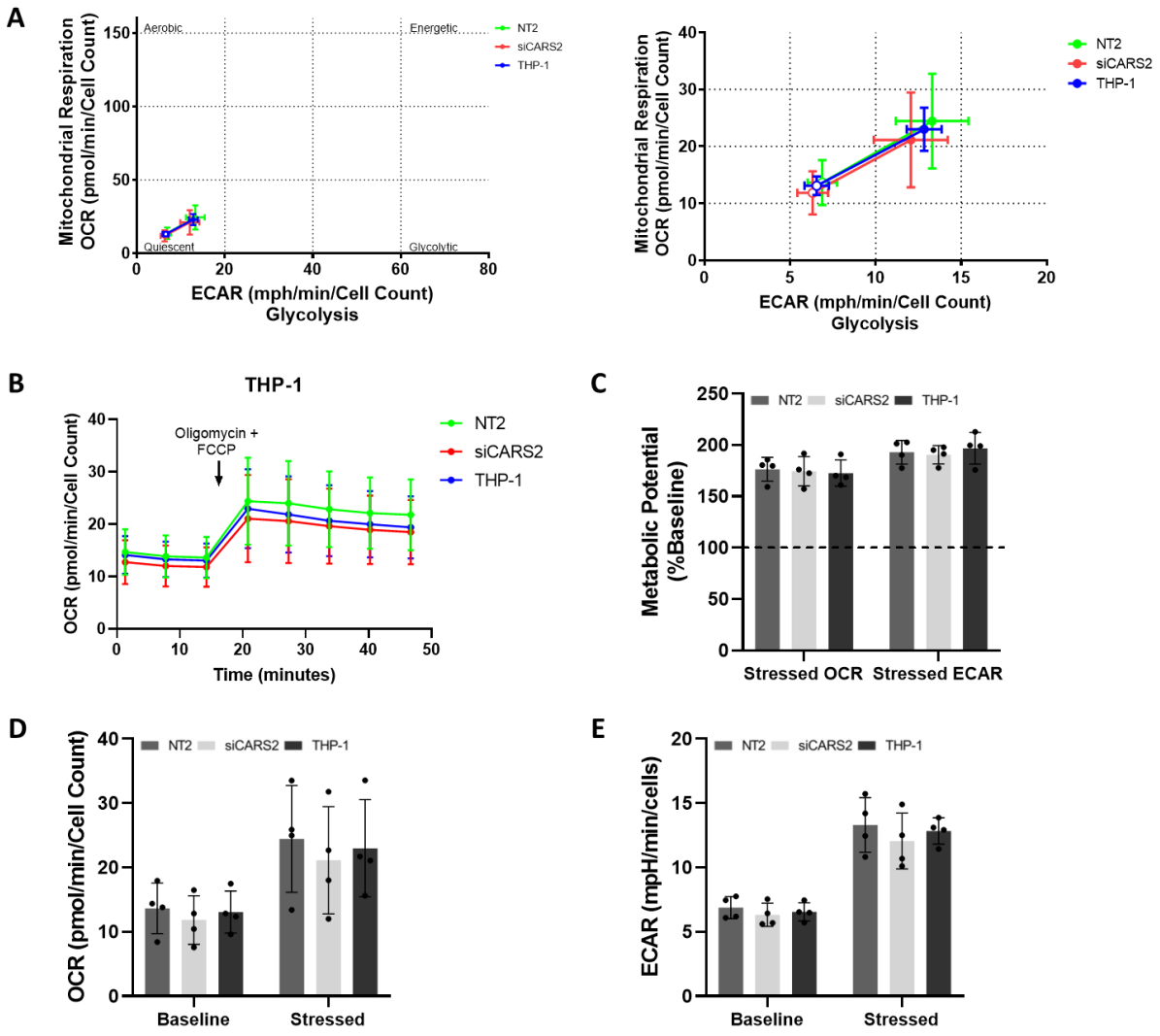

Figure 5.2 Seahorse Cell Energy Phenotype analysis of metabolic potential in THP-1 macrophages. THP-1 macrophages were transfected with *CARS2* or control siRNA for 72 h. The metabolic profile was determined using a Seahorse XF Cell Energy Phenotype assay. The oxygen consumption rate (OCR) and extracellular acidification rate (ECAR) were measured at baseline and under stress conditions (addition of 1 µM Oligomycin A and 0.5 µM FCCP). **(A)** Cell energy diagram showing normalised OCR and ECAR of control, CARS2 knockdown, and untreated THP-1 macrophages under basal (hollow) and stressed (coloured) conditions, with a magnified image. **(B)** OCR levels versus time at baseline and under stress conditions. **(C)** Metabolic Potential is shown as the percent change in OCR and ECAR under stressed over baseline (100%) conditions. Summary data for **(D)** OCR and **(E)** ECAR. Data represent the mean ± SD for n=4.

5.2.3 Mitochondrial membrane potential decreased following lower CARS2 levels.

Tetramethylrhodamine ethyl ester (TMRE) dye was used to assess the mitochondrial membrane potential. Mitochondria were depolarised by the addition of carbonyl cyanide 3-chlorophenylhydrazone (CCCP), a potent mitochondrial phosphorylation uncoupler, as a positive control. Cells were also stained with MitoTracker Green to normalise the total mitochondria. Net TMRE fluorescence decreased when THP-1 cells were treated with CCCP; however, fluorescence decreased in response to reduced *CARS2* levels (**Figure 5.3**). This is consistent with previously reported findings in *CARS2* KO HEK293T cells, where there was a decrease in JC-1 staining for membrane potential[187].

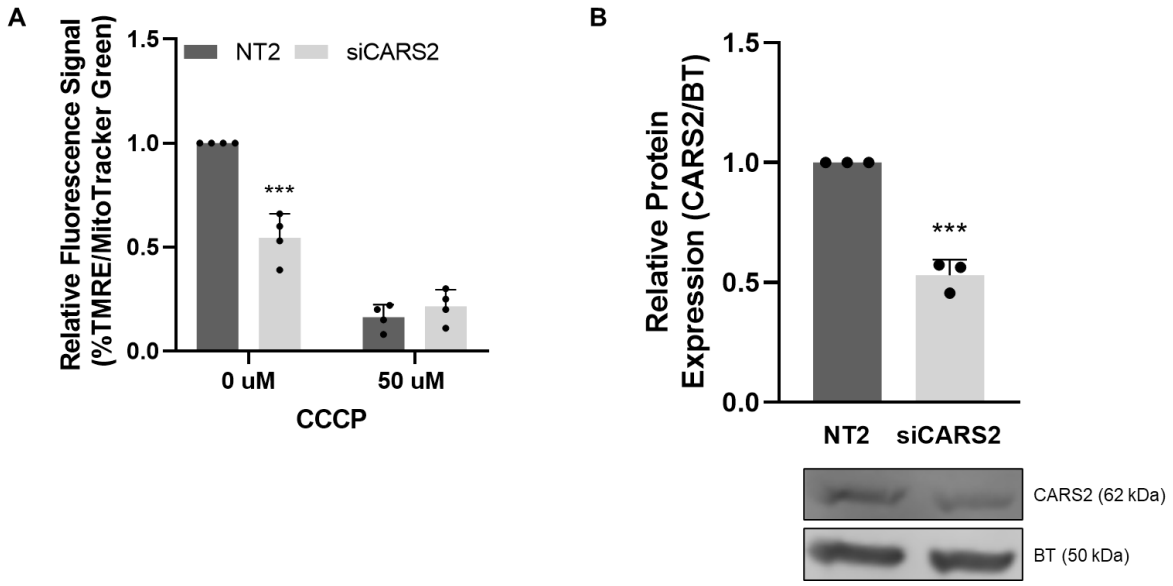

Figure 5.3 CARS2 silencing affects mitochondrial membrane potential in THP-1 cells. (A) Mitochondrial membrane potential was measured using the TMRE assay of *the CARS2* siRNA-mediated knockdown of 96H. The cells were treated with or without 50 μM CCCP for 15 min at 37°C and then stained with 200 nM TMRE and 100 nM MitoTracker Green for 20 min at 37°C. The relative fluorescence signal of TMRE was normalised to that of the NT2 control. **(B)** Western blotting analysis and quantification of CARS2 knockdown in THP-1 macrophages. Data represent the mean ± SD for n=4 and n=3 (western blotting). (Unpaired t-test) * $p<0.05$; ** $p<0.01$; *** $p<0.001$.

5.2.4 Cytosolic mitochondrial DNA release was not affected by reduced CARS2 expression.

A decrease in mitochondrial membrane potential could lead to the release of mitochondrial DNA (mtDNA) into the cytoplasm acting as a danger signal activating downstream innate immune pathways such as the NF-κB signaling pathway as well as the nod like receptor family pyrin domain containing 3 (NLRP3) inflammasome[44]. To measure free mtDNA in the cytosol, we performed cellular fractionation to extract mtDNA from the cytosolic fraction and quantified mtDNA using qPCR. We assessed mtDNA by measuring the mitochondrial genes *MTCO1*, *MTCO3*, and the non-coding region *DLoop*. As shown in **Figure 5.4**, cytosolic mtDNA expression varied greatly across genes in the CARS2 knockdown macrophages. This may be an artifact of the fractionation process. Overall, the free cytosolic mtDNA copy number varied across all the samples. In the whole-cell fraction, the overall mtDNA copy number did not change with knockdown. Unfortunately, the mtDNA results were inconclusive because of variable levels of mtDNA in whole and cytoplasmic fractions. This may be because the technique did not involve clean fractionation or different mitochondrial amounts were present. Column separation may represent a better approach. Despite methodological limitations, these data suggest that the decreased mitochondrial membrane potential does not induce the release of mtDNA into the cytosol.

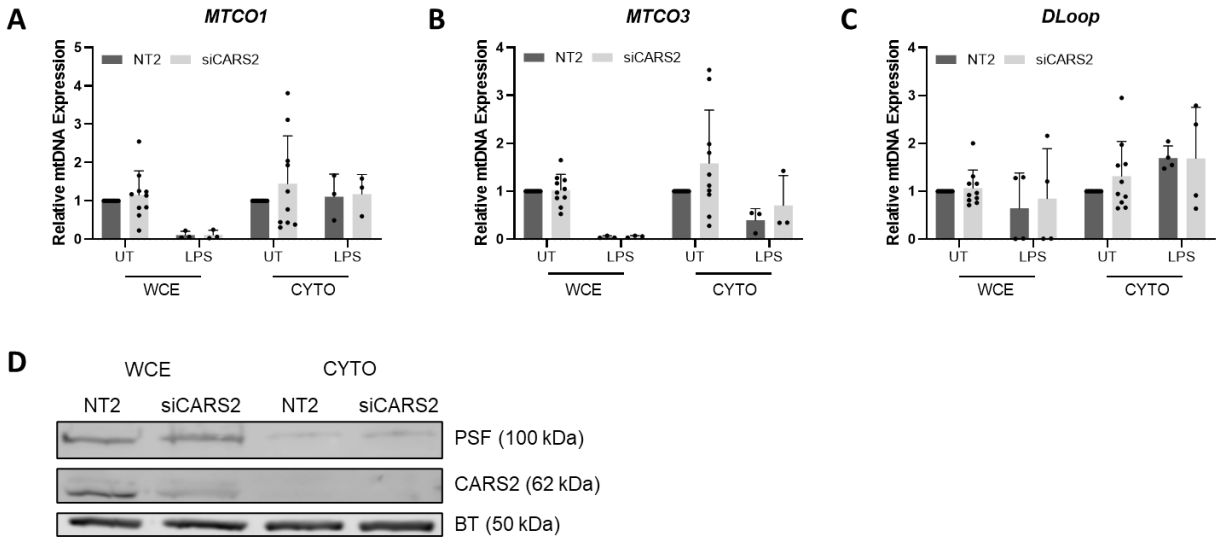

Figure 5.4 Assessment of cytosolic mitochondrial DNA (mtDNA) release. (A) Western blotting of the cellular fractions using PSF to detect the nuclear protein, CARS2 for mitochondria, and Beta Tubulin in the cytosol. WCE, whole-cell extract; CYTO, cytosolic extract. **(B)** THP-1 macrophages were fractionated, and mtDNA quantification was performed using the *MTCO1*, *MTCO3*, and *DLoop* genes in the cytosolic fraction and normalised to the quantification of the nuclear gene *SLCO2B1* in the whole-cell fraction. The data were plotted as fold-changes in expression relative to NT2 control macrophages. The data represent the mean ± SD for n=10, n=3 (LPS-treated samples *MTCO1* and *MTCO3*), and n=4 (LPS-treated samples *DLoop*).

5.2.5 Reduced CARS2 expression decreased reactive oxygen species levels.

Reactive oxygen species (ROS) are believed to play a significant but complex role in atherosclerosis. To understand the mechanism that leads to increased inflammation in response to reduced CARS2 levels, we used the fluorogenic dye DCFDA to measure the ROS levels[188]. Interestingly, ROS levels decreased following knockdown, contrary to the pro-inflammatory effect of reduced CARS2 (**Figure 5.5**). DCFDA responds to changes in intracellular iron signaling or enhanced peroxidase activity.

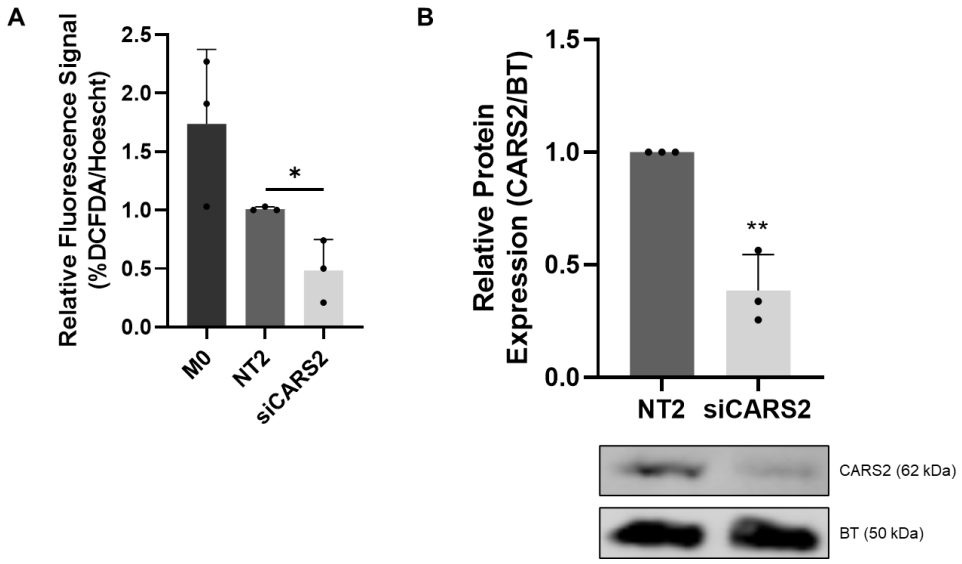

Figure 5.5 Decreased reactive oxygen species (ROS) in macrophages with reduced CARS2 levels. THP-1 macrophages were transfected with *CARS2* or control siRNA for 72 h. ROS levels were measured by the oxidation of DCFDA dye using a fluorescence microplate reader. Cells were stained with 25 μM DCFDA and 1 μM Hoechst for 30 and 5 min, respectively. **(A)** Representative graph of DCF fluorescence relative to control. **(B)** Western blotting analysis and quantification of CARS2 knockdown in THP-1 macrophages. Data represent the mean ± SD for n=3. (Unpaired t-test) * $p<0.05$; ** $p<0.01$; *** $p<0.001$.

5.2.6 Mitochondrial biogenesis, measured by MTCO1 protein expression, is decreased with lower CARS2 levels.

A previous study demonstrated incomplete assembly of mitochondrial complexes in the liver and muscle samples of a patient with compound heterozygous mutations in *CARS2*[185]. To investigate whether *CARS2* affects complex gene expression, representative genes encoding a subunit from the electron transport chain (ETC) complexes and ATP synthases were selected: *NDUFB8* (complex I), *SDHB* (complex II), *UQCRC2* (complex III), COX5A (complex IV), and *ATP5F1A* (ATP synthase). The gene expression of the subunits was measured in CARS2 knockdown THP-1 macrophage samples. There was no change in the subunit gene expression following *CARS2* knockdown (**Figure 5.6**). Knockdown of *CARS2* in THP-1 macrophages did not affect the expression of subunits of the ETC complexes and ATP synthase. Thus, partial knockdown of *CARS2* does not recapitulate the effects of complete *CARS2* deficiency. Consistently, individuals who are haplodeficient for *CARS2* have not been reported to exhibit a clinical CAD phenotype and whole exome sequencing studies did not identify CAD-associated mutations in *CARS2*. MTCO1 is one of three mitochondrial DNA-encoded subunits of the respiratory Complex IV. As CARS2 plays an important role in mitochondrial protein translation, Cytochrome C oxidase subunit 1 (MTCO1) protein expression was assessed in *CARS2* or control siRNA transfected THP-1 macrophages. Interestingly, MTCO1 protein expression was significantly decreased in *CARS2* knockdown THP-1 macrophages, suggesting that *CARS2* may affect protein translation. A ~40% reduction in CARS2 protein expression resulted in decreased MTCO1 expression (**Figure 5.6B**). These non-denatured samples did not contain a reducing agent (BME) and were not boiled. This is consistent with prior data on mutations in *CARS2* that lead to incomplete assembly of mitochondrial complex IV. These findings are consistent with the expectation that reduced CARS2 protein expression affects mitochondrial translation in macrophages.

In the study done by Akaike et al., most of the mitochondrial assays were "fixed" by adding persulfide-active mutants, which rescued persulfide production of CARS2 KO 293T cells[187]. In further studies, it would be informative to investigate specific persulfide activity in macrophages and determine the effects. Of note, H_2S is associated with an anti-atherosclerotic effect and can decrease foam cell formation[189].

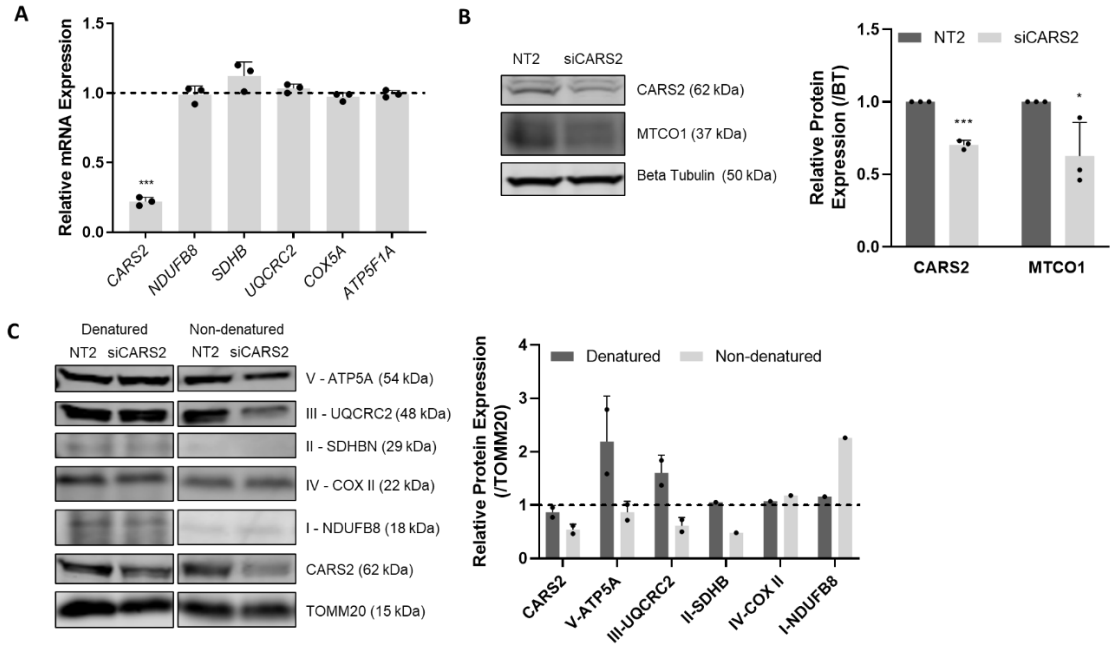

Figure 5.6 CARS2 affects MTCO1 protein expression in THP-1 macrophages. THP-1 macrophages were transfected with *CARS2* or control siRNA for 72 h. **(A)** Gene expression of subunits from the electron transport chain (ETC) complexes and ATP synthase is graphed as a fold change in expression versus NT2 siRNA. The housekeeping gene *SRP14* was used as the internal standard. Data represent the mean ± SD for n=3. **(B)** Western blot analysis and quantification of non-denatured MTCO1 protein levels to assess mitochondrial translation. Data represent the mean ± SD for n=3. **(C)** Western blot analysis and quantification of OXPHOS subunits. The non-denatured samples did not contain a reducing agent (BME) and were not boiled. Data are presented as the mean ± SD for n=2 and n = 1 (II-SDHB, IV-COX II, and I-NDUF8). (Student's t-Test) * $p < 0.05$; *** $p < 0.001$.

5.3 Discussion

Here we have assessed the possible role of mitochondria in the anti-inflammatory effects of CARS2. Our findings demonstrate that reduced CARS2 levels in macrophages decrease mitochondrial membrane potential and MTCO1 protein expression. Unexpectedly, ROS levels decreased and cytosolic mtDNA levels varied across the knockdown conditions. Although the results do not clearly identify a direct link between mitochondrial dysfunction and inflammation, they are consistent with those of previous studies.

CARS2 is a mitochondrial cysteinyl tRNA synthetase that functions as cysteine persulfide synthase affecting mitochondrial biogenesis and bioenergetics[187]. Genetic findings and cell-based studies of altered *CARS2* expression have demonstrated effects on mitochondrial function. A previous case study of a patient with compound heterozygous mutations in *CARS2* showed combined respiratory chain enzyme deficiency associated with severe epileptic encephalopathy[185].

Mitochondria have been shown to play a role in innate immune and inflammatory responses. The mitochondrial antiviral signaling protein (MAVS) mediates the activation of NF-κB and IRF in response to viral infection, leading to the production of pro-inflammatory cytokines and type 1 interferon[190]. Dysfunctional mitochondria, through increased ROS levels, accumulated mitochondrial DNA damage, and progressive respiratory chain dysfunction have been shown to be associated with inflammation and atherosclerosis[191]. Mitochondrial ROS and oxidised mtDNA can trigger NLRP3 inflammasome activation[192–194]. NLRP3 activation is a key event in the inflammatory process of atherosclerosis that leads to IL-1 production[195]. Mitochondrial dysfunction via oxidative damage has been linked to the initiation and progression of atherosclerotic plaques[196].

The expression level of TOMM20, a component of the translocase of the outer mitochondrial membrane, was used to estimate mitochondrial mass and, subsequently, mitochondrial biogenesis[197,198]. Mitochondrial biogenesis is marked by increased expression of components of the protein import machinery and the growth and division of existing mitochondria, leading to increased mitochondrial mass. When assessing TOMM20 protein levels by western blotting, partially reduced CARS2 levels did not elicit changes in the mitochondrial mass. This is likely related to the action of residual CARS2 since in 293T CARS2 KO cells, TOMM20 fluorescence demonstrated alterations in mitochondrial morphology[187], reportedly shrunken and fragmented organelles. In the latter study, quantitative analyses and total mitochondrial mass were not determined. However, performing immunofluorescence on silenced CARS2 macrophages will shed light on mitochondrial morphology.

Metabolically, pro-inflammatory M1 macrophages mainly rely on glycolysis[199], whereas anti-inflammatory M2 macrophages are more dependent on oxidative phosphorylation (OXPHOS)[200]. However, despite an increased inflammatory profile, suggesting a more M1-like phenotype, there were no significant changes in OCR in *CARS2* silenced THP-1 macrophages. These data are in contrast to a previous report of decreased OCR levels in HEK293T CARS2 knockout (KO) cells. This may be explained by differences between the two cell types, THP-1 macrophages versus HEK293T cells, efficacy of knockdown and siRNA methodology. The HEK293T cells continually divide and are highly energetic with robust glycolytic and respiratory activity[201], while THP-1 macrophages, once differentiated no longer divide and seem to be more quiescent. THP-1 macrophages are also harder to transfect[202] compared to HEK293T cells, resulting in only around a 30% protein level knockdown in THP-1 macrophages compared to an 80% knockdown in the HEK293T CARS2 knockout cells[187]. Even so, these authors transfected the HEK293T

CARS2 knockout cells with stealth *CARS2* siRNA on top of that compared to our silencer siRNA, which has less target specificity.

Although no changes were observed in OCR levels, we found decreased MTCO1 protein levels as part of Complex V. This is consistent with the above studies in 293T CARS2 KO cells, suggesting a change in tRNA activity[187].

Consistent with previously reported data in HEK293T CARS2 KO cells, mitochondrial membrane potential decreased in *CARS2* knockdown THP-1 macrophages. Maintenance of the mitochondrial membrane potential is a key function of the electron transport chain and is necessary for other processes, such as mitochondrial biogenesis[203]. Mitochondrial dysfunction is linked to inflammatory responses, with studies linking this response to mitochondrial calcium exchange, ROS generation, and NF-κB activation[204,205]. Of note, degraded mtDNA was found to strongly induce inflammation in astrocytes[206]. The mitochondrial membrane is also negatively affected by inflammatory mediators such as TNF-α and IL-1β[207]. It is unclear as to whether inflammation causes changes in mitochondrial membrane potential or *vice versa*. We next proceeded to investigate this relationship in *CARS2* targeted THP-1 macrophages.

Here, using DCFDA dye, we found that ROS decreased in THP-1 macrophages in response to *CARS2* knockdown. The DCFDA dye detects cytoplasmic ROS but confounders exist since other variables can oxidise DCFH, such as reduced GSH levels, cytochrome c release from mitochondria, and increased peroxidase activity[208]. Other approaches might include the use of Mito-SOX to measure intracellular oxidants and mitochondrial superoxide (O_2) formation to confirm mitochondrial ROS levels in CARS2 silenced cells. Importantly, the relationship of ROS to inflammation is complex. In contrast to the commonly accepted paradigm, several studies have shown that decreased ROS levels lead to increased (rather than decreased) expression of

inflammatory cytokines[209–211]. Specifically, ROS generated by NADPH oxidase 4 (NOX4), can promote the clearance of apoptotic cells and debris, reduce inflammatory responses, and promote tissue repair[209–211].

In summary, partial deficiency of CARS2 does not confer significant mitochondrial dysfunction in contrast to the effects of a complete lack of CARS2, on a genetic or cellular basis. Further investigation of the link between the atheroprotective effects of CARS2 and mitochondrial function is required.

General Discussion and Future Directions

It is well recognized that genetics plays an important role in CAD development. The narrow-sense heritability of CAD has been estimated to be approximately 40%[48,212]. Since 2007, GWAS have identified over 300 loci associated with CAD, explaining less than 25% of CAD heritability[74,213]. This indicates that the majority of genetic variants underlying CAD heritability are still missing. However, over 300 FDR variants ($q<0.05$) have been identified, adding more evidence of association, which together explain approximately 21.2% of CAD heritability[76,77]. This heritability increased to 36.1% when including 897 associations at a significance level ($P < 2.52 \times 10^{-5}$), approximating a 1% FDR[77,213]. The heritability of complex traits such as CAD is the sum of numerous common genetic variants conferring individually minor impacts that do not reach genome-wide significance.

With larger studies, new identified loci will typically have smaller effect sizes[214]. Although the majority of CAD-associated variants have individually minor effects (<20% change in risk)[215], the data derived from GWAS has therapeutic implications[213] in both risk assessment and the identification of novel therapeutic targets. A polygenic risk score consisting of 6.6 million common genetic variants was strongly predictive of CAD risk[216]. In addition, Aragam et al. uncovered common variant associations of weak effects of *HMGCR* and *NPC1L1*, which encode the targets of HMG-CoA reductase inhibitors (statins) and ezetimibe[213]. Statins and ezetimibe are two of the most effective and commonly prescribed medications for CAD prevention and treatment.

During this post-GWAS era, despite the rapid growth in genetic association discoveries, functional genomic studies to determine the causality of GWAS variants and gene mechanisms

have been a slow and tedious process[217]. The subsequent translation of these mechanisms into novel therapeutic targets remains a challenge. The causal genes and functions of over 50% of the CAD GWAS loci have not yet been identified[215]. However, Mendelian randomization analyses of GWAS has confirmed the causal nature of classic CAD risk factors, such as LDL cholesterol, hypertension, and coagulation, as well as highlighted the causal roles of cellular proliferation and adhesion, extracellular matrix, and inflammation[215].

Several factors have made it difficult to bridge the gap between GWAS-associated SNPs and loci for a functional understanding of disease etiology. As discussed in Chapter 1: Introduction, these include the identification of the causal variant(s) and the target gene(s) and determining the relevant cell types for a model system. Even after the identification of a causal gene, understanding its role in the disease can be even more challenging and time-consuming. The 9p21 CAD locus encoding *CDKN2BAS* is presumed to be related in part to its effects on SMC proliferation, but its mechanism(s) remain unclear[82]. It has only recently been reported that this locus controls large gene networks in vascular SMCs, predisposing them to assume atherogenic-like states[218]. Similarly, the functional relationship between GWAS polymorphisms in the *TRIB1* locus and genes remains unclear and is the focus of ongoing research[219], although it is a promising regulator of lipid metabolism. Increased emphasis on downstream functional studies of loci that have already identified GWAS loci may be more fruitful than a continued search for more GWAS loci[217].

The goal of this dissertation was to investigate the functional relationship between the *CARS2* locus and atherosclerosis pathogenesis. The causal SNP rs61969072 is an FDR significant variant in a non-coding region and has a small effect size ((beta = −0.0584)[76], lending further support to the importance of variants that are of small effect size. *CARS2* was found to have a

novel inflammatory role in THP-1 macrophages. Reducing *CARS2* levels led to increased levels of inflammatory cytokines such as TNF-α, IL-6, and IL-1β. Globally, these studies demonstrate that many inflammatory and immune pathways are activated by CARS2 knockdown in macrophages, as demonstrated by expression array analysis. Macrophages promote inflammatory responses and SMC recruitment to atherosclerotic lesions[143]. This also has implications for the crosstalk between macrophages and SMCs, as shown in the co-culture data. Reduced *CARS2* levels in macrophages co-cultured with SMCs resulted in a decreased contractile phenotype and an accompanying increase in inflammatory markers in SMCs. This highlights how the role of CARS2 in inflammation can affect other cell types present in atherosclerotic plaques such as SMCs, potentially affecting their ability to repair and maintain fibrous caps[22].

Although elucidating the mechanism(s) by which CARS2 decreases inflammation has been challenging, we suggest that it may not occur through mitochondrial dysfunction (Chapter 4). However, the mechanism leading to increased inflammation remains unclear. One potential mechanism could be the role of CARS2 as the principal cysteine persulfide synthase (CPERS).

CARS2/CPERS play a role in inflammation-related bone loss via sulfide synthesis[129]. The persulfides produced by CARS2/CPERS are required to degrade 8-nitro-cGMP, a secondary messenger of NO and ROS[129]. In the absence of degradation, 8-nitro-cGMP contributes to inflammation-related reduction of bone mass[129]. In a recently published study, Matsunaga et al. demonstrated increased inflammation in *Cars2*-deficient (*Cars2*$^{+/-}$) mice. Bronchoalveolar lavage fluid (BALF) and lung fluid were collected, and the concentrations of TNF-α and IL-6 were significantly higher in *Cars2*$^{+/-}$ mice than in wild-type (WT) mice[220]. In the same study, glutathione trisulphide (GSSSG), a persulfide produced by CARS2/CPERS, was administered to influenza-infected WT mice, resulting in reduced pathological and inflammatory

consequences[220]. This suggests that oxidised glutathione trisulphide (GSSSG), produced by CARS2, has strong inflammatory effects, can ameliorate cytokine storms, and has specific immune responses, thereby demonstrating protective functions against inflammatory diseases[220]. In another study, GSSSG produced by CARS2 was shown to be effective in lowering pro-inflammatory gene expression in *Slc7a11* knockout mouse peritoneal macrophages[221]. *Slc7a11* encodes a cystine transporter and serves as a major channel for the cysteine supply. Taken together, these data suggest that CARS2/CPERS produces persulfides that promote inflammation resolution.

Other sulfurtransferase enzymes which can produce hydrogen sulfide (H_2S) and persulfides include 3-mercaptopyruvate sulfurtransferase (3-MST), cystathionine β-synthase (CBS), and cystathionine γ-lyase (CSE)[128]. Studies have demonstrated that CSE plays an essential role in the cardiovascular system[222]. CSE-produced H_2S can modify the post-translational thiol to NF-kB, affecting its anti-apoptotic transcriptional activity[223]. However, CARS2 was demonstrated to be the principal enzyme compared to CBS, CSE, and 3-MST, which are primarily responsible for the biosynthesis of reactive persulfides and polysulfides in mammals[128]. The function of CARS2 as a CPERS calls for further research on whether persulfide production can affect inflammation in macrophages.

With respect to future directions in investigating the mechanism of CARS2 involvement in inflammation, examining its role as CPERS may be informative, particularly in the context of human macrophages and atherosclerosis. Thus, the next step would be to characterise the function of CARS2/CPERS in human THP-1 macrophages by altering *CARS2* expression through knockdown and overexpression. The intracellular levels of persulfides (cysteine hydropersulfide (CysSSH), perhydropersulfide (GSSH), and trihydropersulfides (GSSSH)) and

sulfide derivatives can be measured to assess the function of CPERS[127]. Persulfides can also be indirectly quantified by measuring H2S/HS − released by dithiothreitol (DTT) treatment[224]. In the overexpression model, the cells will be supplemented with controlled concentrations of cysteine and cystine as substrates for CPERS function. Following characterisation, the THP-1 macrophages can be treated with GSSSG, a by product of CPERS and inflammation can be measured both at the mRNA and protein level. GSSSG treatment has been shown to inhibit pro-inflammatory cytokine production in glial cells[225].

This study primarily used cell lines to study *CARS2*, which is not reflective of the complex cell types that make up atherosclerotic lesions. The next step would be to study the full body effect of the *CARS2* knockout in a mouse model. The full *CARS2* knockout mouse model is embryonic lethal[127]; however, heterozygous knockout *Cars2*$^{+/-}$ mice demonstrated increased inflammation[220]. Further investigation of plaque progression in these mice may reveal a contribution of decreased persulfide levels.

Conclusion

Over 300 CAD-associated loci have been identified in GWAS studies. However, identifying the causative mechanisms linking causal genes and variants to biological mechanisms remains challenging. This thesis addresses the mechanism by which the FDR-variant, rs61969072, and causal gene *CARS2* are linked to CAD risk. Here, I demonstrated a novel anti-inflammatory role of CARS2, which is linked to the effect of rs61969072 on *CARS2* expression. I demonstrated that reducing *CARS2* levels in macrophages leads to increased inflammation globally. CARS2 also affects specific pathways, such as the NF-kB signaling pathway, and can lower the activation of the anti-inflammatory IL-10 signaling pathway. Also, the increased inflammation in CARS2 reduced macrophages is shown to affect SMC through crosstalk, leading to a more

contractile SMC phenotype. Although the exact mechanism of CARS2 related inflammation has not been elucidated in human macrophages and we have not been able to identify a role for mitochondrial dysfunction, further studies are required. Future directions include exploring the role of CARS2 CPERS in the context of macrophages and atherosclerosis.

References

1. Vaduganathan, M., Mensah, G. A., Turco, J. V., Fuster, V. & Roth, G. A. The Global Burden of Cardiovascular Diseases and Risk. *Journal of the American College of Cardiology* **80**, 2361–2371 (2022).
2. Libby, P., Ridker, P. M. & Hansson, G. K. Progress and challenges in translating the biology of atherosclerosis. *Nature* **473**, 317–325 (2011).
3. Gui, Y., Zheng, H. & Cao, R. Y. Foam Cells in Atherosclerosis: Novel Insights Into Its Origins, Consequences, and Molecular Mechanisms. *Frontiers in Cardiovascular Medicine* **9**, (2022).
4. Sakakura, K. *et al.* Pathophysiology of atherosclerosis plaque progression. *Heart Lung Circ* **22**, 399–411 (2013).
5. Nakashima, Y., Chen, Y.-X., Kinukawa, N. & Sueishi, K. Distributions of diffuse intimal thickening in human arteries: preferential expression in atherosclerosis-prone arteries from an early age. *Virchows Arch* **441**, 279–288 (2002).
6. Stary, H. C. *et al.* A definition of the intima of human arteries and of its atherosclerosis-prone regions. A report from the Committee on Vascular Lesions of the Council on Arteriosclerosis, American Heart Association. *Circulation* **85**, 391–405 (1992).
7. Virmani, R., Kolodgie, F. D., Burke, A. P., Farb, A. & Schwartz, S. M. Lessons From Sudden Coronary Death. *Arteriosclerosis, Thrombosis, and Vascular Biology* **20**, 1262–1275 (2000).
8. Getz, G. S. The Involvement of Lipoproteins in Atherogenesis Evolving Conceptsa. *Annals of the New York Academy of Sciences* **598**, 17–28 (1990).
9. Nakashima, Y., Fujii, H., Sumiyoshi, S., Wight, T. N. & Sueishi, K. Early Human Atherosclerosis. *Arteriosclerosis, Thrombosis, and Vascular Biology* **27**, 1159–1165 (2007).
10. Grundy, S. M. Small LDL, Atherogenic Dyslipidemia, and the Metabolic Syndrome. *Circulation* **95**, 1–4 (1997).
11. Steinberg, D. Low Density Lipoprotein Oxidation and Its Pathobiological Significance *. *Journal of Biological Chemistry* **272**, 20963–20966 (1997).
12. Yoshida, H. & Kisugi, R. Mechanisms of LDL oxidation. *Clinica Chimica Acta* **411**, 1875–1882 (2010).
13. Khan, B. V., Parthasarathy, S. S., Alexander, R. W. & Medford, R. M. Modified low density lipoprotein and its constituents augment cytokine-activated vascular cell adhesion molecule-1 gene expression in human vascular endothelial cells. *J Clin Invest* **95**, 1262–1270 (1995).
14. Takei, A., Huang, Y. & Lopes-Virella, M. F. Expression of adhesion molecules by human endothelial cells exposed to oxidized low density lipoprotein. Influences of degree of oxidation and location of oxidized LDL. *Atherosclerosis* **154**, 79–86 (2001).
15. Navab, M. *et al.* Normal high density lipoprotein inhibits three steps in the formation of mildly oxidized low density lipoprotein: step 1. *Journal of Lipid Research* **41**, 1481–1494 (2000).
16. Mestas, J. & Ley, K. Monocyte-Endothelial Cell Interactions in the Development of Atherosclerosis. *Trends Cardiovasc Med* **18**, 228–232 (2008).
17. Moore, K. J. & Freeman, M. W. Scavenger Receptors in Atherosclerosis. *Arteriosclerosis, Thrombosis, and Vascular Biology* **26**, 1702–1711 (2006).

18. de Villiers, W. J. S. & Smart, E. J. Macrophage scavenger receptors and foam cell formation. *Journal of Leukocyte Biology* **66**, 740–746 (1999).
19. Glass, C. K. & Witztum, J. L. Atherosclerosis: The Road Ahead. *Cell* **104**, 503–516 (2001).
20. Doran, A. C., Meller, N. & McNamara, C. A. The Role of Smooth Muscle Cells in the Initiation and Early Progression of Atherosclerosis. *Arterioscler Thromb Vasc Biol* **28**, 812–819 (2008).
21. Allahverdian, S., Chehroudi, A. C., McManus, B. M., Abraham, T. & Francis, G. A. Contribution of Intimal Smooth Muscle Cells to Cholesterol Accumulation and Macrophage-Like Cells in Human Atherosclerosis. *Circulation* **129**, 1551–1559 (2014).
22. Amento, E. P., Ehsani, N., Palmer, H. & Libby, P. Cytokines and growth factors positively and negatively regulate interstitial collagen gene expression in human vascular smooth muscle cells. *Arterioscler Thromb* **11**, 1223–1230 (1991).
23. Tabas, I. Macrophage death and defective inflammation resolution in atherosclerosis. *Nat Rev Immunol* **10**, 36–46 (2010).
24. Ross, R. Atherosclerosis--an inflammatory disease. *N Engl J Med* **340**, 115–126 (1999).
25. Tedgui, A. & Mallat, Z. Cytokines in Atherosclerosis: Pathogenic and Regulatory Pathways. *Physiological Reviews* **86**, 515–581 (2006).
26. Tsuchiya, S. *et al.* Establishment and characterization of a human acute monocytic leukemia cell line (THP-1). *Int J Cancer* **26**, 171–176 (1980).
27. Qin, Z. The use of THP-1 cells as a model for mimicking the function and regulation of monocytes and macrophages in the vasculature. *Atherosclerosis* **221**, 2–11 (2012).
28. Rainer de Martin, null, Hoeth, M., Hofer-Warbinek, R. & Schmid, J. A. The Transcription Factor NF-κB and the Regulation of Vascular Cell Function. *Arteriosclerosis, Thrombosis, and Vascular Biology* **20**, e83–e88 (2000).
29. de Winther, M. P. J., Kanters, E., Kraal, G. & Hofker, M. H. Nuclear Factor κB Signaling in Atherogenesis. *Arteriosclerosis, Thrombosis, and Vascular Biology* **25**, 904–914 (2005).
30. Brand, K. *et al.* Activated transcription factor nuclear factor-kappa B is present in the atherosclerotic lesion. *J Clin Invest* **97**, 1715–1722 (1996).
31. Tedgui, A. & Mallat, Z. Anti-inflammatory mechanisms in the vascular wall. *Circ Res* **88**, 877–887 (2001).
32. Bogdan, C., Vodovotz, Y. & Nathan, C. Macrophage deactivation by interleukin 10. *J Exp Med* **174**, 1549–1555 (1991).
33. Schottelius, A. J., Mayo, M. W., Sartor, R. B. & Baldwin, A. S. Interleukin-10 signaling blocks inhibitor of kappaB kinase activity and nuclear factor kappaB DNA binding. *J Biol Chem* **274**, 31868–31874 (1999).
34. Donnelly, R. P., Dickensheets, H. & Finbloom, D. S. The interleukin-10 signal transduction pathway and regulation of gene expression in mononuclear phagocytes. *J Interferon Cytokine Res* **19**, 563–573 (1999).
35. Mallat, Z. *et al.* Protective Role of Interleukin-10 in Atherosclerosis. *Circulation Research* **85**, e17–e24 (1999).
36. Ruparelia, N. & Choudhury, R. Inflammation and atherosclerosis: what is on the horizon? *Heart* **106**, 80–85 (2020).
37. Ridker, P. M. *et al.* Antiinflammatory Therapy with Canakinumab for Atherosclerotic Disease. *N Engl J Med* **377**, 1119–1131 (2017).
38. Ibañez, B. & Fuster, V. Cantos. *Circulation Research* **121**, 1320–1322 (2017).

39. Fiolet, A. T. L. *et al.* Efficacy and safety of low-dose colchicine in patients with coronary disease: a systematic review and meta-analysis of randomized trials. *Eur Heart J* **42**, 2765–2775 (2021).
40. Gustafsson, Å. B. & Gottlieb, R. A. Heart mitochondria: gates of life and death. *Cardiovascular Research* **77**, 334–343 (2008).
41. Forte, M. *et al.* The role of mitochondrial dynamics in cardiovascular diseases. *Br J Pharmacol* **178**, 2060–2076 (2021).
42. Peng, W. *et al.* Mitochondrial Dysfunction in Atherosclerosis. *DNA Cell Biol* **38**, 597–606 (2019).
43. Ciccarelli, G. *et al.* Mitochondrial Dysfunction: The Hidden Player in the Pathogenesis of Atherosclerosis? *International Journal of Molecular Sciences* **24**, 1086 (2023).
44. Suárez-Rivero, J. M. *et al.* From Mitochondria to Atherosclerosis: The Inflammation Path. *Biomedicines* **9**, 258 (2021).
45. Yang, S. & Lian, G. ROS and diseases: role in metabolism and energy supply. *Mol Cell Biochem* **467**, 1–12 (2020).
46. Navab, M. *et al.* The Yin and Yang of oxidation in the development of the fatty streak. A review based on the 1994 George Lyman Duff Memorial Lecture. *Arterioscler Thromb Vasc Biol* **16**, 831–842 (1996).
47. Shemiakova, T. *et al.* Mitochondrial Dysfunction and DNA Damage in the Context of Pathogenesis of Atherosclerosis. *Biomedicines* **8**, 166 (2020).
48. McPherson, R. & Tybjaerg-Hansen, A. Genetics of Coronary Artery Disease. *Circ Res* **118**, 564–578 (2016).
49. Zdravkovic, S. *et al.* Heritability of death from coronary heart disease: a 36-year follow-up of 20 966 Swedish twins. *Journal of Internal Medicine* **252**, 247–254 (2002).
50. Lloyd-Jones, D. M. *et al.* Parental Cardiovascular Disease as a Risk Factor for Cardiovascular Disease in Middle-aged AdultsA Prospective Study of Parents and Offspring. *JAMA* **291**, 2204–2211 (2004).
51. Yusuf, S. *et al.* Effect of potentially modifiable risk factors associated with myocardial infarction in 52 countries (the INTERHEART study): case-control study. *The Lancet* **364**, 937–952 (2004).
52. Pulst, S. M. Genetic Linkage Analysis. *Archives of Neurology* **56**, 667–672 (1999).
53. Stitziel, N. O. & MacRae, C. A. A Clinical Approach to Inherited Premature Coronary Artery Disease. *Circ Cardiovasc Genet* **7**, 558–564 (2014).
54. Lehrman, M. A. *et al.* Mutation in LDL Receptor: Alu-Alu Recombination Deletes Exons Encoding Transmembrane and Cytoplasmic Domains. *Science* **227**, 140–146 (1985).
55. Soria, L. F. *et al.* Association between a specific apolipoprotein B mutation and familial defective apolipoprotein B-100. *Proc Natl Acad Sci U S A* **86**, 587–591 (1989).
56. Berge, K. E. *et al.* Accumulation of dietary cholesterol in sitosterolemia caused by mutations in adjacent ABC transporters. *Science* **290**, 1771–1775 (2000).
57. Garcia, C. K. *et al.* Autosomal recessive hypercholesterolemia caused by mutations in a putative LDL receptor adaptor protein. *Science* **292**, 1394–1398 (2001).
58. Abifadel, M. *et al.* Mutations in PCSK9 cause autosomal dominant hypercholesterolemia. *Nature Genetics* **34**, 154 (2003).
59. Altshuler, D. & Hirschhorn, J. N. MEF2A sequence variants and coronary artery disease: a change of heart? *J Clin Invest* **115**, 831–833 (2005).

60. McPherson, R. Genome-Wide Association Studies of Cardiovascular Disease in European and Non-European Populations. *Curr Genet Med Rep* **2**, 1–12 (2014).
61. Altshuler, D., Donnelly, P., & The International HapMap Consortium. A haplotype map of the human genome. *Nature* **437**, 1299–1320 (2005).
62. Frazer, K. A. *et al.* A second generation human haplotype map of over 3.1 million SNPs. *Nature* **449**, 851–861 (2007).
63. Via, M., Gignoux, C. & Burchard, E. G. The 1000 Genomes Project: new opportunities for research and social challenges. *Genome Medicine* **2**, 3 (2010).
64. Risch, N. & Merikangas, K. The future of genetic studies of complex human diseases. *Science* **273**, 1516–1517 (1996).
65. Bush, W. S. & Moore, J. H. Chapter 11: Genome-Wide Association Studies. *PLoS Comput Biol* **8**, e1002822 (2012).
66. Chen, Z., Boehnke, M., Wen, X. & Mukherjee, B. Revisiting the genome-wide significance threshold for common variant GWAS. *G3 (Bethesda)* **11**, jkaa056 (2021).
67. Helgadottir, A. *et al.* A common variant on chromosome 9p21 affects the risk of myocardial infarction. *Science* **316**, 1491–1493 (2007).
68. McPherson, R. *et al.* A common allele on chromosome 9 associated with coronary heart disease. *Science* **316**, 1488–1491 (2007).
69. Samani, N. J. *et al.* Genomewide association analysis of coronary artery disease. *N Engl J Med* **357**, 443–453 (2007).
70. Kathiresan, S. *et al.* Genome-wide association of early-onset myocardial infarction with single nucleotide polymorphisms and copy number variants. *Nat Genet* **41**, 334–341 (2009).
71. Schunkert, H. *et al.* Large-scale association analysis identifies 13 new susceptibility loci for coronary artery disease. *Nat Genet* **43**, 333–338 (2011).
72. Peden, J. F. *et al.* A genome-wide association study in Europeans and South Asians identifies five new loci for coronary artery disease. *Nat Genet* **43**, 339–344 (2011).
73. Deloukas, P. *et al.* Large-scale association analysis identifies new risk loci for coronary artery disease. *Nat Genet* **45**, 25–33 (2013).
74. Zeng, L. *et al.* Contribution of Regulatory-Gene Networks to Heritability of Coronary Artery Disease. *J Am Coll Cardiol* **73**, 2946–2957 (2019).
75. Manolio, T. A. *et al.* Finding the missing heritability of complex diseases. *Nature* **461**, 747–753 (2009).
76. Nikpay, M. *et al.* A comprehensive 1000 Genomes–based genome-wide association meta-analysis of coronary artery disease. *Nature Genetics* **47**, 1121–1130 (2015).
77. Nelson, C. P. *et al.* Association analyses based on false discovery rate implicate new loci for coronary artery disease. *Nat Genet* **49**, 1385–1391 (2017).
78. Schaid, D. J., Chen, W. & Larson, N. B. From genome-wide associations to candidate causal variants by statistical fine-mapping. *Nat Rev Genet* **19**, 491–504 (2018).
79. Farh, K. K.-H. *et al.* Genetic and epigenetic fine mapping of causal autoimmune disease variants. *Nature* **518**, 337–343 (2015).
80. Giral, H., Landmesser, U. & Kratzer, A. Into the Wild: GWAS Exploration of Non-coding RNAs. *Front Cardiovasc Med* **5**, 181 (2018).
81. McPherson, R. Chromosome 9p21.3 Locus for Coronary Artery Disease. *Journal of the American College of Cardiology* **62**, 1382–1383 (2013).
82. Almontashiri, N. A. M. The 9p21.3 risk locus for coronary artery disease: A 10-year search for its mechanism. *Journal of Taibah University Medical Sciences* **12**, 199–204 (2017).

83. Ghoussaini, M. *et al.* Open Targets Genetics: systematic identification of trait-associated genes using large-scale genetics and functional genomics. *Nucleic Acids Res* **49**, D1311–D1320 (2020).
84. Ward, L. D. & Kellis, M. HaploReg: a resource for exploring chromatin states, conservation, and regulatory motif alterations within sets of genetically linked variants. *Nucleic Acids Res* **40**, D930-934 (2012).
85. GTEx Consortium. The Genotype-Tissue Expression (GTEx) project. *Nat Genet* **45**, 580–585 (2013).
86. THE GTEX CONSORTIUM *et al.* The Genotype-Tissue Expression (GTEx) pilot analysis: Multitissue gene regulation in humans. *Science* **348**, 648–660 (2015).
87. Aguet, F. *et al.* Genetic effects on gene expression across human tissues. *Nature* **550**, 204–213 (2017).
88. Koplev, S. *et al.* A mechanistic framework for cardiometabolic and coronary artery diseases. *Nat Cardiovasc Res* **1**, 85–100 (2022).
89. Kojima, Y. *et al.* Cyclin-dependent kinase inhibitor 2B regulates efferocytosis and atherosclerosis. *J Clin Invest* **124**, 1083–1097 (2014).
90. VinuÉ, Á. *et al.* Changes in CDKN2A/2B expression associate with T-cell phenotype modulation in atherosclerosis and type 2 diabetes mellitus. *Translational Research* **203**, 31–48 (2019).
91. Holdt, L. M. *et al.* ANRIL Expression Is Associated With Atherosclerosis Risk at Chromosome 9p21. *Arteriosclerosis, Thrombosis, and Vascular Biology* **30**, 620–627 (2010).
92. Holdt, L. M. *et al.* Circular non-coding RNA ANRIL modulates ribosomal RNA maturation and atherosclerosis in humans. *Nat Commun* **7**, 12429 (2016).
93. Almontashiri, N. A. M. *et al.* Interferon-γ activates expression of p15 and p16 regardless of 9p21.3 coronary artery disease risk genotype. *J Am Coll Cardiol* **61**, 143–147 (2013).
94. Harismendy, O. *et al.* 9p21 DNA variants associated with coronary artery disease impair interferon-γ signalling response. *Nature* **470**, 264–268 (2011).
95. Wolf, Y. I., Aravind, L., Grishin, N. V. & Koonin, E. V. Evolution of Aminoacyl-tRNA Synthetases—Analysis of Unique Domain Architectures and Phylogenetic Trees Reveals a Complex History of Horizontal Gene Transfer Events. *Genome Res.* **9**, 689–710 (1999).
96. Bullwinkle, T. J. & Ibba, M. Emergence and Evolution. *Top Curr Chem* **344**, 43–87 (2014).
97. Ibba, M. & Söll, D. Aminoacyl-tRNA Synthesis. *Annual Review of Biochemistry* **69**, 617–650 (2000).
98. Beebe, K., Mock, M., Merriman, E. & Schimmel, P. Distinct domains of tRNA synthetase recognize the same base pair. *Nature* **451**, 90–93 (2008).
99. Eriani, G., Delarue, M., Poch, O., Gangloff, J. & Moras, D. Partition of tRNA synthetases into two classes based on mutually exclusive sets of sequence motifs. *Nature* **347**, 203–206 (1990).
100. Klipcan, L. & Safro, M. Amino acid biogenesis, evolution of the genetic code and aminoacyl-tRNA synthetases. *Journal of Theoretical Biology* **228**, 389–396 (2004).
101. Sugiura, I. *et al.* The 2.0 Å crystal structure of Thermus thermophilus methionyl-tRNA synthetase reveals two RNA-binding modules. *Structure* **8**, 197–208 (2000).
102. Eriani, G. *et al.* The class II aminoacyl-tRNA synthetases and their active site: Evolutionary conservation of an ATP binding site. *J Mol Evol* **40**, 499–508 (1995).

103. Bonnefond, L. *et al.* Toward the full set of human mitochondrial aminoacyl-tRNA synthetases: characterization of AspRS and TyrRS. *Biochemistry* **44**, 4805–4816 (2005).
104. Wei, N., Zhang, Q. & Yang, X.-L. Neurodegenerative Charcot–Marie–Tooth disease as a case study to decipher novel functions of aminoacyl-tRNA synthetases. *J Biol Chem* **294**, 5321–5339 (2019).
105. Mishra, P. & Chan, D. C. Mitochondrial dynamics and inheritance during cell division, development and disease. *Nat Rev Mol Cell Biol* **15**, 634–646 (2014).
106. Cerini, C. *et al.* A component of the multisynthetase complex is a multifunctional aminoacyl-tRNA synthetase. *EMBO J* **10**, 4267–4277 (1991).
107. Kwon, N. H., Fox, P. L. & Kim, S. Aminoacyl-tRNA synthetases as therapeutic targets. *Nat Rev Drug Discov* **18**, 629–650 (2019).
108. Kyriacou, S. V. & Deutscher, M. P. An important role for the multienzyme aminoacyl-tRNA synthetase complex in mammalian translation and cell growth. *Mol Cell* **29**, 419–427 (2008).
109. Lee, S. W., Cho, B. H., Park, S. G. & Kim, S. Aminoacyl-tRNA synthetase complexes: beyond translation. *J Cell Sci* **117**, 3725–3734 (2004).
110. Nathanson, L. & Deutscher, M. P. Active aminoacyl-tRNA synthetases are present in nuclei as a high molecular weight multienzyme complex. *J Biol Chem* **275**, 31559–31562 (2000).
111. Wakasugi, K. & Schimmel, P. Two distinct cytokines released from a human aminoacyl-tRNA synthetase. *Science* **284**, 147–151 (1999).
112. Wakasugi, K. & Schimmel, P. Highly Differentiated Motifs Responsible for Two Cytokine Activities of a Split Human tRNA Synthetase *. *Journal of Biological Chemistry* **274**, 23155–23159 (1999).
113. Wakasugi, K. *et al.* A human aminoacyl-tRNA synthetase as a regulator of angiogenesis. *Proc Natl Acad Sci U S A* **99**, 173–177 (2002).
114. Wang, M. *et al.* Wars2 is a determinant of angiogenesis. *Nat Commun* **7**, 12061 (2016).
115. Turvey, A. K., Horvath, G. A. & Cavalcanti, A. R. O. Aminoacyl-tRNA synthetases in human health and disease. *Frontiers in Physiology* **13**, (2022).
116. Antonellis, A. *et al.* Glycyl tRNA synthetase mutations in Charcot-Marie-Tooth disease type 2D and distal spinal muscular atrophy type V. *Am J Hum Genet* **72**, 1293–1299 (2003).
117. Zou, Y. *et al.* The regulatory roles of aminoacyl-tRNA synthetase in cardiovascular disease. *Mol Ther Nucleic Acids* **25**, 372–387 (2021).
118. Hallmann, K. *et al.* A homozygous splice-site mutation in CARS2 is associated with progressive myoclonic epilepsy. *Neurology* **83**, 2183–2187 (2014).
119. Coughlin, C. R. *et al.* Mutations in the mitochondrial cysteinyl-tRNA synthase gene, CARS2, lead to a severe epileptic encephalopathy and complex movement disorder. *Journal of Medical Genetics* **52**, 532–540 (2015).
120. Samanta, D., Gokden, M. & Willis, E. Clinicopathologic Findings of CARS2 Mutation. *Pediatr Neurol* **87**, 65–69 (2018).
121. Hu, C. *et al.* Clinical and molecular characterization of pediatric mitochondrial disorders in south of China. *European Journal of Medical Genetics* **63**, 103898 (2020).
122. Wu, T.-H. *et al.* [Mutations in aminoacyl-tRNA synthetase genes: an analysis of 10 cases]. *Zhongguo Dang Dai Er Ke Za Zhi* **22**, 595–601 (2020).
123. Kapoor, D., Majethia, P., Anand, A., Shukla, A. & Sharma, S. Expanding the electro-clinical phenotype of CARS2associated neuroregression. *Epilepsy Behav Rep* **16**, 100485 (2021).

124. Shoffner, J. M. *et al.* Myoclonic epilepsy and ragged-red fiber disease (MERRF) is associated with a mitochondrial DNA tRNA(Lys) mutation. *Cell* **61**, 931–937 (1990).
125. DiMauro, S. *et al.* Clinical features and genetics of myoclonic epilepsy with ragged red fibers. *Adv Neurol* **89**, 217–229 (2002).
126. Wang, F. *et al.* Point mutations in KAL1 and the mitochondrial gene MT-tRNA(cys) synergize to produce Kallmann syndrome phenotype. *Sci Rep* **5**, 13050 (2015).
127. Akaike, T. *et al.* Cysteinyl-tRNA synthetase governs cysteine polysulfidation and mitochondrial bioenergetics. *Nat Commun* **8**, 1177 (2017).
128. Zainol Abidin, Q. H. *et al.* Synthesis of Sulfides and Persulfides Is Not Impeded by Disruption of Three Canonical Enzymes in Sulfur Metabolism. *Antioxidants* **12**, 868 (2023).
129. Kaneko, K. *et al.* 8-Nitro-cGMP suppresses mineralization by mouse osteoblasts. *J Clin Biochem Nutr* **71**, 191–197 (2022).
130. Erdélyi, K. *et al.* Reprogrammed transsulfuration promotes basal-like breast tumor progression via realigning cellular cysteine persulfidation. *Proc Natl Acad Sci U S A* **118**, e2100050118 (2021).
131. Chen, Z. *et al.* Prognostic Assessment of Oxidative Stress-Related Genes in Colorectal Cancer and New Insights into Tumor Immunity. *Oxid Med Cell Longev* **2022**, 2518340 (2022).
132. Perisic, L. *et al.* Gene expression signatures, pathways and networks in carotid atherosclerosis. *J Intern Med* **279**, 293–308 (2016).
133. Folkersen, L. *et al.* Association of Genetic Risk Variants With Expression of Proximal Genes Identifies Novel Susceptibility Genes for Cardiovascular Disease. *Circulation: Cardiovascular Genetics* **3**, 365–373 (2010).
134. Senichkin, V. V., Prokhorova, E. A., Zhivotovsky, B. & Kopeina, G. S. Simple and Efficient Protocol for Subcellular Fractionation of Normal and Apoptotic Cells. *Cells* **10**, 852 (2021).
135. Krämer, A., Green, J., Pollard, J., Jr & Tugendreich, S. Causal analysis approaches in Ingenuity Pathway Analysis. *Bioinformatics* **30**, 523–530 (2014).
136. Bryant, J. D., Lei, Y., VanPortfliet, J. J., Winters, A. D. & West, A. P. Assessing Mitochondrial DNA Release into the Cytosol and Subsequent Activation of Innate Immune-related Pathways in Mammalian Cells. *Current Protocols* **2**, e372 (2022).
137. Yalçınkaya, B., Tastekin, D., Güzelbulut, F., Akgoz, M. & Pençe, S. Quantification of cell-free circulating mitochondrial DNA copy number variation in hepatocellular carcinoma. *Rev Assoc Med Bras (1992)* **68**, 1161–1165.
138. López Rodríguez, M., Arasu, U. T. & Kaikkonen, M. U. Exploring the genetic basis of coronary artery disease using functional genomics. *Atherosclerosis* **374**, 87–98 (2023).
139. ALFA: Allele Frequency Aggregator. https://ncbi.nlm.nih.gov/snp/docs/gsr/alfa/.
140. Wu, C. *et al.* BioGPS: an extensible and customizable portal for querying and organizing gene annotation resources. *Genome Biol* **10**, R130 (2009).
141. Wu, C., MacLeod, I. & Su, A. I. BioGPS and MyGene.info: organizing online, gene-centric information. *Nucleic Acids Res* **41**, D561–D565 (2013).
142. Hutchins, A. P., Diez, D. & Miranda-Saavedra, D. The IL-10/STAT3-mediated anti-inflammatory response: recent developments and future challenges. *Briefings in Functional Genomics* **12**, 489–498 (2013).

143. Moore, K. J., Sheedy, F. J. & Fisher, E. A. Macrophages in atherosclerosis: a dynamic balance. *Nature Reviews Immunology* **13**, 709–721 (2013).
144. Gomez, D. & Owens, G. K. Smooth muscle cell phenotypic switching in atherosclerosis. *Cardiovascular Research* vol. 95 156–164 Preprint at https://doi.org/10.1093/cvr/cvs115 (2012).
145. Kessler, T. & Schunkert, H. Coronary Artery Disease Genetics Enlightened by Genome-Wide Association Studies. *JACC Basic Transl Sci* **6**, 610–623 (2021).
146. Musunuru, K. *et al.* From noncoding variant to phenotype via SORT1 at the 1p13 cholesterol locus. *Nature* **466**, 714–719 (2010).
147. van der Harst, P. & Verweij, N. Identification of 64 Novel Genetic Loci Provides an Expanded View on the Genetic Architecture of Coronary Artery Disease. *Circ Res* **122**, 433–443 (2018).
148. Mauersberger, C., Schunkert, H. & Sager, H. Inflammation-Related Risk Loci in Genome-Wide Association Studies of Coronary Artery Disease. *Cells* **10**, 440 (2021).
149. Allahverdian, S., Chaabane, C., Boukais, K., Francis, G. A. & Bochaton-Piallat, M.-L. Smooth muscle cell fate and plasticity in atherosclerosis. *Cardiovasc Res* **114**, 540–550 (2018).
150. Yurdagul, A., Finney, A., Woolard, M. D. & Orr, A. W. The Arterial Microenvironment: The Where and Why of Atherosclerosis. *Biochem J* **473**, 1281–1295 (2016).
151. Yurdagul, A. Crosstalk Between Macrophages and Vascular Smooth Muscle Cells in Atherosclerotic Plaque Stability. *Arteriosclerosis, Thrombosis, and Vascular Biology* **42**, 372–380 (2022).
152. Owens, G. K., Kumar, M. S. & Wamhoff, B. R. Molecular Regulation of Vascular Smooth Muscle Cell Differentiation in Development and Disease. *Physiological Reviews* **84**, 767–801 (2004).
153. Jobin, P. G. *et al.* Matrix metalloproteinases inactivate the proinflammatory functions of secreted moonlighting tryptophanyl-tRNA synthetase. *Journal of Biological Chemistry* **294**, 12866–12879 (2019).
154. Liu, H., Shi, B., Huang, C.-C., Eksarko, P. & Pope, R. M. Transcriptional diversity during monocyte to macrophage differentiation. *Immunol Lett* **117**, 70–80 (2008).
155. Becker, S., Warren, M. K. & Haskill, S. Colony-stimulating factor-induced monocyte survival and differentiation into macrophages in serum-free cultures. *The Journal of Immunology* **139**, 3703–3709 (1987).
156. Martinez, F. O., Gordon, S., Locati, M. & Mantovani, A. Transcriptional Profiling of the Human Monocyte-to-Macrophage Differentiation and Polarization: New Molecules and Patterns of Gene Expression1. *The Journal of Immunology* **177**, 7303–7311 (2006).
157. Moore, K. W., Malefyt, R. de W., Coffman, R. L. & O'Garra, A. Interleukin-10 and the Interleukin-10 Receptor. *https://doi-org.proxy.bib.uottawa.ca/10.1146/annurev.immunol.19.1.683* **19**, 683–765 (2003).
158. Dagvadorj, J. *et al.* Interleukin (IL)-10 attenuates lipopolysaccharide-induced IL-6 production via inhibition of IiB-activity by Bcl-3. **15**, 217–224 (2009).
159. Chen, H. J., Tas, S. W. & de Winther, M. P. J. Type-I interferons in atherosclerosis. *Journal of Experimental Medicine* vol. 217 Preprint at https://doi.org/10.1084/jem.20190459 (2020).
160. Mesev, E. V., LeDesma, R. A. & Ploss, A. Decoding type I and III interferon signalling during viral infection. *Nat Microbiol* **4**, 914–924 (2019).

161. Cheung, S. H., Kwok, W. K., To, K. F. & Lau, J. Y. W. Anti-Atherogenic Effect of Hydrogen Sulfide by Over-Expression of Cystathionine Gamma-Lyase (CSE) Gene. *PLOS ONE* **9**, e113038 (2014).
162. Mani, S. *et al.* Decreased Endogenous Production of Hydrogen Sulfide Accelerates Atherosclerosis. *Circulation* **127**, 2523–2534 (2013).
163. Dhar, A. The Role of PKR as a Potential Target for Treating Cardiovascular Diseases. *Current cardiology reviews* **13**, 28–31 (2017).
164. Fiordelisi, A., Iaccarino, G., Morisco, C., Coscioni, E. & Sorriento, D. NFkappaB is a Key Player in the Crosstalk between Inflammation and Cardiovascular Diseases. *International Journal of Molecular Sciences* **20**, (2019).
165. Zandi, E., Rothwarf, D. M., Delhase, M., Hayakawa, M. & Karin, M. The IkappaB kinase complex (IKK) contains two kinase subunits, IKKalpha and IKKbeta, necessary for IkappaB phosphorylation and NF-kappaB activation. *Cell* **91**, 243–252 (1997).
166. Zhu, Y. *et al.* Research Progress on the Relationship between Atherosclerosis and Inflammation. *Biomolecules* **8**, 80 (2018).
167. Wolf, D. & Ley, K. Immunity and Inflammation in Atherosclerosis. *Circ Res* **124**, 315–327 (2019).
168. Boshuizen, M. C. S. & de Winther, M. P. J. Interferons as Essential Modulators of Atherosclerosis. *Arteriosclerosis, Thrombosis, and Vascular Biology* **35**, 1579–1588 (2015).
169. Orecchioni, M., Ghosheh, Y., Pramod, A. B. & Ley, K. Macrophage Polarization: Different Gene Signatures in M1(LPS+) vs. Classically and M2(LPS–) vs. Alternatively Activated Macrophages. *Frontiers in Immunology* **10**, (2019).
170. Sato, M. *et al.* Positive feedback regulation of type I IFN genes by the IFN-inducible transcription factor IRF-7. *FEBS Letters* **441**, 106–110 (1998).
171. Au, W. C., Moore, P. A., LaFleur, D. W., Tombal, B. & Pitha, P. M. Characterization of the interferon regulatory factor-7 and its potential role in the transcription activation of interferon A genes. *J Biol Chem* **273**, 29210–29217 (1998).
172. Sato, M. *et al.* Distinct and Essential Roles of Transcription Factors IRF-3 and IRF-7 in Response to Viruses for IFN-α/β Gene Induction. *Immunity* **13**, 539–548 (2000).
173. Günthner, R. & Anders, H.-J. Interferon-regulatory factors determine macrophage phenotype polarization. *Mediators Inflamm* **2013**, 731023 (2013).
174. Au-Yeung, N., Mandhana, R. & Horvath, C. M. Transcriptional regulation by STAT1 and STAT2 in the interferon JAK-STAT pathway. *JAKSTAT* **2**, e23931 (2013).
175. Zamanian-Daryoush, M., Mogensen, T. H., DiDonato, J. A. & Williams, B. R. G. NF-κB Activation by Double-Stranded-RNA-Activated Protein Kinase (PKR) Is Mediated through NF-κB-Inducing Kinase and IκB Kinase. *Mol Cell Biol* **20**, 1278–1290 (2000).
176. Bonnet, M. C., Weil, R., Dam, E., Hovanessian, A. G. & Meurs, E. F. PKR Stimulates NF-κB Irrespective of Its Kinase Function by Interacting with the IκB Kinase Complex. *Mol Cell Biol* **20**, 4532–4542 (2000).
177. Zhang, P. & Samuel, C. E. Induction of Protein Kinase PKR-dependent Activation of Interferon Regulatory Factor 3 by Vaccinia Virus Occurs through Adapter IPS-1 Signaling. *J Biol Chem* **283**, 34580–34587 (2008).
178. Ahn, S. B., Jang, K., Jun, D. W., Lee, B. H. & Shin, K. J. Expression of Liver X Receptor Correlates with Intrahepatic Inflammation and Fibrosis in Patients with Nonalcoholic Fatty Liver Disease. *Digestive Diseases and Sciences* **59**, 2975–2983 (2014).

179. Yeh, M. M. & Brunt, E. M. Pathological Features of Fatty Liver Disease. *Gastroenterology* **147**, 754–764 (2014).
180. Stål, P. Liver fibrosis in non-alcoholic fatty liver disease - diagnostic challenge with prognostic significance. *World J Gastroenterol* **21**, 11077–11087 (2015).
181. Brea, A. *et al.* Nonalcoholic Fatty Liver Disease Is Associated With Carotid Atherosclerosis. *Arteriosclerosis, Thrombosis, and Vascular Biology* **25**, 1045–1050 (2005).
182. García, M. A. *et al.* Impact of protein kinase PKR in cell biology: from antiviral to antiproliferative action. *Microbiol Mol Biol Rev* **70**, 1032–1060 (2006).
183. Kumar, A., Haque, J., Lacoste, J., Hiscott, J. & Williams, B. R. Double-stranded RNA-dependent protein kinase activates transcription factor NF-kappa B by phosphorylating I kappa B. *Proc Natl Acad Sci U S A* **91**, 6288–6292 (1994).
184. Monaco, C. *et al.* Canonical pathway of nuclear factor κB activation selectively regulates proinflammatory and prothrombotic responses in human atherosclerosis. *Proc Natl Acad Sci U S A* **101**, 5634–5639 (2004).
185. Coughlin, C. R. *et al.* Mutations in the mitochondrial cysteinyl-tRNA synthase gene, *CARS2,* lead to a severe epileptic encephalopathy and complex movement disorder. *Journal of Medical Genetics* **52**, 532–540 (2015).
186. Akaike, T., Motohashi, H., Fukuto, J. & Nagy, P. L-58 - Cysteinyl-tRNA synthetase (CARS) controls endogenous hydropersulfide production and mitochondrial respiration. *Free Radical Biology and Medicine* **120**, S21 (2018).
187. Akaike, T. *et al.* Cysteinyl-tRNA synthetase governs cysteine polysulfidation and mitochondrial bioenergetics. *Nature Communications* **8**, 1177 (2017).
188. Kalyanaraman, B. *et al.* Measuring reactive oxygen and nitrogen species with fluorescent probes: challenges and limitations. *Free radical biology & medicine* **52**, 1 (2012).
189. Hu, H.-J. *et al.* Hydrogen sulfide improves ox-LDL-induced expression levels of Lp-PLA2 in THP-1 monocytes via the p38MAPK pathway. *Mol Med Rep* **23**, 358 (2021).
190. Seth, R. B., Sun, L., Ea, C.-K. & Chen, Z. J. Identification and Characterization of MAVS, a Mitochondrial Antiviral Signaling Protein that Activates NF-κB and IRF3. *Cell* **122**, 669–682 (2005).
191. Madamanchi, N. R. & Runge, M. S. Mitochondrial Dysfunction in Atherosclerosis. *Circulation Research* **100**, 460–473 (2007).
192. Zhou, R., Yazdi, A. S., Menu, P. & Tschopp, J. A role for mitochondria in NLRP3 inflammasome activation. *Nature* **469**, 221–227 (2011).
193. Nakahira, K. *et al.* Autophagy proteins regulate innate immune response by inhibiting NALP3 inflammasome-mediated mitochondrial DNA release. *Nat Immunol* **12**, 222–230 (2011).
194. Shimada, K. *et al.* Oxidized Mitochondrial DNA Activates the NLRP3 Inflammasome during Apoptosis. *Immunity* **36**, 401–414 (2012).
195. Grebe, A., Hoss, F. & Latz, E. NLRP3 Inflammasome and the IL-1 Pathway in Atherosclerosis. *Circulation Research* **122**, 1722–1740 (2018).
196. Ballinger, S. W. *et al.* Mitochondrial Integrity and Function in Atherogenesis. *Circulation* **106**, 544–549 (2002).
197. Yano, M. *et al.* Functional Analysis of Human Mitochondrial Receptor Tom20 for Protein Import into Mitochondria *. *Journal of Biological Chemistry* **273**, 26844–26851 (1998).

198. Wurm, C. A. *et al.* Nanoscale distribution of mitochondrial import receptor Tom20 is adjusted to cellular conditions and exhibits an inner-cellular gradient. *Proc Natl Acad Sci U S A* **108**, 13546–13551 (2011).
199. Freemerman, A. J. *et al.* Metabolic Reprogramming of Macrophages. *J Biol Chem* **289**, 7884–7896 (2014).
200. Jha, A. K. *et al.* Network Integration of Parallel Metabolic and Transcriptional Data Reveals Metabolic Modules that Regulate Macrophage Polarization. *Immunity* **42**, 419–430 (2015).
201. Claus, C., Fritz, R., Schilling, E. & Reibetanz, U. The Metabolic Response of Various Cell Lines to Microtubule-Driven Uptake of Lipid- and Polymer-Coated Layer-by-Layer Microcarriers. *Pharmaceutics* **13**, 1441 (2021).
202. Maeß, M. B., Wittig, B. & Lorkowski, S. Highly Efficient Transfection of Human THP-1 Macrophages by Nucleofection. *J Vis Exp* 51960 (2014) doi:10.3791/51960.
203. Vasan, K. *et al.* Genes Involved in Maintaining Mitochondrial Membrane Potential Upon Electron Transport Chain Disruption. *Frontiers in Cell and Developmental Biology* **10**, (2022).
204. Cillero-Pastor, B. *et al.* Mitochondrial dysfunction activates cyclooxygenase 2 expression in cultured normal human chondrocytes. *Arthritis Rheum* **58**, 2409–2419 (2008).
205. Ichimura, H., Parthasarathi, K., Quadri, S., Issekutz, A. C. & Bhattacharya, J. Mechano-oxidative coupling by mitochondria induces proinflammatory responses in lung venular capillaries. *J Clin Invest* **111**, 691–699 (2003).
206. Mathew, A. *et al.* Degraded Mitochondrial DNA is a Newly Identified Subtype of the Damage Associated Molecular Pattern (DAMP) Family and Possible Trigger of Neurodegeneration. *Journal of Alzheimer's Disease* **30**, 617–627 (2012).
207. López-Armada, M. J. *et al.* Mitochondrial activity is modulated by TNFα and IL-1β in normal human chondrocyte cells. *Osteoarthritis and Cartilage* **14**, 1011–1022 (2006).
208. Zielonka, J. & Kalyanaraman, B. "ROS-generating mitochondrial DNA mutations can regulate tumor cell metastasis"—a critical commentary. *Free Radic Biol Med* **45**, 1217–1219 (2008).
209. Schröder, K. *et al.* Nox4 Is a Protective Reactive Oxygen Species Generating Vascular NADPH Oxidase. *Circulation Research* **110**, 1217–1225 (2012).
210. Mongue-Din, H. *et al.* NADPH Oxidase-4 Driven Cardiac Macrophage Polarization Protects Against Myocardial Infarction–Induced Remodeling. *JACC Basic Transl Sci* **2**, 688–698 (2017).
211. Gray, S. P. *et al.* Reactive Oxygen Species Can Provide Atheroprotection via NOX4-Dependent Inhibition of Inflammation and Vascular Remodeling. *Arteriosclerosis, Thrombosis, and Vascular Biology* **36**, 295–307 (2016).
212. Nikpay, M., Stewart, A. F. R. & McPherson, R. Partitioning the heritability of coronary artery disease highlights the importance of immune-mediated processes and epigenetic sites associated with transcriptional activity. *Cardiovasc Res* **113**, 973–983 (2017).
213. Aragam, K. G. *et al.* Discovery and systematic characterization of risk variants and genes for coronary artery disease in over a million participants. *Nat Genet* **54**, 1803–1815 (2022).
214. Visscher, P. M. *et al.* 10 Years of GWAS Discovery: Biology, Function, and Translation. *Am J Hum Genet* **101**, 5–22 (2017).
215. Shu, L., Blencowe, M. & Yang, X. Translating GWAS Findings to Novel Therapeutic Targets for Coronary Artery Disease. *Front Cardiovasc Med* **5**, 56 (2018).

216. Khera, A. V. *et al.* Genome-wide polygenic scores for common diseases identify individuals with risk equivalent to monogenic mutations. *Nat Genet* **50**, 1219–1224 (2018).
217. Gallagher, M. D. & Chen-Plotkin, A. S. The Post-GWAS Era: From Association to Function. *Am J Hum Genet* **102**, 717–730 (2018).
218. Lo Sardo, V. *et al.* Unveiling the Role of the Most Impactful Cardiovascular Risk Locus through Haplotype Editing. *Cell* **175**, 1796-1810.e20 (2018).
219. Jadhav, K. S. & Bauer, R. C. Trouble With Tribbles-1. *Arterioscler Thromb Vasc Biol* **39**, 998–1005 (2019).
220. Matsunaga, T. *et al.* Supersulphides provide airway protection in viral and chronic lung diseases. *Nat Commun* **14**, 4476 (2023).
221. Takeda, H. *et al.* Sulfur metabolic response in macrophage limits excessive inflammatory response by creating a negative feedback loop. *Redox Biology* **65**, 102834 (2023).
222. Wang, R. Physiological Implications of Hydrogen Sulfide: A Whiff Exploration That Blossomed. *Physiological Reviews* **92**, 791–896 (2012).
223. Sen, N. *et al.* Hydrogen sulfide-linked sulfhydration of NF-κB mediates its anti-apoptotic actions. *Mol Cell* **45**, 13–24 (2012).
224. Filipovic, M. R., Zivanovic, J., Alvarez, B. & Banerjee, R. Chemical Biology of H2S Signaling through Persulfidation. *Chem. Rev.* **118**, 1253–1337 (2018).
225. Tawarayama, H. *et al.* Glutathione trisulfide prevents lipopolysaccharide-induced retinal inflammation via inhibition of proinflammatory cytokine production in glial cells. *Sci Rep* **13**, 11513 (2023).

Curriculum Vitae

Anh-Thu Dang

EDUCATION

University of Ottawa, Ottawa, ON
Doctorate in Philosophy Science, Biochemistry with Specialization in Human and Molecular Genetics
2018 – Present

- Working thesis title: "*Functional Relationship of the CARS2 locus to coronary artery disease*"

University of Ottawa, Ottawa, ON
Master of Science, Biochemistry with Specialization in Human and Molecular Genetics
2016 – 2018; Transfer Date: May 2018

University of Ottawa, Ottawa, ON
Bachelor of Science, Honours with Specialization in Biochemistry
2012 – 2016

- Thesis: "Effect of magnesium deficiency on genome stability and cellular senescence"

RESEARCH AND PROFESSIONAL EXPERIENCE

University of Ottawa Heart Institute, Ottawa, ON
Graduate Researcher, Sept 2016 – Present

- Planned, designed, and executed research for a scientific thesis project to investigate the functional relationship of a gene locus (*CARS2*) associated with coronary artery disease inflammation.
- Interpreted and presented results at departmental seminars and conferences to audiences with varying backgrounds of scientific expertise.

Faculty of Medicine, University of Ottawa, Ottawa, ON
Alumni Trajectory Project Team Member, May 2019 – Mar 2020

- Tracked past graduate students in the Faculty of Medicine from 2008-2018 (791 alumni) and was able to access 74% as part of a cyclical project.
- Co-authored report to inform teaching strategies to improve graduate education.
- Developed a resource for students to explore successful alumni career trajectories.

Health Canada, Nutrition Research Division, Ottawa, ON
Undergraduate Researcher, Sept 2015 – April 2016

- Conducted experiments to study the impact of magnesium deficiency on genome stability and cellular senescence.
- Prepared and presented research results in a seminar and poster session effectively communicating to both peers and researchers.

PUBLICATIONS

Dang, A.-T., A.W. Turner, P. Lau, D. Mohottalage, Y.K. Stephanie Fong, P. Eriksson, L. Folkersen, L. Matic, U. Hedin, S. Soubeyrand, and R. McPherson. 2022. A novel anti-inflammatory role links the CARS2 locus to protection from coronary artery disease. Atherosclerosis. 348:8–15. doi:10.1016/j.atherosclerosis.2022.03.024.

Laframboise, S.J., T. Bailey, **A.-T. Dang**, M. Rose, Z. Zhou, M.D. Berg, S. Holland, S.A. Abdul, K. O'Connor, S. El-Sahli, D.M. Boucher, G. Fairman, J. Deng, K. Shaw, N. Noblett, A. D'Addario, M. Empey, and K. Sinclair. 2023. Analysis of financial challenges faced by graduate students in Canada. Biochem Cell Biol. doi:10.1139/bcb-2023-0021.

Soubeyrand, S., P. Lau, M. Nikpay, **A.-T. Dang**, and R. McPherson. 2022. Common Polymorphism That Protects From Cardiovascular Disease Increases Fibronectin Processing and Secretion. Circ Genom Precis Med. 15:e003428. doi:10.1161/CIRCGEN.121.003428.

Beehler, K., M. Nikpay, P. Lau, **A.-T. Dang**, T.A. Lagace, S. Soubeyrand, and R. McPherson. 2021. A Common Polymorphism in the FADS1 Locus Links miR1908 to Low-Density Lipoprotein Cholesterol Through BMP1. Arterioscler Thromb Vasc Biol. 41:2252–2262. doi:10.1161/ATVBAHA.121.316473.

Soubeyrand, S., M. Nikpay, A. Turner, **A.-T. Dang**, M. Herfkens, P. Lau, and R. McPherson. 2019. Regulation of MFGE8 by the intergenic coronary artery disease locus on 15q26.1. Atherosclerosis. 284:11–17. doi:10.1016/j.atherosclerosis.2019.02.012.

SCHOLARSHIPS AND AWARDS

- Honourable Mention for a Basic Science Poster at the Ottawa Cardiovascular Research Day (2022)
- Award of Excellence (Silver category), National Research Poster Presentation (2021)
- Canadian Institutes of Health Research Travel Award, $1000 (2020)
- University of Ottawa Admission Scholarship - Doctorate (2018)
- University of Ottawa Admission Scholarship (2012)

CONFERENCES

Oral Presentations

- Canadian Lipoprotein Conference, Whistler, BC, Canada (2022)
- Ottawa Cardiovascular Research Day, Cancelled: Selected for a talk (2020)
- Canadian Lipoprotein Conference, Banff, AB, Canada (2019)
- Ottawa Cardiovascular Research Day, Ottawa, ON, Canada (2019)

Poster Presentations

- Canadian Student Health Research Forum, Virtual (originally Winnipeg, MB, Canada) (2021)
- Arteriosclerosis, Thrombosis and Vascular Biology Annual Meeting, Virtual (originally Chicago, Illinois, USA) (2020)
- Arteriosclerosis, Thrombosis and Vascular Biology Annual Meeting, San Francisco, California, USA (2018)
- Ottawa Heart Conference, Ottawa, ON, Canada (2018)
- 5th International Ottawa Heart Conference, Ottawa, ON, Canada (2017)

Chairing/Moderating

- Moderator: "Monocyte Subsets in the Vasculature" and "Taming Cardiovascular Complications and Improving Patient Outcomes: PCSK9 Inhibitors Forging the New Frontier", 5th International Ottawa Heart Conference (2017)

- Chair: "Oral Presentation Session #2: Discovery & Translational Innovations", Ottawa Cardiovascular Research Day (2019)

COMMUNITY AND VOLUNTEER ACTIVITIES

Ottawa Science Policy Network

Cofounder/VP Administration, 2021 – Present

- Established the network at uOttawa as a cofounder.
- Responsible for the keeping of minutes at General and Executive meetings and distribution.
- Handle official correspondence of the organization via email.

Soapbox Science

Volunteer, 2022

- Worked with other volunteers to coordinate responsibilities and shifts.
- Assisted speakers by engaging the public in scientific conversation.

Let's Talk Science

Heart Institute Team Leader/Volunteer, 2016-2021

- Recruited and trained volunteers to support outreach activities.
- Led and supported a team of 8 volunteers at the University of Ottawa Heart Institute site.

oHEART Trainee Committee

Communication Officer, 2021-2022

- Creating and publishing communication content on behalf of the oHEART Committee to highlight trainees, advertise events and share resources.

Evaluator, 2021

- Critically evaluated publications for Publication Excellence Award (2021)

Social Coordinator, 2017-2019

- Initiated, organized, and executed events for graduate students such as workshops, social events, and scientific talks.

Copyright Statement

This thesis contains published and unpublished work. Modifications to the texts and figures have been made in this thesis.

The introduction, material and methods, Table 3.1 - 3.4, Figure 3.1-3.10, associated figure legends, text and discussion of Chapter 3 and Figure 4.1, associated figure legends and text of Chapter 4 are included in the original publication:

Dang, A.-T. *et al.* A novel anti-inflammatory role links the CARS2 locus to protection from coronary artery disease. *Atherosclerosis* **348**, 8–15 (2022).

Specific contributions from co-authors and collaborations are described below:

Anh-Thu Dang: Writing – original draft, carried out the experiments and drafted the first version of the manuscript, and provided input into the experimental design.
Adam W. Turner: Supervision, supervised.
Paulina Lau: Methodology, provided supervision and methodological input.
Dhanuddara Mohottalage: assisted with one experiment.
Yuet Kay Stephanie Fong: assisted with one experiment.
Per Eriksson: provided data from the ASAP study, and.
Lasse Folkersen: provided data from the ASAP study.
Sébastien Soubeyrand: directed the laboratory studies, provided intellectual input throughout and edited the manuscript,
Ruth McPherson: secured funding, designed the study and edited the final manuscript.